Journal of

Jnde

Non Destructive Testing
and Evaluation

ISSN 0973 - 9610

March 2023
Volume 20 ● Issue 1

**An Official Journal of the
Indian Society for
Non Destructive Testing**

If Undelivered Return To :

Indian Society For Non-Destructive Testing
Module Nos.60 & 61,
Readymade Garment Complex,
Sidco Industrial Estate,
Guindy, Chennai-600032.
Tel: 044-22500412

An ISNT Publication

www.isnt.in

Indian Society for
ISNT
Non Destructive Testing

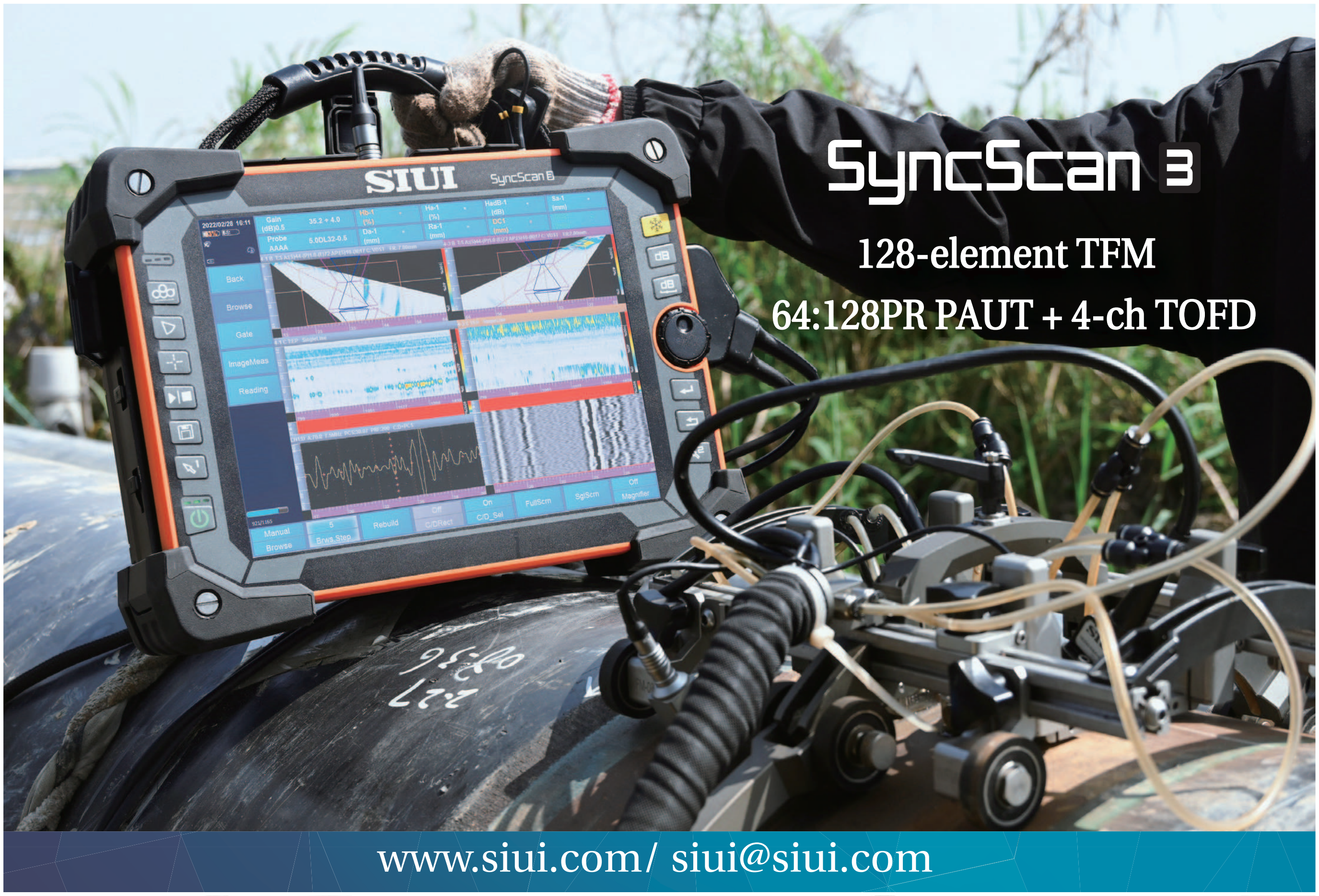

Dual Matrix Array probes

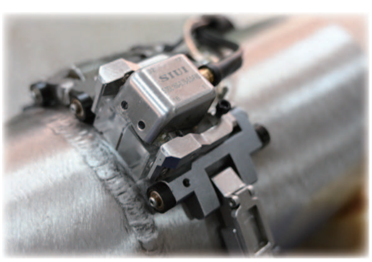

Low-profile scanner with PA probes

*All compatible with Olympus and other brands.

See the future

SIUI

Contents

2 LETTERS
- President Talk
- Managing Editor's Talk
- Guest Editor's Talk

3 CHAPTERS

4 NGC/NCB MEMBERS

6 CHAPTER ACTIVITIES

20 TRAINING MANAGEMENT BOARD

24 REPORT OF ANNUAL CONFERENCE AND EXHIBITION ON NDE (NDE 2022)

29 TECHNICAL PAPERS

- **Pulsed Thermal NDT of Material Discontinuities by Using the Concept of Equivalent Effusivity/Diffusivity Variations**
  A.O. Siddiqui, Y.L.V.D. Prasad, V.P. Vavilov, D. Yu. Kladov
- **Infrared Machine Vision for Detection and Characterization of Defects Present in a Mild Steel Material**
  Pranav Yogesh Mahajan, Aneesh Bajwa, Keshav, Nandani Bansal, Geetika Dua, Amanpreet Kaur and Vanita Arora
- **Defect Detection Capabilities of Barker-Coded Thermal Wave Imaging in Titanium Alloy (Ti-6AL-4V)**
  Anshul Sharma, Vanita Arora, Ishant Singh, Priyanka Das and Ravibabu Mulaveesala
- **Numerical Approach for Characterization of Structural Steel Sample using Frequency Modulated Thermal Wave Imaging**
  Vanita Arora, Ravibabu Mulaveesala, Anshul Sharma, Geetika Dua and Suresh Kumar Bhambhu
- **Neural Network Based Automatic Defect Detection in Infrared Thermography**
  Geetika Dua, Pranav Yogesh Mahajan, Aneesh Bajwa and Vanita Arora
- **Reliability of Thermal Images and Numerical Modelling on Passive Infrared Thermography for Concrete Structures**
  Kavya R. Nair, Vimal Mohan, P. Srinivasan

75 NDE PATENTS

Journal of Non Destructive Testing and Evaluation

MARCH 2023
Volume 20 - Issue 1

on the COVER Page

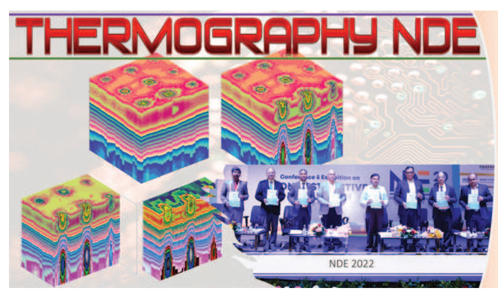

Cover page depicts the spatio-temporal resolvability provided by the matched filter based post processing approach for testing and evaluation of structural steel sample having subsurface defects of various shapes and lateral dimensions using frequency modulated thermal wave imaging.

(Release of Souvenir at the Inaugural function of NDE2022 held during 24-26 Nov 2022)

OBJECTIVE - This Journal of Non Destructive Tesing & Evaluation (JNDE) is published quarterly by the Indian Society for Non Destructive Testing (ISNT) for promoting NDT Science & Technology. The objective of this Journal is to provide a forum for dissemination of knowledge in NDE & related fields. Papers will be accepted on the basis of their contribution to the growth of NDE Science & Technology.

PUBLISHED BY: Mr. Bikash Ghose - Managing Editor, JNDE

For JNDE Subscription / Advertisement / New / Renewal of ISNT Membership Inquiries Contact:
Indian Society for Non-Destructive Testing (ISNT)
Modules 60& 61, 3rd Floor, Readymade Garment Complex,
SIDCO Industrial Estate,
Guindy, Chennai - 600 032, India
Tel: 044-2250 0412 / 4203 8175 Email: headoffice@isnt.in

PRESIDENT TALK

DIWAKAR JOSHI
President – ISNT
president@isnt.in

Greetings!

December2022 issue of JNDE was on NDE 4.0. It was well received by the readers, thanks to Dr. Shyamsunder, our guest editor. You will be happy to know that Dr. Shyamsunder is coordinating the 3rd International Conference on NDE which will be hosted by ISNT in India during Feb 2025.

Let us have a quick look at what's happening around!

The Program Formulation and Management Board (PFMB) will be releasing a few programs in different regions of India in the year 2023. National Certification Board (NCB) is in the process of getting ICN scheme revised to ISO 9712:2021. BIS 13805 will also get revised shortly. The Training Management Board (TMB) is in the process of auditing ATCs for final authorisation. There is a visible increase in Chapter activities including webinars, training programs and workshops, which is a good sign.

You will be happy to note that NDE 2023 will be conducted in Pune from 7th to 9th Dec, 2023. The theme for NDE 2023 is 'Transformative NDE: Unleashing the Power of Advanced Technologies'. We must agree that there cannot be a more apt theme than this in the presentscenario in industry and the emerging NDE 4.0. Our conference and exhibition has always beena spectacle of latest technology, and with this theme we can definitely expect much more.Without doubt, this would build our skills further and enhance our competence, leading to abetter us and advancing the nation further!

Prof. K. Balasubramaniam, President Elect ISNT,was elected as the Vice President of APFNDT during the meeting of APFNDT members in Melbourne on 2nd March 2023. With his leadership, ISNT will contribute a lot in international activities in the coming years.

The present issue is devoted to Infrared Thermography which is playing an important role in Detection and Characterization of defects. I am sure the readers will get a very good Insight on the latest trends in thermography in this issue.

I thank all authors, the editorial board, advertisers, and the whole team for releasing this issue in time, and request readers to share their feedbacks and suggestions.

Diwakar D. Joshi
President
president@isnt.in

MANAGING DIRECTOR TALK

BIKASH GHOSE

You now have in your hand the JNDE's first issue of the year 2023. This special issue on Infrared Thermography, edited by Dr. Ravibabu Mulaveesala, will be of much interest to you all. Many thanks to Dr. Ravibabu for bringing out the issue on time.

I welcome three new editors to the editorial board. From this issue onwards, ISNT-JNDE will regularly publish six research articles instead of four, along with the other regular features.

This special issue on Infrared Thermography presents six original research papers on "Pulsed Thermal NDT using the Concept of Equivalent Effusivity/Diffusivity Variations, Infrared Machine Vision, Barker-Coded Thermal Wave Imaging, Frequency Modulated Thermal Wave Imaging, ADR in Infrared Thermography and Passive Infrared Thermography for Concrete Structures".

The chapter activities section summarizes the activities conducted by various chapters in the last three months (Dec 2022 – Feb 2023). It also outlines the first physical NDE (NDE 2022) after the pandemic, conducted in Nov 2022. ISNT will conduct the next grand event, NDE 2023, at The Hotel Orchid in Pune during 7-9 Dec 2023.

My heartfelt thanks to all the advertisers and contributors of this issue who helped release the issue before time. One can now submit the original research articles to JNDE through the online portal of JNDE http://jnde.isnt.in.

Bikash Ghose
Managing Editor, JNDE
me.jnde@isnt.in

EDITORIAL TALK

DR. RAVIBABU MULAVEESALA

This volume of the Journal of Non-destructive Testing and Evaluation (NDT&E) contains research articles within the common denominator of Testing and Evaluation various materials using infrared thermography. This issue tried to demonstrate the breadth of applications for which one can use Thermal NDT&E (TNDT&E), together with very recent research developments, some clear demonstrations of the method at work in applications and some of the necessary background theory that underpins the basic signal, image and video processing methods commonly adopted for improved defection capabilities of subsurface defects.

The aim of this TNDT&E special issue is to provide a snapshot of state-of-the-art research from wide selection of key researchers involved in TNDT&E area from various research and academic institutes. Contributors have also been encouraged to submit high standard relevant articles that act as a review of their own work up to the current boundaries of their focused research specialization.

I am sure that the readers will find theissue as highly informativeand useful reference. Finally, I would like to thank all thecontributing authors for providing their valuable piece of research work to this issue. It has been a great pleasure to prepare this specialissue and hope that you will enjoy its reading.

Dr. Ravibabu Mulaveesala
Email: mulaveesala@sense.iitd.ac.in

CHAPTERS

CHAPTER Chairmen & Secretary

CHAPTER CHAIRMEN/SECRETARIES

Shri Hemant Kumar
Chairman– ISNT-Ahmedabad Chapter
Head – Reliability Static
CAB-1st Floor, SEZ Refinery,
Reliance Industries Ltd, VP-CES,
Jamnagar-361142, Gujarat, India,
(Off)+91 288 6621826 / Mobile:0'9998215033
hemantk.kumar@ril.com / hemant.ril2013@gmail.com

Shri Jayesh Prajapati
Secretary– ISNT-Ahmedabad Chapter
CEO, Ultratech Engineers, 28, N.K. Industrial Park Part-1,
Bakrol-Dhamatvan Road, Bakrol (Bujrang),
Ahmedabad-382430
Mobile: 9824396155
jayeshprajapati82@gmail.com

Shri Shashidhar P. Pallaki
Chairman- ISNT-Bangalore Chapter
CEO, Pallakki NDT Excellence Center
No-411, A, 4th Phase, Peenya Industrial Area
Bangalore – 560058 / Cell: 0'9448060717
pallakki@pallakkindt.com

Shri Prakash Balasubramanian
Hon. Secretary, ISNT-Bangalore Chapter
Mb:9845192860
prakash@sasthascientific.com

Shri RG. Ganesan
Chairman- ISNT -Chennai Chapter
"Chief Executive,
BETZ ENGINEERING & TECHNOLOGY ZONE,"
"Door # 21, Dharakeshwari Nagar,
1st Street, Sembakkam, "
Tambaram to Velacherry Main Road, .
Chennai – 600 073
Mb: 9840175179
rg_ganesan@yahoo.com

Shri P. Anandan
Hon. Secretary, ISNT-Chennai Chapter
Technical Manager & NDT Level-III
Scaanray Metallurgical Services, Plot C-12,
Industrial Estate, Mogappair West, Chennai – 600 037
Mb: 9884036985
ap@scaanray.com

Shri P. Murali
Chairman, ISNT- Coimbatore Chapter
Mb: 9443491823
murlinaveen@gmail.com

Shri A. Rathinam
Hon. Secretary, ISNT-Coimbatore Chapter
Cell:0'9843011031
everestndt@gmail.com
isntcoimbatorechapter@gmail.com

Shri Raj Kumar Singh
Chairman, ISNT-Delhi Chapter
Cell : 0'9312433853
rajinspection001@gmail.com

Shri F. Siddiqui
Hon. Secretary, ISNT-Delhi Chapter
541/2, Group-I, Hastal, Uttam Nagar,
New Delhi – 110059
Cell: 0'9811466220
isntdelhi@gmail.com / delhindt@yahoo.com

Dr S.K Jha
Chairman, ISNT Hyderabad Chapter
Chairman & Managing Director of Midhani
Mob: 9100033949
skjha@midhani-india.in

Dr Phani Surya Kiran
Secretary, ISNT Hyderabad Chapter
Mob:8106609567
kiranmps@gmail.com

Shri S Balamurugan
Chairman, ISNT- Jamshedpur Chapter
Head, Non-Destructive Testing & Sensors (NDT&S) Research Group
Research & Development Division, Tata Steel Limited
Jamshedpur 831001 / Ph: 0657 2648915
Mb:9204651390 / s.balamurugan@tatasteel.com

Shri Rohit Kumar Agrawal
Hon. Secretary, ISNT- Jamshedpur Chapter
Principal Researcher, Non-Destructive Testing & Sensors (NDT&S) Research Group
Research & Development Division, Tata Steel Limited
Jamshedpur 831001 / "PH: 0657 6648915
Mb:9897521586 / rohit.agrawal1@tatasteel.com

Shri S. Athmalingam
Chairman, ISNT Kalpakkam Chapter,
Associate Director, HSEG & Head - QAD
IGCAR, Kalpakkam - 603 102
Ph: 044-27480071/27480500 (Ext.23490)
Cell:0'9444501819
athma@igcar.gov.in

Shri M.V. Kuppusamy
Hon. Secretary, ISNT Kalpakkam Chapter
Head-QA Projects Section
Quality Assurance Division, SQ & RMG,
IGCAR, Kalpakkam 603 102
(Off) Phone:044-27480500 Extn. : 22388
Cell:0'8056090071
masikuppu@igcar.gov.in

Shri Sathyan V
Chairman, ISNT- Kochi Chapter
SM (Project), Bharat Petroleum Corp. Ltd. (Kochi Refinery)
PO Ambalamugal 682 302, Ernakulam, Kochi
0484-2822109 (O)
Cell:0'9446086345
sathyanv@bharatpetroleum.in

Shri Sibi Ignatius
Hon. Secretary, ISNT-Kochi Chapter
BPCL Kochi Refinery,
Ambalamugal 682302, Ernakulam, Kochi
Ph. No. 0484-2821121 / Cell:0'9446385611
sibiignatius@bharatpetroleum.in

Shri Dipankar Gautam
Chairman, ISNT- Kolkata Chapter
AB 121, Salt Lake, Kolkata – 700 064
Ph. No. 033 23581072
Cell: 98048 13030 / 98302 03223
dgautam1956@gmail.com / dipankargautam@yahoo.co.in

Shri Sreemoy Saha
Hon. Secretary, ISNT- Kolkata Chapter
No. 123 Ramlal Agrawal Lane
Megdoot Apartment, Block A, Flat 2B,
Kolkata 700050.
Cell: 9830291416
sreemoy4u@gmail.com

Shri S.K. Verma
Chairman, ISNT- Kota Chapter
NPCIL, PO - Anushakti,
Via - Kota (Raj) - 323 307
Cell:0'9413356402
surendrakverma@npcil.co.in

Shri Ranjeet Singh Rajpurohit
Hon. Secretary, ISNT Kota Chapter
Scientific Officer-E, -Quality Assurance Section
Rawatbhata Rajasthan Site, Unit 3&4
Nuclear Power Corporation of India
Ph. No. 01475-242052
Cell:9413358189
rsrajpurohit@npcil.co.in

Dr. P.P. Nanekar
Chairman–ISNT Mumbai Chapter
Head, Post Irradiation Examination Division
BARC, Trombay, Mumbai – 400 085
Off: 022-25594867 / 25564258
Cell: 0'9892161750
pnanekar@barc.gov.in / paritoshn@yahoo.com

Shri Samir K. Choksi
Hon. Secretary, ISNT - Mumbai Chapter
Choksi Imaging Ltd., 4 & 5, Western India House,
Sir P. M. Road, Fort, Mumbai- 400 001
Ph. No. 022-2610 1113 / Cell: 0'9821011113
Choksiindia@yahoo.co.in

Shri Jeevan Ghime
Chairman, ISNT-Nagpur Chapter
M/s. Becquerel Industries Pvt. Ltd.
33, Rushikesh Modern Co-op. Hsg. Society
Ingole Nagar, Wardha Road, Nagpur - 440005
Cell: 0'9822565879 / jeevan@biplndt.com

Shri Parag W. Pathak
Hon. Secretary, ISNT - Nagpur Chapter
M/s. NDT Solutions Saket - Pruthvi Appt
Plot No-. A+ B, Second Floor, Surendra Nagar, Nagpur - 440015
Cell: 0' 7709047371/ paragwpathak@yahoo.com

Shri Jayaprakash Hiremath
Chairman –ISNT Pune Chapter
C2, 301, Woodsville Phase 1,
Borhadewadi , Near Gail Pump
House, Moshi, Pune, Maharashtra, 412105
Mb: 9423569802
hiremath@tuv-nord.com

Shri Rahul Kulkarni
Hon. Secretary –ISNT Pune Chapter
C / O - KQSPL, Plot No. 55, Scheme
No. 4, Sector No. 4, Yamunanagar, Nigdi, Pune- 411044
Mb: 9822547797
hon.secretaryisntpune@gmail.com / rahul.kulkarni@kqspl.com

Shri B. Munirathinam
Chairman, ISNT Sriharikota Chapter
General Manager, QCCF, SPROB&SPP
Sriharikota – 524124
(Off) Phone:08623-225711
(Mobile):0'9490439735 / bmuni@shar.gov.in

Shri V. Rajasekhar
Hon. Secretary, ISNT Sriharikota Chapter
Chapter Sci/Eng.-SD, NDT, SPP,
SDSC – SHAR, Sriharikota – 524124
Off) Phone:08623-225923 / (Mobile):0'9989898932
rajasekhar.v@shar.gov.in /vrajasekhar55@gmail.com

Shri Vinay Thattey
Chairman, –ISNT Tarapur Chapter
Scientific Officer H+ and Training Superintendent ,
Tarapur Atomic Power Station -1&2 ,
Nuclear Power Corporation of India Limited
Type A-2/21, AnuShri Township, PO: TAPP,
TAL & DIST.: PALGHAR, PIN -401 504, MAHARASHTRA STATE,
Cell: 9423982722 / vthattey@npcil.co.in

Shri S. K. Acharya
Hon. Secretary –ISNT Tarapur Chapter
Scientific Officer, Tarapur Atomic Power Station 1&2 ,
Nuclear Power Corporation of India Limited
Type A-2/21, AnuShri Township, PO: TAPP,
TAL & DIST.: PALGHAR, PIN -401 504, MAHARASHTRA,
Cell: 8552000192
skacharya@npcil.co.in /skacharya17@gmail.com

Dr. T Gurunathan
Chairman, ISNT -Trichy Chapter,
General Manager/Quality & BE,
BHEL/Trichy, Tamilnadu, PIN-620014
Mobile: 9442627082 /Ph-0431-2575877
tguru@bhel.in

Shri H. Nikhil
Hon. Secretary, ISNT-Trichy Chapter
Deputy Manager/ATP-NDTL Quality
BHEL, Trichy, Tamilnadu, Pin-620014
Mb:9489320982
hnikhil@bhel.in / trichy@isnt.in

Dr. Mohan Kumar L
Chairman-ISNT- Trivandrum Chapter
GENERAL MANAGER, ROCKET PROPELLANT PLANT,
VSSC, ISRO P.O. THIRUVANANTHAPURAM, PIN – 695 022
Ph. No. 0471-256 3822 (O)
Mob. No. 94461 77376
l_mohankumar@vssc.gov.in / lmkdrn@yahoo.com

Shri Girish N Namboodri
Hon. Secretary, ISNT- Trivandrum Chapter
SCI/ENGR SE, NDTF/RPP,
VSSC, ISRO P.O. THIRUVANANTHAPURAM-PIN – 695 022
Ph. No. 0471-256 2599/3340
Mob. No. 75618 39768
girish.nampoothiri@gmail.com / isnttvm@gmail.com

Shri R. Venkatasubramanian
Chairman-ISNT-Vadodara Chapter
"C/o Industrial X-Ray and Allied Radiographers India Pvt. Ltd.,"
C-17 / 78, Krishana Industrial Estate,
Opposite to BIDC, Gorwa,
Vadodara – 390 016 Gujarat, India
(O) 0265 – 2280756 / Mb: 9825244941
rmani1511@gmail.com / chairmanisntvc@gmail.com

Shri Kashyap Niranjan Bhatt
Hon. Secretary, ISNT - Vadodara Chapter
Rushikesh Engineering Resources
306, Vrajsiddhi Tower, Market Char Rasta,
Rajmahel Road, Vadodara: 390001
GUJARAT, INDIA.
(Mb:) 9825245886
info@rushikeshengg.com / secretaryisntvc@gmail.com

NGC/NCB

NGC/NCB Members

NATIONAL GOVERNING COUNCIL (NGC)

1. **Shri Diwakar D. Joshi**
   President
   Mb- 9822263475
   president@isnt.in

2. **Dr. Krishnan Balasubramaniam**
   President Elect
   Mb: 9840200369
   balas@iitm.ac.in

3. **Dr. Jaiteerth R. Joshi**
   Vice President
   Mb: 9440049272
   joshidrdl@gmail.com

4. **Shri Rajul R. Parikh**
   Vice President
   Mb: 9820192953
   rajulparikh@eecindia.com

5. **Dr. M.T. Shyamsunder**
   Vice President
   Mb: 9880508266
   mandayam.shyamsunder@gmail.com

6. **Shri Bikash Ghose**
   Hon. Gen. Secretary
   Mb: 91 9890127524
   secretary@isnt.in

7. **Shri R. Vivek**
   Hon. Jt. Secretary
   Mb: 9840023015
   vivek@electromagfield.com

8. **Shri Nerurkar K.A**
   Hon. Treasurer
   Mb: 9822525518
   treasurer@isnt.in

9. **Shri S. Viswanathan**
   Hon. Co-Treasurer
   Mb: 9894945482
   viswa@igcar.gov.in

10. **Dr. B. Venkatraman**
    Immediate Past President
    Ph: (Off) 044-27480240
    qadbvr@gmail.com

11. **Dr. R.J. Pardikar**
    Past President
    Cell: 9003096843
    r.j.pardikar@gmail.com

MEMBERS

12. Shri Anil V. Jain
13. Shri Anandan. P
14. Balamurugan. S
15. Shri V. Deepesh
16. Shri Dharmveer Singh
17. Shri R.G. Ganesan
18. Prof. S. Gopalakrishnan
19. Shri S. Hari Krishna
20. Shri P. Mohan
21. Shri Mukesh Arora
22. Ms. Menaka. M
23. Ms. Navita Gupta
24. Shri Bhausaheb Krishnaji Pangare
25. Shri Partha Pratim Brahma
26. Dr. Ravibabu Mulaveesala
27. Shri Ravindran S.R
28. Shri Sadasivan. N
29. Shri Samir K. Choksi
30. Shri Shashidhar Pallaki
31. Shri M. S. Shendkar
32. Shri Uday Kale
33. Shri Umakanthan Anand
34. Shri R. Venkatasubramanian
35. Shri M.N.V. Viswanath
36. Shri G. Surya Prakash (Co-opt)
37. Shri Raja Narendra Mallampati (Co-opt)

Permanent Invitee:

38. Shri G. Ramachandran

PAST PRESIDENTS

39. Shri V.R. Deenadayalu
40. Shri K. Balaramamoorthy
41. Shri A. Srinivasulu
42. Shri K. Viswanathan
43. Shri S. I. Sanklecha
44. Shri Dilip P. Takbhate
45. Dr. P. Kalyanasundaram
46. Shri V. Pari
47. Shri D.J. Varde

ALL CHAIRMAN/SECRETARY OF CHAPTERS

EX-OFFICIO MEMBERS

48. Dr. P. P. Nanekar, Chairman, NCB
49. Shri V. Manoharan, Chief Controller of Exams
50. Prof. Krishnan Balasubramaniam,
    President, QUNEST Fdn.

NATIONAL CERTIFICATION BOARD (NCB)

1. **Dr. Paritosh P. Nanekar**
   Chairman, NCB
   Bhabha Atomic Research Centre
   Chairman.ncb@isnt.in

2. **Shri M.V. Kuppusamy**
   Hon. Secretary, NCB
   Indira Gandhi Centre for Atomic Research
   secretary.ncb@isnt.in

3. **Shri V. Manoharan**
   Chief Controller of Examinations, NCB
   Principal Technologist
   VisiConsult-X-Ray Systems & Solutions
   coe.ncb@isnt.in

4. **Shri S. Viswanathan**
   Hon. Treasurer, NCB
   Indira Gandhi Centre for Atomic Research
   treasurer.ncb@isnt.in

MEMBERS

5. Shri G.V. Shiva Rao, DRDL, Hyderabad
6. Shri A.K. Das, National Thermal Power Corporation Ltd.
7. Shri S. Ramakrishnan, Brakes India Ltd.
8. Shri Umakanthan Anand, Reliance Industries Ltd.
9. Shri Tushar Mukherjee, Reliance Industries Ltd.
10. Shri Anand Bagdare, Godrej & Boyce Mfg. Co. Ltd.
11. Shri Sathyan. V, BPCL Kochi Refinery
12. Shri Sanjay Narang, Larsen & Toubro Ltd.
13. Shri Raghvendra. P, Larsen & Toubro Ltd.
14. Shri Muraleedharan Nair, IRClass, Indian Register of Shipping
15. Shri Jayaprakash Hiremath, TUV India Pvt. Ltd.
16. Shri Uday Kale, KUB Quality Services Pvt. Ltd.

POTENTIAL NCB AUTHORIZED EXAMINATION CENTER

17. Shri R.G. Ganesan, ISNT Chennai Chapter
18. Shri N. Sadasivan, ISNT Mumbai Chapter
19. Ms. Navita Gupta, Satyakiran School for NDT, Delhi

EX-OFFICIO MEMBERS

20. Shri Diwakar D. Joshi,
    President, ISNT
21. Prof. Krishnan Balasubramaniam,
    President-Elect, ISNT
22. Shri Bikash Ghose,
    Hon. Gen. Secy., ISNT
23. Dr. B. Venkatraman,
    Immediate Past President, ISNT

23\. Dr. M.T. Shyam Sunder,
    Chairman-Training Management Board -ISNT

24. Shri Partha Pratim Brahma,
    Controller of Authorisation -ISNT

ARORA

Arora Technologies (P) Limited

MaNufacturing | Distribution | AuTomation

AUL SERIES

Manufacturing of NDT Products

- LED UV Lamps
- UV/White Light Meter
- Yokes | Power Pack | Bench Machine
- MPI/LPT Chemicals & Accessories
- UT Probes | Cables | Couplant
- LED Film Viewer & Densitometer

Distribution of NDT Solutions

- Ultrasonic Installed Sensors
- PAUT/TOFD Equipments
- Eddy Current Equipments
- Wire Rope Tester
- Remote Visual Inspection (RVI)
- Digital Radiography

ECTANE 3

NORDISCAN-PL

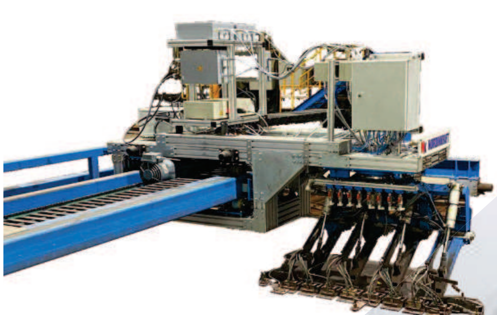

Automated NDT Systems

- Magnetic Particle Inspection Systems
- Eddy Current & Ultrasonic Rotating Systems
- Ultrasonic Systems
  - Off-line Ultrasonic Examination of Plates
  - In-line Ultrasonic Systems for Ferrous/Non-Ferrous, Plates, Ingots, Bars and Billets, Pipes, Rails
  - Systems for Automatic Non-Contact Detection of Hard Spots
  - Plate Surface Cleaning System
- Radiography Systems

Plot No. D-183/8, MIDC, TTC Nerul, Navi Mumbai, Maharashtra 400706, India.

info@arorandt.com www.arorandt.com +91 22 6138 0600

CHAPTER ACTIVITIES For the period from Dec 2022 to Feb 2023

AHMEDABAD

Annual General Meeting on 18/02/2023.

BENGALURU

Courses & Exam. Conducted :

ISNT Bengaluru Chapter conducted 5 days hybrid mode Training programme RTFI (Radiographic Film Interpretation) at premises of Pallakki NDT Excellence Center Pvt. Ltd, Bengaluru during 19 to 24 January 2023. Total 16 Participants were attended from Nuclear Power Corporation, Ordnance Factory, ASME U Stamp Fabricators and NDT service providers.

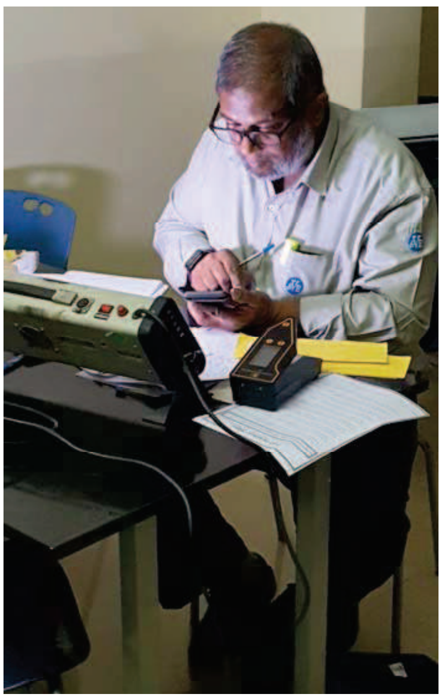

CHENNAI

Courses & Exam. Conducted :

Radiographic Testing Level-II course and examination was held on 14th December 2022 to 24th December 2022. Number of candidates attended the course was 9 and examination was 11.

Surface NDT MT & PT Level-II course and examination was held on 19th January 2023 to 28th January 2023 Number of participants attended the course course and examination was 11.

Ultrasonic Testing Level-II course and examination was held on 31st January 2023 to 11th February 2023. Number of candidates attended the course and examination was 13.

Technical Talk:

Advanced Phased Array UT: Basics to Applications with Demo" by Prof.Krishnan Balasubramanian, Institute Professor – IITM Chennai and Mr.Cyril Thibault, AOS and the Phased Array Company Nantes, France on 30.11.2022 at IITM, Chennai

Other Activity:

EC Meeting was held on 13th November 2022

EC Meeting was held on 18th December 2022

EC Meeting was held on 29th January 2023

Flaw-Guide®

NDT Products

(Manufactured By Pradeep Group of Industries)

Contact Address : 707, Lodha Supremes Bldg.1, Road 22, Wagle Estate, Thane 400604 (India)
Email : sales@pradeepndt.com **Tel.Nos 91 22 25836001 / 2 / 3 Website** www.pradeepndt.com

7th E-Newsletter – Sound Bytes were released on 13th January 2023.

ISNT Chennai Chapter received the Best Chapter Award for the year 2022 during the inaugural function of NDE 2022 on 24.11.2022 at “Mahatma Mandir Convention and Exhibition Center (MMCEC), Gandhinagar, Gujarat, India, at Gujarat.

20th January 2023 was a red letter day for ISNT Chennai Chapter. Since it was on that day that a MOU was signed at Anna University between Anna University & ISNT Chennai Chapter by the vice chancellor of Anna University and the Chairman of ISNT Chennai Chapter in the presence of dignitaries of Anna University and representatives from ISNT Chennai Chapter.

The MOU shall be valid for 3 years and can be extended by mutual consents.

S. No.	Month	Course Code	Courses	Training Period		Exanunation Date	course Fees Rs.	Last date of receipt of application form
				From	To			
1.	April	ST-2301	Surface NDT Level-II (MT & PT)	26.04.23	03.05.23	05.05.23 & 06.05.23	12,500/ -	21.04.2023
2.	May	UT-2302	Ultrasonic Testing Level-II	16.05.23	24.05.23	26.05.23 & 27.05.23	15,000/ -	10.05.2023
3.	Jtme	RT-2303	Radiographic Testing Level-II	14.06.23	21.06.23	23.06.23 & 24.06.23	14,000/ -	09.06.2023
4.	July	VT-2304	Visual Testing Level-II	03.07.23	06.07.23	08.07.23	7,500/ -	27.06.2023
5.	July	ST-2305	Surface NDT Level-II (MT & PT)	20.07.23	26.07.23	28.07.23 & 29.07.23	12,500/ -	14.07.2023
6.	August	ET-2306	Eddy Current Testing Level-II	07.08.23	16.08.23	18.08.23 & 19.08.23	20,000/ -	01.08.2023
7.	August	UT-2307	Ultrasonic Testing Level-II	22.08.23	30.08.23	01.09.23 & 02.09.23	15,000/ -	15.08.2023
8.	September	LT-2308	Leak Testing Level-II	04.09.23	15.09.23	16.09.23	22,000/-	29.08.2023
9.	October	RT-2309	Radiographic Testing Level-II	04.10.23	11.10.23	13.10.23 & 14.10.23	14,000/ -	29.09.2023
10.	November	ST-2310	Surface NUT Level-II (MT & PT)	16.11.23	22.11.23	24.11.23 & 25.11.23	12,500/-	10.11.2023
11.	December	UT-2311	Ultrasonic Testing Level-II	12.12.23	20.12.23	22.12.23 & 23.12.23	15,000/ -	07.12.2023
12.	February	RT-2312	Radiographic Testing Level-II	31.01.24	07.02.24	09.02.24 & 10.02.24	14,000/ -	26.01.2024

Important Note: All courses, examinations and Certifications are based on IS 13805 (NCB) Prevailing Examination fee for IS 13805 (NCB) scheme is Rs.5,000/- plus GST, same shall be paid directly to NCB. Link for making this payment will be shared / provided including registration.

Multiple applications
Research & Development
Corrosion Mapping
Immersion Tanks
Weld Inspection
With Scanners
& Crawlers
& Robots
Explorer 128/ 128
Probe connector
EXPLORER
INTEGRATION MADE EASY
for all inspection systems
contact@tpac-ndt.com
TPAC
Explorer 64/128
HIGH PERFORMANCE & SPEED PHASED ARRAY & FMC/TFM

The salient points are:

1. To conduct research pertaining to NDT jointly by both the parties for the benefit of the country as a whole.
2. Application oriented projects on NDT for industrial sector to be undertaken by the students.
3. The training courses, programs, conferences, workshops and lectures on NDT shall be executed jointly with Anna University.
4. To focus on the syllabus of the related subject and make NDT as a subject in verticals.
5. To provide consultancy services in the areas of NDT for public and private organization.

Members present: S/Shri. RG. Ganesan, Chairman, ISNT CC, K. Viswanathan, Past President, G. Ramachandran, Advisor, B. Ram Prakash, Advisor, R. Balakrishnan, Chairman Elect, P.Anandan, Hon. Secretary, A. R. Parthasarathy, Hon. Treasurer, and EC Members P.N. Udayasankar, R. Jayagovindan, Prof. Dr. S. Sathiyamurthy, Prof. Dr. S. Balasivanandha Prabhu, Prof. Dr. Rajendra Boopathy

ISNT Chennai Chapter - Course Calendar for 2023-2024

SOUND BYTES

Decibel 22
Frequency 4
December 2022 issue
Email ID: soundbytesisnt@gmail.com

Official Newsletter of ISNT Chennai Chapter

Beyond the Boundaries Created (continued).

Dear Members,

We are glad to contact you all through this wonderful mouth piece once again. If you recollect in the best issue of SB we had probed the mind of our chairman to fathom his version of vision for ISNT CC for the next two years.

Though he is the captain of this ship of ours, to convert his navigational skills into reality we need an able chief engineer. We have one such as our Shri. P.Anandan. So this time SB tied up to meet with him and collate information regarding the steps taken to transform the vision to mission.

Following is the excerpt

S.B: Greetings from SB to you, Secretary. Chairman unfolded a grandiose plan for our chapter in the next two years. Is it possible to go through each step to inform the members about the road map drawn? Let us go one by one.

P.A: A committee has been formed for propagating & promoting SB. The committee is as follows:
Publication & Award Committee-PWC
Mentor : Mr. G.R.Ramachandran, Chairman : Mr.B. Ram Prakash
Members: 1) Mr R G Ganesan, 2) Mr P Anandan, 3) Mr Parthapratim Brahma, 4) Dr Prabhu Rajagopal, 5) Dr Balasivanandha Prabu 6) Mr R Balakrishnan

The responsibilities of the committee are to ensure that it compiles articles from authors (both members & non members), scout for advertisers and publish the newsletter quarterly. The committee can add more members as they deem it fit.

S.B: We welcome the members on board and wish to emphasize that we need more young blood (especially from the student community) to perpetuate the publication. Next in line is Training & Certification. Can you elaborate on the action plan?

P.A: For this important field of our activities yet another committee has been formed as follows:
Training Management Committee-TMC
Mentor : Mr.K.Viswanathan Chairman : Mr.S.R.Ravindran
Member s: 1) Mr C Srinivasan, 2) Mr K Subramaniam, 3) Mr Chockalingam, 4) Mr R Subbaraman, 5) Mr A Vimal Raj, 6) Mr S Velumani, 7) Mr S Saravanan - KKNPP.

This committee's responsibilities will be to guarantee that the course notes, specimens for practical and the required appropriate equipment are made available to make our training comparable to world class. Hence the group is a strong one in the field of practicing NDT.

S.B: Excellent. We are with you & them. But the path is a tough one and needs continuous improvements in all the areas of training cooperation of all involved is invited. Next is academics.

P.A: The committee for Research & Technical Management Committee - RTMC
Mentor : Dr. Krishnan Balasubramaniam Chairman : Dr. Prabhu Rajagopal
Members: 1) Mr R Vivek, 2) Mr Dharmaraj, 3) Mr P N Udhayasankar, 4) Mr K S Lakshmanan, 5) Mr Kasi Viswanthan

Indian Society for Non-Destructive Testing , Chennai Chapter
Module 59, 3rd floor, Readymade Garment Complex, SIDCO Industrial Estate, Guindy, Chennai 600 032.
Phone 044-45532115, 7200086075.

MUMBAI

Courses & Exam conducted

MPT Level II was conducted at NPCIL from 28th Nov - 02nct Dec ,22 for 16 nos.candidates. LPT Level]] was conducted at NPCIL from 05th Dec - 10th Dec, 22 for 20 nos. of candidates.

Technical Talk

21th Jan 2023,

Topic - Flaw Detection and Characterization in tubes using Eddy Current Testing by Shri. Arbind Kumar

18th Feb 2023,

Topic - NDT: Risk & Cognetive Biases by Mr. Santosh Gupte.

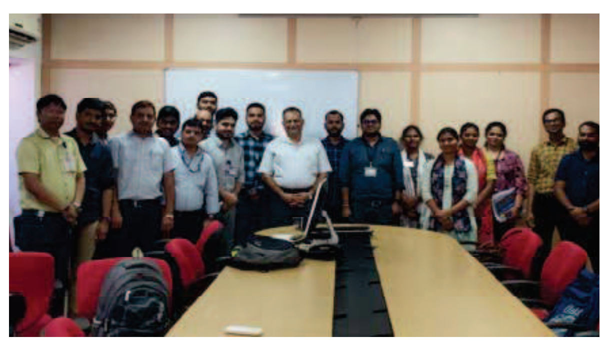

PUNE

Other Activities :

EC meeting No. 8 Conducted on dated 03.12.2022

EC Meeting No. 9 will be conducted on dated 25.02.2022

KOTA

Course & Exam

Re-examination of Ultrasonic Testing level- II (13.12.2022).

Practical examination for recertification of NDT certificate (PT-L-II & ET-L-II) (15.12.2022).

Technical Talk :

Line management training on Visual Inspection of pressure tube rolling to QA engineers and Supervisors. (16.01.2023 to 17.01.2023)

Other Activity

Executive Body Meeting on 12.12.2022

KOLKATA

Course & Exam

Level-II Training Course as per IS-13805 in Ultrasonic Testing was conducted during 27th

January, 2023 – 10th February, 2023. Total 7 (Seven) candidates attended the course & appeared in exam.

2 EC Meetings were conducted.

TARAPUR

Course & Exam

Visual Testing level II training program was held on 06.02.2023 and examination was conducted on 11.02.2023. Total 24 candidates were participated during the program.

Technical Talk

Chapter conducted technical demonstration on videoscopes in association with M/s Maarg Technologies, Mumbai and were demonstrated all the available equipment's and elaborated its application. They also presented the technical specification through power point presentation.

Other Activity

During the year total 04 EC meetings was held for different activity of the chapter. Chapter has prompted the activities and total 06 new members were enrolled as a life member.

ISNT Tarapur conducted its 27th AGM on 20.11.2022 at WANO Hall,NPCIL Tarapur Guest House Advisor Shri A.B. Deshmukh, Site Director, TMS, Shri. S.M. Mulkalwar, Station Director, Tarapur Atomic Power Station 1&2 along with Shri. R Murali, Chief superintendent of Tarapur Atomic Power Station 1&2, Tarapur also present during AGM.

New executive committee taken over and Shri R. Murali elected as a Chairman, Shri Nagendra kumar as an Hon. Secretary and Shri Chetan Mali as an Hon. Treasurer.

Chapters E bulletin, 5th issue inaugurated during AGM by Advisor Shri. A.B. Deshmukh, Site Director, TMS.

Welcome to Shri. A.B.Deshmukh, Site director, Tarapur Maharashtra Site, NPCIL by Treasurer during Inauguration of VT level II training programme

Welcome to Shri. S.M.Mulkalwar, Station Director, Tarapur Atomic Power Station 1&2, NPCIL by secretary during Inauguration of VT level II training programme

Welcome to Shri. R.Murali, Chief superintendent and chairman, Tarapur Atomic Power Station 1&2, NPCIL by EC member during Inauguration of VT level II training programme

Introduction of participant during VT level II training programme


Practical demonstration to all candidates during VT level II training programme


Videoscope practical demonstration to participants during VT level II training programme


Videoscope practical demonstration to participants during VT level II training programme


Practical demonstration & presentation by M/s MARRG technologies during VT level II training programme


Participation certificate distribution by chairman & secretary during VT level II training programme


Participation certificate distribution by chairman & secretary during VT level II training programme


Lecture by chairman Shri. R.Murali during VT level II training programme


Prof. K. Balasubramaniam, Chairman Organsing committee along with Co chairman Shri. N.K.Roy and Treasurer Shri. Chetan Maliin NDE 2022

ISNT EC members in 27th Annual General Body Meeting

Advisors in 27th Annual General Body Meeting

TRICHY

Course and Exam

BARC Training Cum Certification Course on Radiation Safety for Industrial Radiographer

First Batch (37 Candidates) 28.11.2022 – 09.12.2022

Second Batch (40 Candidates) 30.01.2023 – 10.02.2023

Technical Talk

- 06-12-22 The Future of Entrepreneurship - Covid & Beyond
- 13-12-22 Energy Conservation DAY Theme: Contribution of Solar Energy for Energy conservation.
- 18-12-22 SOFT SKILLS FOR SUCCESS
- 27-12-22 Materials for Additive Manufacturing: Recent Trends and Processing Issues.
- 03-01-23 E-Vehicle Technology
- 10-01-23 Information Technology Advancements
- 13-01-23 Road Safety Week 2022 -theme -Save Yourself to Save Your Family.
- 17-01-23 Latest Techniques in Building Construction (Autoclaved Aerated Cement Blocks and binders.
- 24-01-23 Thermal Insulation System.
- 31-01-23 Power Sources for Welding
- 07-02-23 Electric Vehicle Systems - An Insight

Other Activity

EC Meeting conducted:

1. 09.12.2022
2. 02.01.2023

Membership addition

1. 15 Life Members
2. 1 Associate member

Annual General Body Meeting conducted on 05.02.2023

Next EC Meeting Planned: 20-02-2023 @ 05:45PM

VADODARA

Course and Exam

At the request of NCB, Basic examination for NDT Level III certification for two candidates were organized by ISNT Vadodara Chapter on 21-February-2023.

Other Activity:

ISNT Vadodara Chapter has successfully completed two days workshop on Phased Array Ultrasonic Testing at M/s. Gujarat Narmada Valley Fertilizers & Chemicals Limited, Bharuch on 21st and 22nd February 2023.

The workshop covered both - theory and practical demonstration.

Mr. R. Venkatasubramanian, Mr. Krutik Shah and Mr. Kashyap Bhatt were faculty members from ISNT Vadodara Chapter.

Total 20 candidates from GNFC actively participated in the workshop with good interaction between faculty members and participants.

The workshop found highly useful to all participants for their plant inspection activities. Very good appreciation received by ISNT Vadodara Chapter for organizing the workshop.

HYDERABAD

Technical Talk

One day National Workshop on "Non destructive Testing and Evaluation," on 4th March, 2023 at Government City College, Hyderabad.

Other Activity:

EC Meeting on 10th March, 2023

TRAINING MANAGEMENT BOARD

TRAINING MANAGEMENT BOARD

Office Bearers:

Dr. M.T. Shyamsunder, Chairman
Mr. S. Harikrishna, Hon. Secretary
Mr. Partha Pratim Brahma, Controller of Authorisation

Members :

Ms. Navita Gupta
Mr. N. Sadasivan
Mr. Mincheri Ravi
Mr. Thamanna Ravikumar
Mr. M. Manimohan
Mr. Arbind Kumar
Mr. Chintamani Khade
Mr. R.V.S. Mani
Mr. Anandan Pari
Dr. R.J. Pardikar
Mr. V. Pari

Ex-Officio Members :

President, ISNT
President Elect, ISNT
Hon. Gen. Secretary, ISNT
Hon. Treasurer, ISNT
Immediate Past President -ISNT
Chairman –NCB
Chief Controller of Exams –NCB

Training Management Board (TMB) – ISNT

Over the last three decades, the training and certification activities of ISNT have been coordinated mainly by the National Certification Board (NCB) of ISNT, especially for the IS 13805 scheme, where BIS had authorized ISNT to be the sole body for this purpose. With NCB-ISNT getting formal accreditation by NABCB in accordance with ISO 17024 for initiating a new scheme based on ISO 9712 and having an international reach in the name of International Certification in NDT (ICN), it also became imperative that the training and the certification activities have to be operated independently to avoid conflict-of-interest and confidentiality issues. In view of this, ISNT has decided to form a Training Management Board (TMB) with the below-given objectives and scope,whose sole responsibility would be to manage all the training related activities and policies for the certification schemes of ISNT.The National Governing Council (NGC) of ISNT has formally approved the formation of TMBin the meeting held on 29th January 2022, and it was put in place immediately thereafter with a set of 15 members and 7 Ex-Officio members.

Objectives of TMB

Training

- Standardize and Harmonize the Content, Quality and Delivery of Training courses (leading to certification) being conducted by any authorized entity under the ISNT banner
- Key focus on Level 1, 2 and 3 certification courses being conducted by ISNT Chapters and Other Institutes
- Act as a nodal agency for addressing all NDT/Inspection related special Training needs of the Indian industry

Authorization of Training Centre's

- Streamline and create a Robust process to establish Authorized Training Centres (ATC) for IS13805 and ICN across the country (and abroad if needed) to help spread ISNT's schemes more widely

Scope

- Training activities related to IS13805 certification
- Training activities related to ICN certification
- Any Special Training programs of interest and relevance to be organized by ISNT based on current trends OR on request from Industry to help spread NDE Science and Technology across the country
- Developing, implementing and executing the method and process of Authorizing Training Centre's for both IS 13805 and ICN
- Establishing a self-sustaining model for revenue generation for continued operations and growth of TMB

PROGRAM FORMULATION AND MANAGEMENT BOARD

PROGRAM FORMULATION AND MANAGEMENT BOARD (PFMB)

I wish to inform you that the Program Formulation and Management Board of ISNT (PFMB) has been constituted with Shri V. Manoharan as the Chairman, Dr. Deepesh Vimalan as Hon. Secretary and 14 technology/industry experts as members of the board.

PFMB has formed 4 technology groups –Radiological Imaging, Electromagnetic NDE, Thermal Imaging, and Acoustic NDE and Chairman for each working group were identified.

Office Bearers

Shri V. Manoharan, Chairman

Shri Deepesh Vimalan, Hon. Secretary

Members :

Dr. S. Thirunavukkarasu	Prof. Kavitha Arunachalam	**Ex-Officio Members**
Mr. A.K. Das	Mr. P. Vijayaraghavan	Mr. Diwakar D. Joshi, President -ISNT
Dr. Phani Suryakiran	Prof. Ravibabu	Mr. Bikash Ghose, Hon. Gen. Secretary -ISNT
Mr. Bhausaheb Pangare	Mr. Komma Reddy Vamshi	Mr. Kalesh Nerurkar, Hon. Treasurer ISNT
Dr. Arumugam. M	Dr. Debasish Mishra	**Invitees**
Prof. Prabhu Rajagopal	Mr. Umankanthan Anand	Dr. Paritosh Nanekar, Chairman-NCB
Dr. Menaka	Dr. Ramadas Chennamsetti	Dr. M.T. Shyamsunder, Chairman -TMB

Objectives

The main Objectives of PFMB are as follows:

- To conceptualize, formulate and organise various non-certification programs such as Webinars, Workshops, Conferences, Seminars etc. to create platform for constant interaction with ISNT members, meet the requirement of industry, academia and research community.
- To interact with other international NDT societies, National technical societies to formulate and organise joint programs.

Scope

- To plan and organise two annual conferences of maximum 2 days' duration (other than NDE) and execute through an organizing committee nominated by PFMB
- To conceptualize, formulate and execute programs such as Webinars, Workshops, Conferences, Seminars etc. of relevance to the NDT community to be organised by ISNT throughout the year across the country.
- To publicize the proposed program
- Develop and implement mechanism for executing the programs along with ISNT Chapters or independently (only if no chapter is interested).
- Create various topical working groups within PFMB and formulate programs as stated above for meeting specific requirement.
- To connect with various industries / institutes and formulate program to meet the specific needs
- Interact with international NDT societies (ISNT partner societies with MOUs) for conducting joint programs, predominantly Webinars
- Interact with national technical societies for conducting joint programs
- Establishing a model for sustained revenue generation for continued operations and growth of PFMB

Themes for the Special Issues of Journal of Nondestructive Testing and Evaluation (JNDE)

The issues of Journal of Non Destructive Testing and Evaluation (JNDE) are published quarterly and the special issues are focused on specific theme. Each of the special issue features articles and research papers on the latest developments and advancements in the specific theme.

For the current special issue, the theme is "Infrared Thermography". The issue editor for this issue is Dr Ravibabu Mulaveesala, who is a leading expert in the field of IR NDT. He has curated a selection of articles that highlight the latest advancements in this area.

In the same line, the upcoming special issues will feature leading experts as issue editors who will select articles and papers on the following different themes that will be of great interest to researchers, practitioners, and industry professionals alike.

Issue	Theme	Issue Editor
June 2023	Radiological NDE	Dr Debashish Mishra, GE Research
September 2023	NDE of Civil Infrastructure	Dr Surendra Beniwal, IIT Jammu Dr Debdutta Ghosh, CBRI-CSIR
December 2023	NDE 4.0	Dr Shyamsunder Mandayam, Azareri Pvt Ltd

Interested authors are requested to submit articles in these areas by visiting the online portal of the journal at https://jnde.isnt.in/index.php/JNDE/about/submissions. Authors need to register with the journal prior to submitting or, if already registered, can simply log in and begin the five-step process to submit article. The submissions are accepted throughout the year.

NDE 2022

Report of Annual Conference and Exhibition on NDE (NDE 2022)

The annual flagship event of the Indian Society for Nondestructive Testing (ISNT), "Conference and Exhibition on NDE (NDE 2022)," was conducted in physical form after a gap of three years from 24th - 26th November 2022 at the Mahatma Gandhi Convention and Exhibition Center (MMCEC), Gandhinagar, Gujarat. The conference was held in the state of Gujarat after long years. The Inaugural function of the conference was held on 24th November 2022. Shri Nilesh M Desai, Distinguished Scientist & Director, Space Application Center-ISRO was the Chief Guest; Shri Manish Kumar Srivastava, Executive Director (Engineering) from National Thermal Power Corporation (NTPC) & Shri Umakanthan Anand, Reliance Industries were the Guests of Honours for the inaugural function. Dr Sajeesh K Babu, Chairman ICNDT was the special guest for the inaugural function of NDE 2022. Prof. Krishnan Balasubramaniam, Chair Professor IIT Madras was the Chairman and Bikash Ghose, Group Director of HEMRL, DRDO was the convener of the conference.

More than 550 participants attended the conference, represented by various Service and Manufacturing Industries, Academia, NDE Entrepreneurs, R&D Institutions from Space, Defence, Atomic Energy, Power, Railway etc. A special session on Career Opportunities was organised exclusively for the students. Shri V Manoharan moderated the session, and Prof Vishesh Badheka from PDEU led the same. A special session on NDE 4.0 was organised by Dr Ripi Singh and was moderated by Dr Shaymsunder Mandayam. JNDE special issue of December 2022 on NDE 4.0 was released on this occasion. For the first time, an Industrial session on "Challenges for NDE for Power Sector" was organised and was led by Shri A K Das from NTPC. Shri Umaknathan Anand from Reliance Industries led an interactive session on NDE for Oil and Gas. Three NDE Conference tutorials were held on online mode on 3rd & 4th Dec 2022. There were two Memorial talks, four Plenary talks, and more than 34 invited talks were delivered in the conference. More than 150 papers were presented in 32 sessions spread over three days by the researchers working in the different areas of NDE. Dr Ravibabu Mulaveesala & Dr Phani Mylavarapu have spearheaded the technical committee of the NDE conference, and Dr Deepesh Vimalan spearheaded the Pre-Conference Tutorial. Dr Baldev Raj memorial talk was delivered by Dr Ripi Singh, and Dr Komal Kapoor from NFC has delivered the Rameshbhai Parikh memorial talk.

About 57 national and international exhibitors showcased their products in the exhibition. M/s Evident Olympus was the Principal Sponsor of the Conference. M/s Reliance Industries, M/s TATA Steel, and M/s Bharat Forge have supported the event as non-exhibition sponsors. M/s Fuji Film was the Diamond Sponsor whereas M/s Blue Star and M/s EECI were the Gold Sponsors under the exhibition category.

NDE 2022, another landmark event from ISNT in the annual series, was back in physical form after a gap of three years and has ensured fulfilling experiences of all delegates, speakers, invitees, and exhibitors on all fronts.


Reliance
Industries Limited
FUJIFILM
TATA STEEL
Thank You


EVIDENT
OLYMPUS
Reliance
FUJIFILM
TATA STEEL
NDE 2022
NOV 24-26, 2022 • GANDHINAGAR
Conference & Exhibition on
NON DESTRUCTIVE


Exhibition on
TRUCTI
ATION
GOLD
A STEEL
Tomorrow
BLUE
INDUSTRIAL S
ndtt


NDE 2022
NOV 24-26, 2022 • GANDHINAGAR
ISNT
Conference & Exhibition on
NON DESTRUCTIVE
EVALUATION
EVIDENT
OLYMPUS
Reliance
FUJIFILM
TATA STEEL


EVIDENT
OLYMPUS
Reliance
Industries Limited
FUJIFILM
TATA STEEL


EVIDENT
OLYMPUS


NON DESTRUCTIVE EVALUATION
EVIDENT


NDE 2022
OLYMPUS
FUJIFILM


NOV 2022
GANDHINAGAR, GUJARAT
OUR SPONSORS
PRINCIPAL
EVIDENT
OLYMPUS
PLATINUM
Reliance
Industries Limited
DIAMOND
FUJIFILM
Value from Innovation
GOLD
BLUE STAR
TATA STEEL

Pulsed Thermal NDT of Material Discontinuities by Using the Concept of Equivalent Effusivity/Diffusivity Variations

A.O. Siddiqui[1a], Y.L.V.D. Prasad[1], V.P. Vavilov[2], D. Yu. Kladov[2]

[1]Advanced Systems Laboratory, Kanchanbagh P.O., Hyderabad 500058
[2] National Research Tomsk Polytechnic University 634050 Tomsk, Lenin Av., 30, Russia
[a]*Email: ahmedovais.asl@gov.in*

Abstract

Subsurface material discontinuities lead to local variations of apparent thermal effusivity and diffusivity. The analysis of equivalence between such variations and defect parameters is useful from both theoretical and practical points of view. Classical heat conduction solutions contain effusivity/diffusivity as important parameters, which can be used for defect characterization. Also, conversion of temperature images into maps of thermal propertiesmay enhance defect visibility, for example, by transiting from the temperature domain into the time domain, as it appears in the case of diffusivity measurement. A 60J impact damage in carbon fiber reinforced polymer is characterized by effusivity/diffusivity variation from 20 to 40 %.

Keywords: *Nondestructive testing, Infrared thermography, Defect, Diffusivity, Effusivity*

1.Introduction:

In pulsed thermal nondestructive testing (NDT), subsurface defects of materials are detected by analyzing dynamic temperature distributions on the surface of test samples excited by a pulse or waves of thermal energy. Several types of thermal stimulation can be used but typically it is performed by means of flash tubes and halogen lamps [1]. In one-sided tests, front (F) surface temperature signals, which appear over defects, essentially decay by amplitude and delay in time with increasing defect depth l, while on the rear (R) surface temperature signals and their evolution in time are weakly dependent on l, see the test scheme in figure 1. In the last decade, thermal NDT appeared as a powerful tool for evaluating quality of composite materials, see the recent review [2] and some topical papers [3-5].

Classical analytical solutions of heat conduction in solids are typically one-dimensional (1D) and involve material thermal properties as solution parameters, namely, thermal effusivity$e$ and thermal diffusivity a. The concept of pulsed thermal NDT accepted in this study assumes that a discontinuity-like defect phenomenologically can be considered as a local variation of the above-mentioned parameters Δe(F-surface procedure) and Δa(R-surface procedure). This concept wasearlier used for analyzing severity of impact damage in carbon fiber reinforced polymer (CFRP) composites [6,7]. The investigations were conducted on large series of CFRP samples which contained impact damages in a wide range of energy, while the samples were subjected to temperature cycling tests and moistening.

In this study we, first, analyze the theoretical aspects of the relationship between discontinuity-like defects and thermal property variations by using 3D modeling and afterwards supply an experimental illustration for both one- and two-sided inspection of impact damage in CFRP.

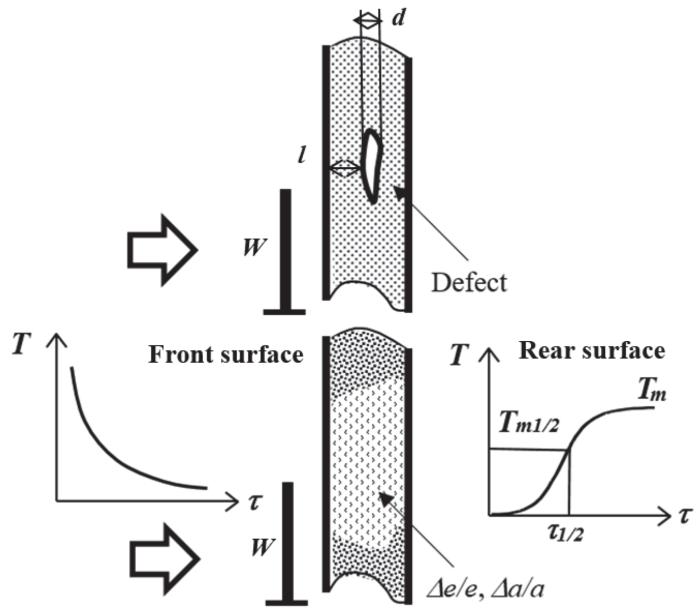

Fig.1 One-and two-sided thermal NDT procedures: equivalence between defects and apparent variations of thermal properties

2.Theory: back to basics

The Dirac-pulse heating of an adiabatic homogeneous plate is described with the two well-known expressions:

$T = \frac{Wa}{\lambda L}\ [1 + 2\sum_{n=1}^{\infty} e^{-n^2\pi^2 Fo}]$ on the F-surface;

$T = \frac{Wa}{\lambda L}\ [1 + 2\sum_{n=1}^{\infty}(-1)^n e^{-n^2\pi^2 Fo}]$, on the R-surface (1)

Here: W is the absorbed energy, λ is the thermal conductivity,$a$is the thermal diffusivity, L is the plate thickness, and $Fo = a\tau/L^2$ is the Fourier number. The plots of the functions above are schematically shown in figure1.The three material thermal properties (C , the heat capacity, ρ, the density and thermal conductivity $\lambda = C\rho a$) cannot be determined without having measured absorbed energy; note that the dimensions of these quantities contain energy in Joules. Oppositely, thermal diffusivity$a$, of which dimension is m^2/s, can be evaluated by analyzing some inflection points in the R-surface$T^R(\tau)$ functions. Such inflection points naturally appear in $T^R(\tau)$ curves, while the processing of F-surface $T^F(\tau)$ curves requires using some mathematical "tricks", such as non-linear fitting [8, 9]. Reliability of the corresponding estimates on the R-surface is typically higher than those on the F-surface. Physically, this is explained by the fact, that in a two-sided procedure the heat energy travels across a sample thus being affected by material bulk properties, unlike a one-sided procedure where the influence of material properties on the surface temperature strongly decays with increasing depth.

It is worth noting that Eqs. (1) contain the infinite number of exponential members which are often interpreted as pulsed thermal waves travelling between the F- and R-surfaces of the plate. Front-surface solutions become much simpler if a plate can be replaced with a semi-infinite body, of which Dirac-pulse heating is described by the equation:

$T = \frac{W}{e\sqrt{\pi}} \frac{1}{\sqrt{\tau}}$,(2)

Where $e = \sqrt{C\rho\lambda}$ is the effusivity, or thermal inertia. Obviously, the determination of absolute values of

$e = W/(T\sqrt{\pi\tau})$(3)

is also linked to measuring absorbed energy but in thermal NDT one often analyzes the temporal behavior of the $e/W = 1/(T\sqrt{\pi\tau})$function. It is also worth noting that any plate behaves as the respective semi-infinite body at shorter observation times that follows from Eq. (1) at short Fo times. It is important noting that experimentally determined e values are apparent and vary in time.

In a two-sided procedure, thermal diffusivity is typically determined by using the Parker formula [10]:

$$a = \frac{0.139L^2}{\tau_{1/2}} \quad (4)$$

where $\tau_{1/2}$ is the so-called half-rise-time easily determined in a $T^R(\tau)$ curve, see the plot in figure 1.

3. Effusivity and diffusivity *vs.* subsurface defect parameters – sensitivity analysis

In this section we analyze how the presence of subsurface defects changes apparentlocal thermal properties of a material under test: effusivity in a one-sided procedure and diffusivity in a two-sided procedure.The underlying concept is to model some defect situations where air-filled defects having different thickness d and located at different depths l modify the values of local apparent effusivitycalculated by Eq. (3) and diffusivity calculated by Eq. (4) to compare to the respective "non-defect" values.

3.1 Test model description

Two CFRP sampleswith the thickness of 1 and 6 mm were analyzed in both one- and two-sided procedures. The heating time was 1 second and the heating power - 10 kW/m^2. Four synthetic image sequences have been produced to determine variations in apparent local effusivity and diffusivity, i.e. at the points located over the centers of the air-filled defects. Defect depth and thickness varied to study influence of these parameters on thermal property variations. Since defect lateral dimensions greater than 10 mm weakly influence surface temperature signals [1], in this model only 10x10 mm defects have been analyzed according to the scheme in figure 2a. The examples of apparent effusivity and diffusivity maps are presented in figure 2b, c.

It is worth noting again the principal difference between maps of effusivity and diffusivity. Diffusivity is a unique integral parameter which characterizes a sample in a particular heating procedure. Diffusivity values are calculated by processing a whole synthetic sequence. Effusivity can be regarded as a unique parameter only if Dirac-pulse heating of an adiabatic semi-infinite body is involved. In our case, we deal with square-pulse heating of non-adiabatic plates, therefore, effusivity is to be calculated for each single image in a synthetic sequence varying from image to image through the sequence. In the analysis below, effusivity variation for each defect has been calculated at the time when a differential temperature signal for this particular defect achieves a maximum value.

For the 1 mm-thick sample, the synthetic sequence included 150 images with the acquisition interval being 0.1s; whereas, for 6 mm-thick sample, the synthetic sequence included 100 images with the acquisition interval being 1s.

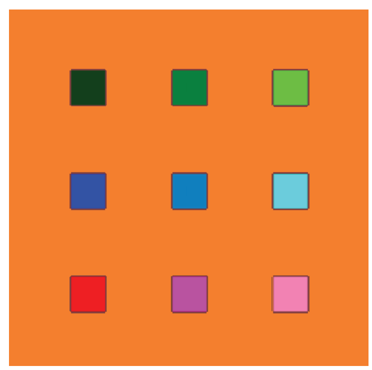

Fig.2a Scheme of defects

Sample 1: L=1 mm: defect depth 0.2, 0.5 and 0.8 mm, defect thickness 0.05, 0.10 and 0.15 mm

Sample 2: L=6 mm: defect depth 1, 3 and 5 mm, defect thickness 0.05, 0.10 and 0.20 mm

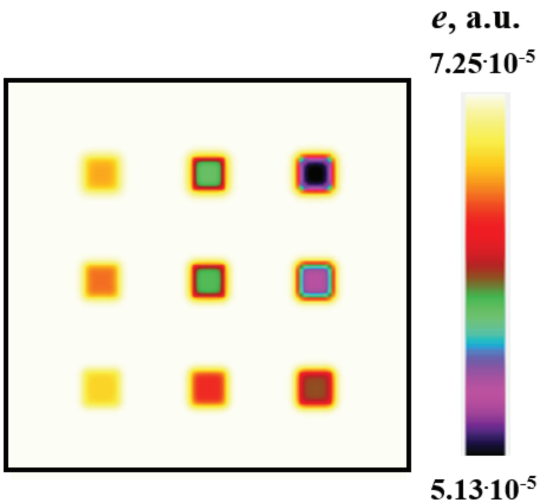

Fig.2b Effusivity map (1 mm-thick CFRP sample)

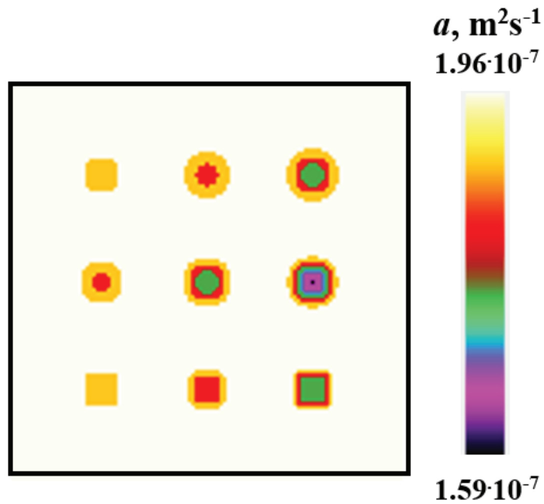

Fig.2c Diffusivity map (6 mm-thick CFRP sample).

Fig.2 Test model for analyzing relationship between defect parameters and local variations of effusivity/diffusivity (all defects 10×10 mm):

3.2 Modeling results and discussion

All results are presented in Table1 where relative variations (in percent) of effusivity and diffusivity are given for each particular defect (36 test cases in total). The same results are graphically shown in figure3. Notice that there are no results for the defects at the depth 0.8 mm in the 1 mm-thick sample because of the so-called inversion phenomenon. The concept of this phenomenon is that, in a two-sided procedure, the defects located close to the rear surface first produce negative temperature signals (defect areas are colder than the background) and then become positive thus making the corresponding values of diffusivity variations in Table 1 "non-uniform" (these values are specified with **). The inversion phenomenon deserves further exploration.
In fact, the obtained relationships qualitatively repeat those which take place for differential signals, namely, relative effusivity variations decay linearly with depth and increase linearly with defect thickness, while diffusivity variation is maximal for the defects located in the middle of the sample, and the corresponding relationships $\Delta a/a\ (l)$are close to linear.

4. Experimental illustration

The theory above was illustrated by evaluating a CFRP sample with thickness of 4.7 mm subjected to a standard impact damage test characterized by the energy of 60 J and velocity of 7 m/s (Figure 4a).The sample was tested on both F- and R-surfaces performing one- and two-sided tests to produce 4 sets of the IR image sequences, which were analyzed for variations of apparent effusivity and diffusivity. The sample was heated with 2 flash tubes (6.4 kJ energy in total, 5 ms pulse duration). On the F-surface, the impact damage was hardly detected (the so called Barely Visible Impact Damage-BVID), while the major delaminations appeared on the R-surface in the well-known "butterfly" form (see figure 4a). It is worth noting that, unlike the theoretical cases analyzed above, an impact damage defect represents a complicated conglomerate of delaminations and cracks located at different depths and oriented along the fiber direction. Often, a main body of impact damage appears closely to the sample rear surface.

Table.1 Effusivity/diffusivity variations over air-filed defects in 1 and 6 mm-thick CFRP samples (model from Fig. 2)

Defect depth$l$, mm	Defect thickness$d$, mm	One-sided procedure $\|\Delta e/e\|$, % *	Two-sided procedure $\|\Delta a/a\|$, %
1 mm-thick sample			
0.2	0.05	32.4	21.1
	0.10	44.4	34.6
	0.15	51.3	40.0
0.5	0.05	16.9	28.6
	0.10	25.1	44.3
	0.15	29.6	48.1
0.8	0.05	5.50	21.1**
	0.10	10.1	21.1**
	0.15	14.7	11.9**
6 mm-thick sample			
1	0.05	11.5	3.6
	0.10	18.0	7.1
	0.20	27.1	10.7
3	0.05	3.1	7.1
	0.10	5.9	10.7
	0.20	9.6	15.8
5	0.05	0.96	3.6
	0.10	1.3	7.1
	0.20	2.3	10.7

* These values are determined for the times when the differential temperature signals over particular defectsbecome maximal.

** These values correspond to a special case where temperature signals on the rear surface experience the so-called inversion, i.e. change the sign.

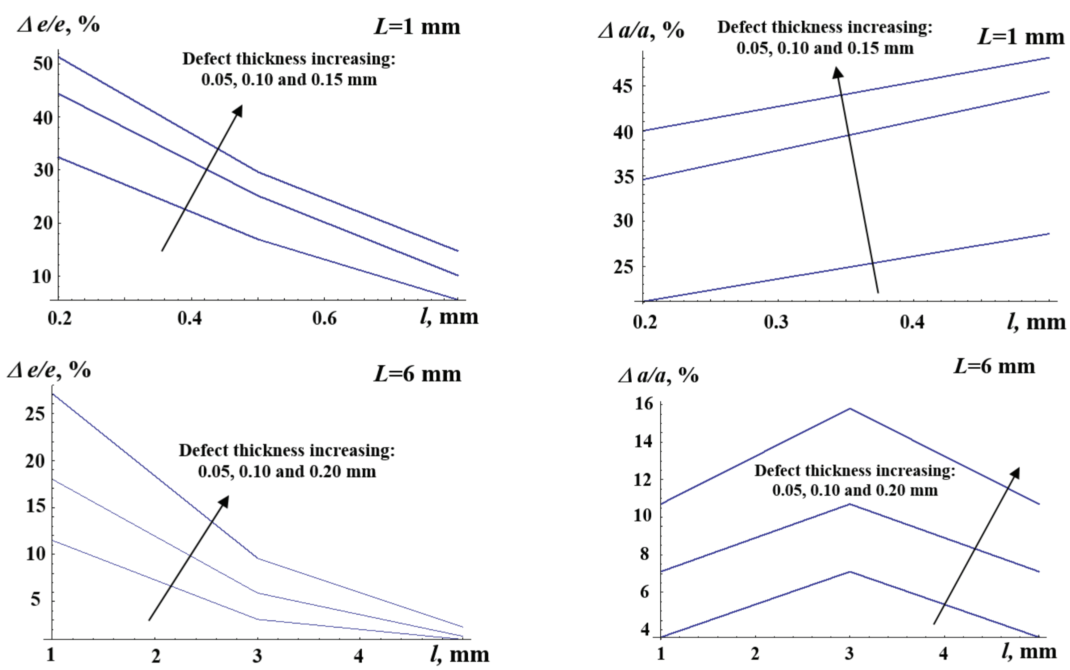

Fig.3 Effusivity/diffusivity variations over air-filled defects in 1 and 6 mm-thick CFRP samples (data from Table 1)

The evolution of the F-surface temperature distribution over the impact damage in a one-sided test procedure is shown in figure 4b. It is seen that immediately after the heat pulse one can see the thin superficial delamination while the main body of the defect appears later. The analysis of the in-depth structure of impact damage defects is beyond the scope of this study; the use of dynamic thermal tomography for 3D reconstruction of impact damage was discussed in [11].

Figure 4c shows the evolution of signal-to-noise ratio (*SNR*) through the recorded source image sequencethatwasroutinely calculated for defect (D) and non-defect (ND) areas chosen by the operator. It follows that the defect can be detected best of all at about 1 s. Then the source sequence was converted into the sequence of apparent effusivity images according to Eq. (3).

The corresponding $e(\tau)$ plot is presented in figure 4d to illustrate that immediately after the heat pulse the effusivity magnitude in the chosen (D and ND) areas is the same, and a noticeable difference occurs in the interval from 0.4 to 4 s. An F-surface map of $e(i,j)$is shown in figure 4e to illustrate 19 % variation of thermal effusivity over the impact damage. It is worth reminding that $e(\tau)$values vary in time and an absolute value of $\Delta e/e\ (\tau)$ reaches maximum at a particular time (at about 1s in figure 4e).

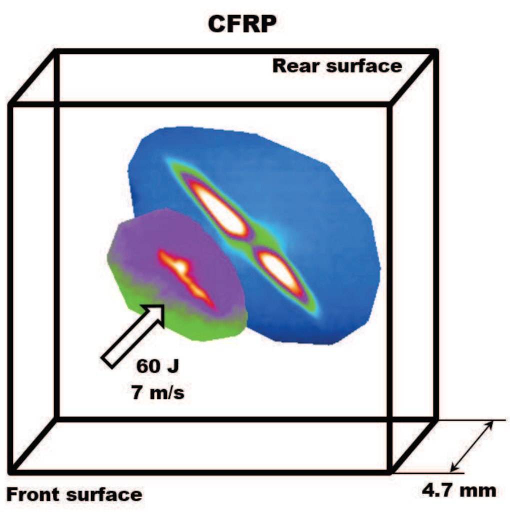

Fig.4a Test scheme and examples of temperature distributions on F- and R-surfaces

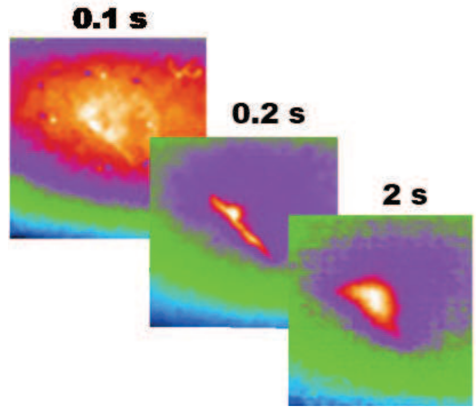

Fig.4b F-surface temperature evolution

Fig. 4c SNR vs time

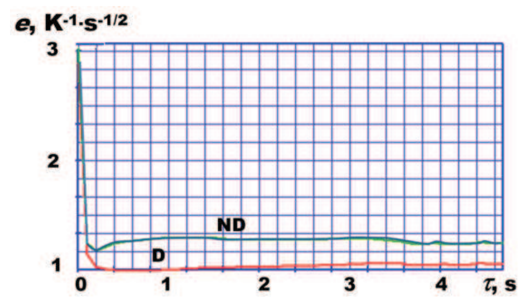

Fig.4d Effusivityvs time in defect (D) and non-defect (ND) areas

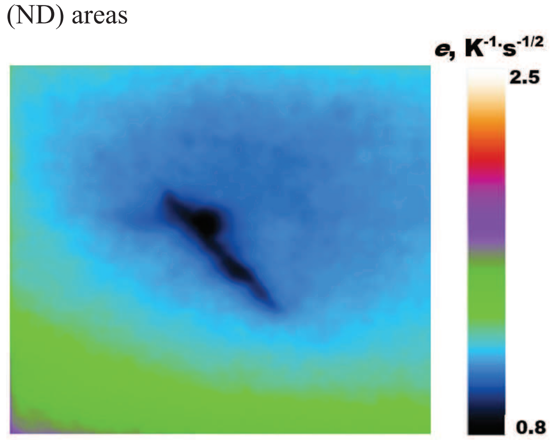

Fig.4e Effusivity map at 1s (19 % effusivity variation over impact damage)

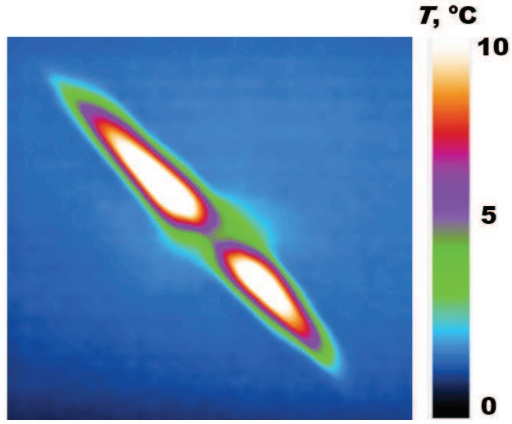

Fig.5a R-surface temperature distribution at 2.6 s

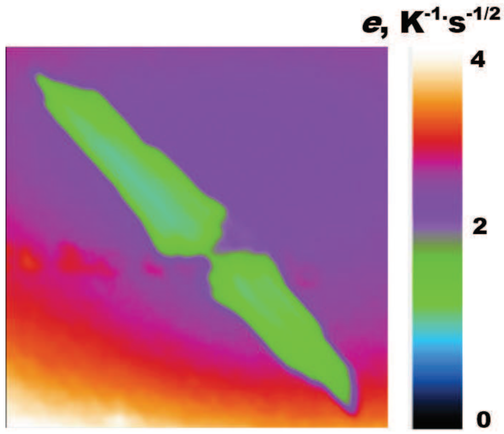

Fig.5b Eeffusivity map at 2.6s (42% effusivity variation over impact damage)

Fig.5 Evaluating R-surface effusivity in a one-sided test procedure (pulsed heating of 4.7 mm-thick CFRP sample subjected to 60 J impact

In a one-sided test procedure, the sample excess temperature *T* reached 10^{o}C, and the defect was clearly seen on the R-surface in the "butterfly" form (Fig. 5a). This means that the main body of the impact damage located closely to the R-surface to produce effusivity variation of 42 % (Fig. 5b). The results in Fig. 4 and 5 prove that one-sided values of effusivity are strongly dependent on time and defect depth.

In the two-sided procedure of diffusivity measurement, first, the F-surface was heated, and the R-surface temperature was captured (figure 6a). The temperature profiles were of the classical Parker shape (see figure 6b), and the respective diffusivity image is presented in figure 6c. In non-defect areas, the composite diffusivity was (3-3.5)$\cdot$10^{-7} m$^2\cdot$s^{-1}, that is a typical value for CFRP composite, while over the defect it dropped down to (2-2.4)$\cdot$10^{-7} m$^2\cdot$s^{-1}. The average diffusivity variation over the defect was about 44 %.

In the case of heating the R-surface and determining diffusivity on the F-surface, the results were very similar to those on the R-surface (Figure 7, diffusivity variation 43 %) that is explained by the known fact that material diffusivity measurements are independent on which surface is heated and which - monitored. By other words, two-sided thermal NDT tests are preferable if defects might be located at any depth.

The experimental results obtained for the impact damage defect, which is characterized by a complicated structure of single delaminations, demonstrate that relative variations of thermal properties are of the same order of magnitude as it appears in the case of a theoretical model containing single air-filled defects.

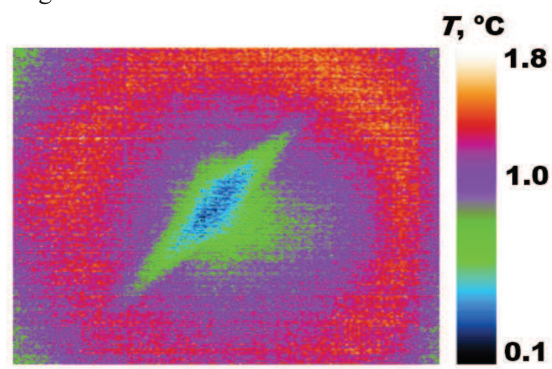

Fig.6a R-surface temperature distribution at 10s

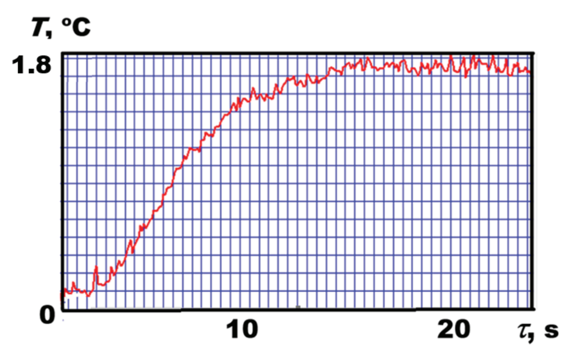

Fig.6b R-surface temperature evolution in time

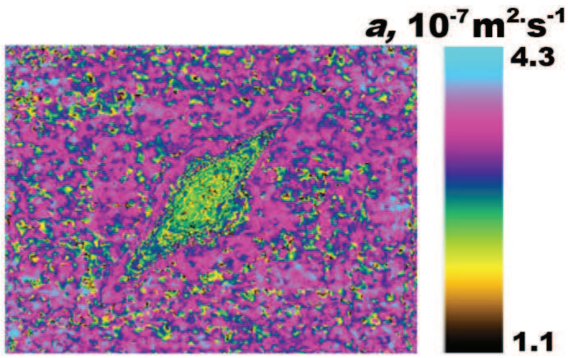

Fig.6c R-surface diffusivity map (diffusivity variation over defect 44 %)

Fig.6 Evaluating R-surface diffusivity in a two-sided test procedure (pulsed heating of 4.7 mm-thick CFRP sample subjected to 60 J impact)

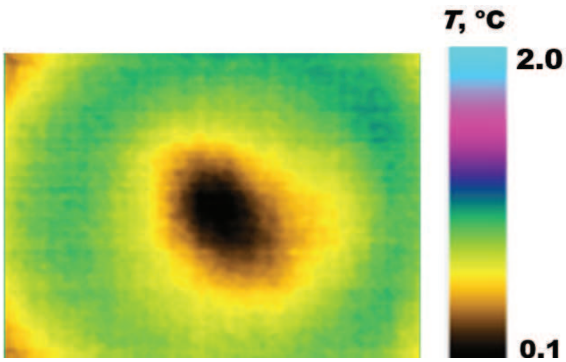

Fig.7aF-surface temperature distribution at 10 s

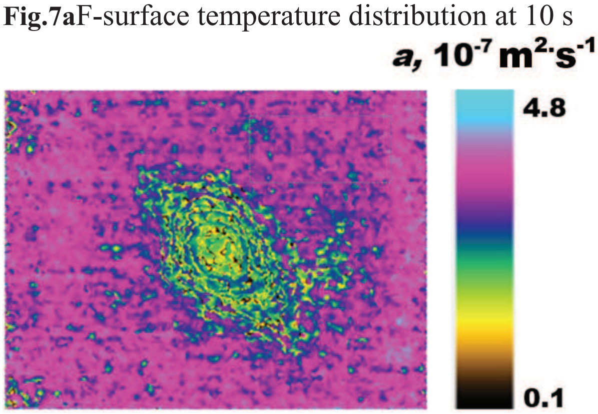

Fig.7b F-surface diffusivity map (diffusivity variation over defect 43 %)

Fig.7 Evaluating F-surface diffusivity in a two-sided test procedure (pulsed heating of 4.7 mm-thick CFRP sample subjected to 60 J impact)

5 .Conclusions

- In one-sided thermal NDT procedures, the effusivity parameter can be used for characterizing hidden defects. Effusivity magnitude depends on defect depth thus allowing defect depth evaluation, mainly, for subsurface defects. The main disadvantages of this technique are as follows: 1) an image sequence cannot be replaced with a single image of effusivity, because effusivity estimates vary in time, 2) effusivity variations in defect areas strongly decay with defect depth, 3) effusivity is linearly related to absorbed energy.
- Over subsurface defects, apparent local effusivity variation linearly decays with defect depth and increases with defect thickness.
- In two-sided thermal NDT procedures, the modified Parker method is recommended for evaluating diffusivity distributions. This technique is implemented in the time domain that ensures its better noise resistance compared to effusivity measurements that are fulfilled in the temperature domain.
- Over subsurface defects, local diffusivity variation reaches maximum in the middle of the sample and increases linearly with defect thickness.
- A 60 J impact damage in a 4.7 mm-thick CFRP sample is characterized by effusivity variations from about 20 to 40 % and diffusivity variations of about 40 %.
- The future research will be devoted to the analysis of whether relative variations of composite effusivity/diffusivity can be used for evaluating defect parameters.

6. References

[1] Vavilov V., Burleigh D. (2020), “Infrared thermography and thermal nondestructive testing”, Springer Nature Switzerland, DOI: 10.1007/978-3-030-48002-8.

[2] Bing W., Shuncong Z., Tung-Lik L., Fancey K.S., JiaweiMi (2020), “Non-destructive testing and evaluation of composite materials/structures: A state-of-the-art review”, Adv. in Mech. Eng., 12 (4), pp. 1-28.

[3] Chulkov A.O., Sommier A., Pradere C., Vavilov V.P., Siddiqui A.O., Prasad Y.L.V.D. (2021), “Analyzing efficiency of optical and THz infrared thermography in nondestructive testing of GFRPs by using the Tanimoto criterion”, NDT & E Intern., vol. 117, 102383. DOI: 10.1016/j.ndteint.2020.102383.

[4] Mulaveesala R., Rani A., Kher V., Mishra P., Kaur (2021), "J. Infrared non-destructive testing and evaluation for inspection of carbon fiber reinforced polymer materials", Proc. Thermosense: Thermal Infrared Applications XLIII conf., vol. 11743, 117430Q, DOI: 10.1117/12.2593390.
[5] Dua G., Arora V., Mulaveesala R. (2018), "An aperiodic digitized frequency modulated thermal wave imaging for testing and evaluation of carbon fiber reinforced polymer materials", JNDE, 16 (12), pp. 30-32.
[6] Vavilov V., Chulkov A., Smotrov A., Smotrova S., Moskovchenko A. (2019), "Characterizing impact damage in GFRP/CFRP composites by determining thermal effusivity/diffusivity", Measurement Science and Technology, vol. 30, 034003, DOI: 10.1088/1361-6501/ab018e.
[7] Vavilov V.P., Chulkov A.O., Smotrova S.A., Smotrov A.V., Scherbakov V.N., Storozhenko V.A. (2022), "Infrared thermographic analysis of thermal property variations in composites subjected to impact damage, thermal cycling and moisture saturation",. Composite Structures, vol. 296, 115927, DOI: 10.1016/j.compstruct.2022.115927
[8] Zalameda J.N., Winfree W.P. (2004), "Improved sampling of thermal transients using Focal Plane Array infrared imagers", Proc. Thermosense: Thermal Infrared Applications XXVI conf., vol. 5405, pp. 374-381.
[9] Winfree W.P., Zalameda J.N. (2002), "Single sided thermal diffusivity imaging in composites with a shuttered thermographic inspection system", Proc. Thermosense: Thermal Infrared Applications XXIV conf., vol. 4710, pp. 536-544.
[10] Parker W.J., Jenkins R.J., Butler C.P., Abbot G.L. (1961), "Flash method of determining thermal diffusivity, heat capacity and thermal conductivity", J. of Appl. Phys., vol. 32, pp.1679-1684.
[11] Vavilov V.P., Shirayev V.V., Kuimova M.V. (2018), "Time- and phase-domain thermal tomography of composites", Photonics, 5 (4), pp. 31-42. DOI: 10.3390/photonics5040031.

Infrared Machine Vision for Detection and Characterization of Defects Present in a Mild Steel Material

Pranav Yogesh Mahajan[1], Aneesh Bajwa[1], Keshav[1], Nandani Bansal[1], Geetika Dua[1a],Amanpreet Kaur[1], Vanita Arora[2]
[1]Thapar Institute of Engineering and Technology, Patiala.147004
[2]Indian Institute of Information Technology Una, Vill. Saloh, Teh. Haroli, Distt. Una Himachal Pradesh, India-177209.
[a]Email: *geetikadua09@gmail.com*

Abstract

Significant advancements in machine vision and thermal imaging have provided an advantage in non-destructive testing and evaluating different materials. This work presents an approach to combining thermal wave imaging with machine vision for a fast, accurate way to detect and characterize the sub-surface defects and their features present in a solid material. Machine vision-based defect detection approaches attract the research community due to their reliable performance in employing the stimulated thermal response in active thermal wave imaging. A thermal source stimulates the material surface while the infrared camera captures its thermal response, extracts features from the thermal pattern, and feeds them into a machine vision-based algorithm for characterization. This proposed method improves the detectability reliability regarding qualified characteristics of defects.

Keywords: *MachineVision; Non-destructive testing; Scale-invariant feature transform, Watershed transform*

1.Introduction

Infrared thermography (IRT) has emerged widely as a method for non-destructive testing as it offers non-contact, comprehensive area detection of material defects. The principle of infrared thermography is based on the physical phenomenon that any object of a temperature above absolute zero emits electromagnetic radiation. The infrared camera further covers the emitted radiation into temperature and displays the images showing thermal variations [1-6].

Infrared thermography is further classified as passive thermography and active thermography. In passive thermography, without any external known source, a natural thermal response on the test material surface is used to identify subsurface defects. An external heat source stimulates the test sample in active thermography, and the corresponding thermal response is recorded using an infrared camera. Various processing methods can do further subsurface defect detection.

Depending on the external stimulus, the active thermography is classified as Pulsed thermography (PT) [2-3], Pulse phased thermography (PPT) [4-5], Lock-in thermography (LT) [6-7], and other aperiodic thermal wave imaging methods like Frequency Modulated Thermal Wave Imaging (FMTWI) [8-9].In Pulsed thermography (PT), the surface of the test material is energized using a high peak power source within a short duration of time, and the corresponding thermal response is collected from the surface of the test material. Because of the high peak power and short duration of time, the total test sample cannot absorb heat uniformly and enters two problems non-uniform emissivity and non-uniform radiation. In lock-in thermography (LT), instead of high peak power, a mono-frequency continuous wave is used as an external stimulus, and the infrared camera captures the corresponding thermal response. The thermal response collected from the infrared camera is analyzed using phase-based analysis, which is less sensitive to non-uniform radiation and non-uniform emissivity. Because of mono frequency, repetition of the experiment is needed to detect the defects at various depths.

Pulse-phase thermography (PPT) combines pulse and lock-in thermography, like pulse energy for stimulation and phase-based analysis for defect detection. This experimentation is like pulse thermography, but Fourier Transform carries analysis applied over thermal response to extract the phase delay. Frequency modulated thermal wave imaging.

(FMTWI) [8-12] is introduced to overcome the above problems. This method imposed a suitable band of frequencies over the test sample within single experimentation.Frequency modulated thermal wave imaging, where the heating waveform phase relations are adjusted over bandwidth in such a way that chirps (frequency modulated) signal, with much-reduced peak power, is produced. FMTWI, while retaining all characteristics of lock-in thermography, has the added advantage of overcoming the blind frequency problem. The captured thermograms are further processed using matched filtering (pulse compression) [12-16].

The main objective of this paper is to propose a method to detect and classify defects in solid materials. This work presents an approach combining thermal wave imaging with machine vision for a fast, accurate way to detect and classify the sub-surface defects and their features in a mild steel material. A machine vision-based discrimination modality has been proposed for an aperiodic analysis to be used for sub-surface characterization. This proposed modality improves testability and reliability presents the best detection in terms of quantified characteristics of the defects.

Machine-vision algorithms provide us with valuable information about the defects present [17-20]. Various signal and image processing schemes are generally applied to observed thermal response to validate defect detection, depth quantification, and material property estimation [20]. However, in the present scenario where artificial intelligence and machine learning are ruling the world, these signal processing and manual inspection-based modalities also lag the performance, quality, and time. Machine vision techniques are utilized to overcome such cases and be synchronized with the present world scenario to detect and characterize the defects placed in materials.

In this paper, machine learning techniques like Scale-invariant feature transform (SIFT) is employed on pre-processed thermal response acquired from numerically simulated mild steel sample with various types of defects placed at different depths. The sample is excited by frequency-modulated heat flux. Further, the watershed transform-based region-based segmentation approach is employed for localizing the defects accurately.

2. Modeling and simulation

In this work, a 3D Finite element analysis (FEA) has been carried out on a steel sample using COMSOL Multiphysics. This software simulates designs, devices, and processes in all engineering, manufacturing, and scientific research fields [21-22]. COMSOL Multiphysics is a simulation platform that provides fully coupled multiphysics and single-physics modeling capabilities. The Model Builder includes all of the steps in the modeling workflow, from defining geometries, material properties, and the physics that describe specific phenomena to solving and post-processing models for producing accurate results. The two mild steel sample (one training and the other testing) models with eighteen defects, six each of three different material, air, water, and oil (shown in Fig.1), has been modeled with a finer mesh using 3D tetrahedral elements.

(a)

(b)

Fig.1 Layout of the modeled mild steel sample with inclusions. (a) Training sample (b). Testing sample

The defects are further placed at different depths having the same diameter (20 mm). The defect's depths are shown in Table 1.The FEA is carried out by imposing an LFM heat flux (with frequency varying from 0.01 Hz to 0.1 Hz for 100 s) over the surface of the test material, and the infrared camera captures the resultant surface thermalresponse at a frequency of 25 Hz. The simulations are carried out under adiabatic boundary conditions, with the sample at an ambient temperature of 300 K.

Table.1 Depths of different defects

S.No. (Oil (o), Air(a), Water (w))	Depth (mm)	S.No. (Oil, Air, Water)	Depth (mm)
1	1	7	0.8
2	1.4	8	1.2
3	1.8	9	1.6
4	2.2	10	2
5	2.6	11	2.4
6	3	12	2.8

The thermal properties of the materials used are as given in Table 2.

Table 2. Thermal properties

Material	Density (ρ) (Kg/m^3)	Thermal Conductivity (k) W/(m*K))	Specific Heat (c) (J/(Kg*K))
Air	1.23	0.025	1007
Water	1000	0.5576	4200
Oil	1510	0.162	749
Mild Steel	7850	60.5	434

The simulated data is further processed using signal processing and machine vision based algorithms as described in the next section.

3. Post processing methods

3.1 Polynomial Fitting

The recorded thermal response is first processed to obtain a zero mean thermal response using an appropriate polynomial fit. Using this method, we model or represent a data spread by assigning the best fit function (curve) along the entire range [8-10, 23].

3.2 Pulse Compression

Pulse compression is a statistical technique for determining how one variable changes with the other variable. It gives us an idea of the relationship between the two variables. It is a bi-variate analysis measure that describes the association between different variables. We used correlation to find how the size of the defect varies in the thermal image when the depth radius of the defect is varied and tried to develop a relationship between them. After finding a relationship between these parameters, it became easier to train and tests the machine vision-based model [12-15,17].

3.3 Watershed Transform

The watershed transformation can be classified as a region-based segmentation approach. The intuitive idea underlying this method comes from geography. Watershed algorithms are used in image processing primarily for object segmentation, that is, for separating different objects in an image. The algorithm allows for counting the number of defects or for further analysis of the separated object [24].

3.4 SIFT

Scale-invariant feature transform (SIFT) is a machine-vision algorithm to detect, describe, and match local features in images (thermograms). Interesting points can be extracted for any object in an image to provide a "feature description" of the object. This description, extracted from a training image, can then be used to identify the object when attempting to locate the object in a test image containing many other objects. To perform reliable recognition, extracting features from the training image to be detectable even under changes in image scale, noise, and illumination is essential. Such points usually lie on high-contrast regions of the image, such as object edges [18, 24-27].

In this work, SIFT is first applied, determining a few best frames from the 4999 frames (pulse-compressed thermograms) dataset. Then, the best frame is determined using this technique.

4. Results and discussions

The present works highlight the capability of the proposed approach in detecting and characterizing defects present in a structural mild steel sample. In this approach, the test material can undergo a known controlled frequency modulated thermal stimulation sweeping their entire frequency range from 0.01Hz to 0.1 Hz in 100 s, and the infrared camera captures the corresponding thermal response over the surface.

Additive white Gaussian noise with a signal-to-noise ratio being 30 dB is added to the obtained thermal response for the imposed incident heat flux. Noise is artificially added to test the capability of the proposed approach to detect the subsurface density variations. The temporal mean raise from the noisy thermal response is removed using an appropriate polynomial fit. Fig.2. shows the corresponding mean-zero thermograms for the training and testing modeled samples.

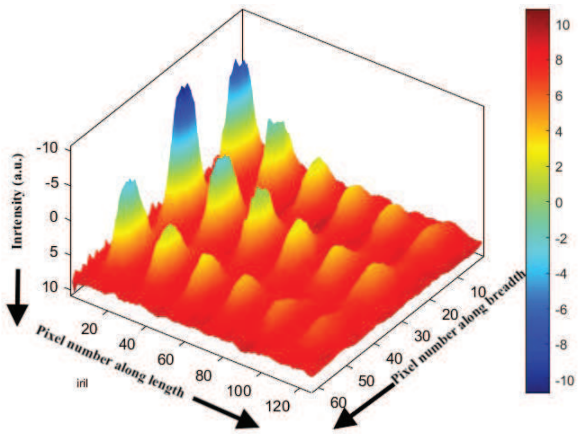

(a)

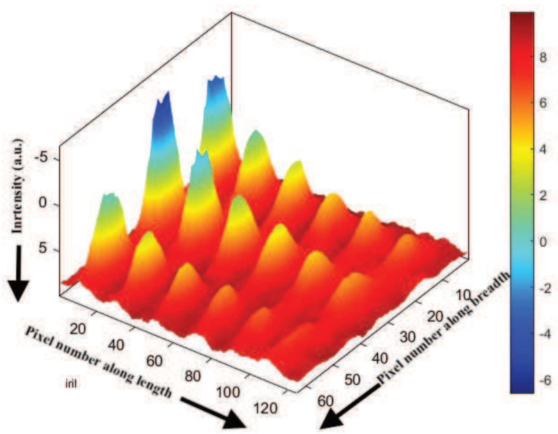

(b)

Fig.2 Zero mean thermograms. (a) Training sample (b). Testing sample

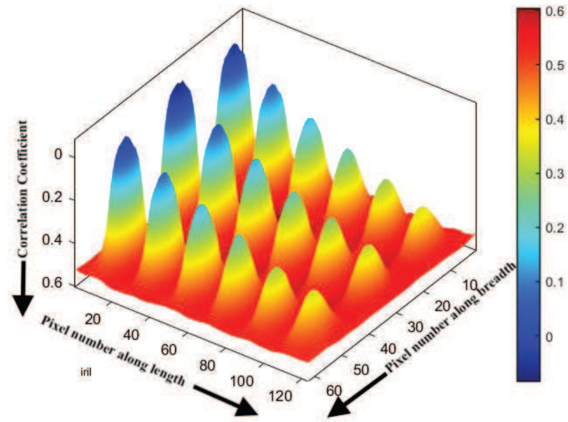

(a)

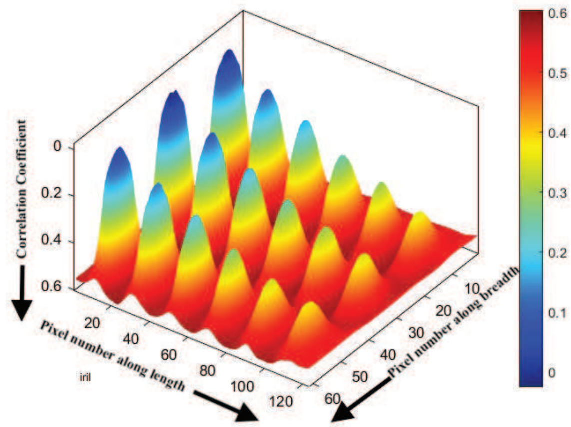

(b)

Fig.3 Pulse-compressed thermograms. (a) Training sample (b). Testing sample

As shown in this section, the aforementioned signal processing, and machine vision-based techniques are further applied to mean zero data and results.Pulse compression analysis is performed on the mean zero data for the training and testing sample data. The resulting thermograms are obtained,and the best frame is selected using SIFT algorithm. It is obtained at 1.5 s.

Fig.3. shows the pulse-compressed thermograms.

Further, applying the watershed algorithm to the chosen best frame provides the segmented thermogram. The algorithm also determines the count of the defects present in the sample. The resulting thermograms are as shown in Fig.4.

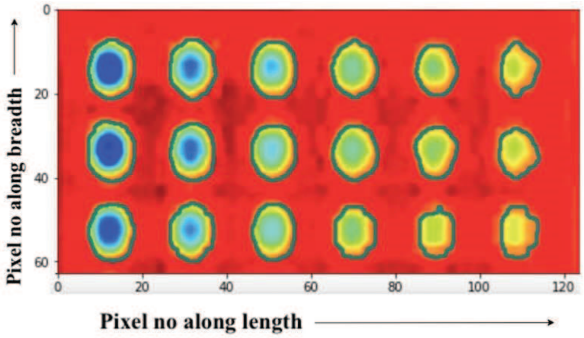

(a)

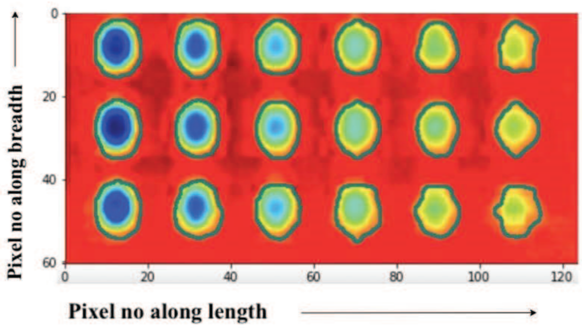

(b)

Fig.4 Segmented thermograms. (a) Training sample (b). Testing sample

Furthermore, pulse compression results are used to determine the type of material (air, water, or oil). The relationship between correlation peak shifts and depths of defects present, a set of pixels (3x3 region around the center of each defect) are chosen, and their correlation coefficient is calculated with that of chosen reference pixel.

Peak shifts are determined for the peak of auto-correlation of reference pixels. Moreover, a relationship between depths and these peak shifts is constructed.

This process is repeated for defects containing different materials: air, water, and oil. The results show the maximum variation in defects with air and defects with water has the minimum, which is true as water has the highest thermal effusivity and air has the lowest. The results are verified for the training sample and plotted as shown in the bar diagram in Fig.5.

5. Conclusions

The present manuscript demonstrates the capability of Frequency modulated infrared thermographic technique combined with the machine vision algorithms.This infrared machine vision technology provides the accurate detection ad characterization of the defects.

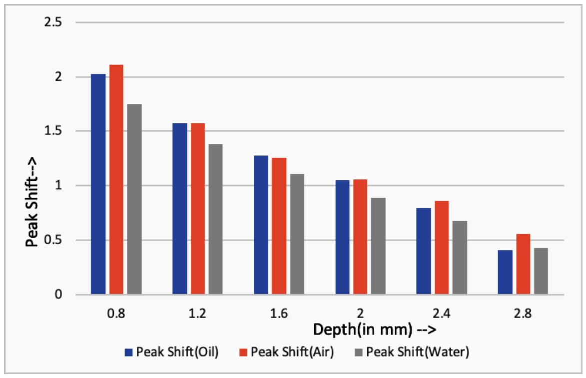

Fig.5 Variation of Peak shifts with Depth for three different materials

FMTWI technique is applied on a mild steel sample with defects of different types and placed at different depths. Pulse-compressed thermogram obtained from post-processing is considered as input to the machine vision algorithms. Further, defects characterization is done to determine the relationship between a different material's peak shift and depth. The relation obtained can also be used in the future to determine the depths of the defect. The count of defects has been calculated using the watershed algorithm.

6. References

[1] X. P. V. Maldague (2001), “Theory and Practice of Infrared Thermography for Non- Destructive Testing,” John Wiley & Sons Inc.

[2] D. P. Almond and S. K. Lau (1994), “Defect sizing by transient thermography I: An analytical treatment,” Journal of Physics D: Applied Physics, 27 (5), pp. 1063-1069.

[3] D. L. Balageas, J.C. Krapez, P. Cielo (1986), “Pulsed photothermal modeling of layered materials,” Journal of Applied Physics, 59 (2), pp. 348-357.

[4] X. Maldague and S. Marinetti (2003), “Pulse Phase Infrared Thermography,” Review of Scientific Instruments, 74 (1 II), pp. 417-419.

[5] X. Maldague and S. Marinetti (1996), “Pulse phase infrared thermography,” Journal of applied physics, vol. 79, no. 5, pp. 2694-2698.

[6] G. Busse (1979), “Optoacoustic phase angle measurement for probing a metal,” Applied Physics Letters, 35 (10), pp. 759-760.

[7] G. Busse, D. Wu, W. Karpen, “Thermal wave imaging with phase-sensitive modulated thermography,” Journal of Applied Physics, 71 (8), pp. 3962-3965, 1992.

[8] R. Mulaveesala and S. Tuli (2006), "Theory of frequency modulated thermal wave imaging for nondestructive subsurface defect detection," Applied Physics Letters, 89 (19), art.no. 91913.

[9] S. Tuli and R. Mulaveesala, "Defect detection by pulse compression in frequency modulated thermal wave imaging," Quantitative InfraRed Thermography Journal, vol. 2(1), pp. 41-54, 2005.

[10] Ghali V S and Mulaveesala R 2010 Frequency modulated thermal wave imaging techniques for non-destructive testing, Insight: Non-Destructive Testing and Condition Monitoring52, 475-480

[11] Arora V, Mulaveesala R and Bison P 2016 Effect of Spectral Reshaping on Frequency Modulated Thermal Wave Imaging for Non-destructive Testing and Evaluation of Steel Material, Journal of Nondestructive Evaluation35, 1-7.

[12] Kaur K and Mulaveesala R (2019), "An efficient data processing approach for frequency modulated thermal wave imaging for inspection of steel material", Infrared Physics and Technology, 103, 103083.

[13] Dua G, Arora V and Mulaveesala R (2021), "Defect Detection Capabilities of Pulse Compression Based Infrared Non-Destructive Testing and Evaluation", IEEE Sensors Journal21, 7940-7947.

[14] Arora V, Mulaveesala R, Rani A, Kumar S, Kher V, Mishra P, Kaur J, Dua G and Jha R (2021),"Infrared Image Correlation for Non-destructive Testing and Evaluation of Materials", Journal of Nondestructive Evaluation, 40, 1-7.

[15] Mulaveesala R, Arora V and Dua G (2021),"Pulse Compression Favorable Thermal Wave Imaging Techniques for Non-Destructive Testing and Evaluation of Materials", IEEE Sensors Journal, 21, 12789-12797.

[16] Kaur K and Mulaveesala R (2019), "Experimental investigation on noise rejection capabilities of pulse compression favourable frequency-modulated thermal wave imaging", Electronics Letters, 55, 352-353.

[17] Duan Y, Liu S, Hu C, Hu J, Zhang H, Yan Y, Tao N, Zhang C, Maldague X and Fang Q (2019), "Automated defect classification in infrared thermography based on a neural network", NDT & E International 107, 102147.

[18] Hossein-Nejad Z, Agahi H, ad Mahmoodzadeh A (2020), "Detailed review of the scale invariant feature transform (sift) algorithm; concepts, indices and applications", Journal of Machine Vision and Image Processing, 7(1), 165-190.

[19] Dudek G, Dudzik. S 2018 Classification Tree for Material Defect Detection Using Active Thermography, Advances in Intelligent Systems and Computing, 655, 118-127

[20] Fang Q, Nguyen B D, Castanedo C I, Duan Y and Maldague II X (2020), "Automatic defect detection in infrared thermography by deep learning algorithm", Thermosense: thermal infrared applications XLII SPIE) pp 180-195.

[21] Mulaveesala R and Dua G (2016), "Non-invasive and non-ionizing depth resolved infra-red imaging for detection and evaluation of breast cancer: A numerical study", Biomedical Physics and Engineering Express, 2, 055004.

[22] Arora V, Mulaveesala R, Dua G and Sharma A (2020), "Thermal non-destructive testing and evaluation for subsurface slag detection: Numerical modeling", Insight: Non-Destructive Testing and Condition Monitoring, 62, 264-268.

[23] Cardone, Daniela, EdoardoSpadolini, David Perpetuini, Chiara Filippini, Antonio Maria Chiarelli, and Arcangelo Merla (2021), "Automated warping procedure for facial thermal imaging based on features identification in the visible domain", Infrared Physics & Technology, 112, 103595.

[24] Gamarra, Margarita, Eduardo Zurek, Hugo Jair Escalante, Leidy Hurtado, and Homero San-Juan-Vergara (2019), "Split and merge watershed: A two-step method for cell segmentation in fluorescence microscopy images, Biomedical signal processing and control, 53, 101575.

[25] Mery D, da Silva R R, Calôba L P and Rebello J M (2003),"Pattern recognition in the automatic inspection of aluminium castings", Insight-Non-Destructive Testing and Condition Monitoring, 45, 475-483.

[26] Li, Henan, Shigang Wang, Yan Zhao, Jian Wei, and Meilan Piao (2021), "Large-scale elemental image array generation in integral imaging based on scale invariant feature transform and discrete viewpoint acquisition", Displays, 69, 102025.

[27] Jubair, Aliaa S., Aliaa Jaber Mahna, and H. I. Wahhab (2019), "Scale invariant feature transform based method for objects matching", International Russian Automation Conference (RusAutoCon), pp. 1-5.

Defect Detection Capabilities of Barker-Coded Thermal Wave Imaging in Titanium Alloy (Ti-6AL-4V)

Anshul Sharma[1], Vanita Arora[2], Ishant Singh[1], Priyanka Das[1] Ravibabu Mulaveesala[1a]

[1]InfraRed Imaging Laboratory (IRIL) Laboratory, Centre for Sensors, Instrumentation and cyber-physical Systems Engineering (SeNSE), Indian Institute of Technology Delhi, Hauz Khas, New Delhi-110016, India
[2]Indian Institute of Information Technology Una, Vill. Saloh, Teh. Haroli, Distt. Una Himachal Pradesh, India-177209.
[a]*Email: mulaveesala@sense.iitd.ac.in*

Abstract

Pulse compression favorable active infrared thermographic techniques have emerged as highly promising evaluation methodologies among various thermal non-destructive testing and imaging modalities for identifying subsurface anomalies in the test specimen. Because they outperform commonly utilized pulse and periodically modulation-based conventional thermal wave imaging modalities regarding defect detection sensitivity and resolution while employing low peak power heat sources and a comparatively moderate amount of experimenting time. Recently proposed Barker-Coded Thermal Wave Imaging (BCTWI) has offered these advantages over other infrared thermographic techniques. Several data processing methodologies are also be developing to characterize the anomalies from the depicted thermal data. This study highly recommends pulse compression-based data processing approaches for the Barker-coded thermal wave imaging technique. This is because it enhances the localization of supplied thermal energy into the main lobe of cross-correlation data and dispenses significantly less energy into the sidelobes. Current study focused on the application of BCTWI modality with time domain-based and frequency domain data processing approaches such as time domain correlation, time domain phase and frequency domain phase analysis for defect detection in Titanium alloy (Ti-6Al-4V). The results show that the pulse compression-based time domain analysis of the captured thermal data over the test specimen has improved the visibility, contrast, and detectability of the anomalies regarding the frequency domain. Further, the findings depicted using the various approaches have been contrasted using the correlation coefficient as the figures of merit.

Keywords: *Barker-Coded Thermal Wave Imaging (BCTWI); Pulse compression; Titanium alloy (Ti-6Al-4V); signal-to-noise ratio; correlation coefficient*

1 Introduction

Recent technological advancements have seen a huge surge in the usage of titanium-based alloys in different sectors such as in industrial applications, aerospace, medical implants, marine, and automotive construction. Titanium alloys offer certain unique properties including high strength-to-weight ratio, corrosion resistance, and biocompatibility [1, 2]. However, during the production and manufacturing of titanium alloys, there might exist the probability of an unavoidable delamination or occurrence of sub-surface defects. This leads to severe disruption in the architectural uniformity and in-service application of the product and can negatively impact the native properties and overall performance of the manufactured material. Out of the various titanium alloys, Ti-6Al-4V is one of the most commonly used alloys, which contains 6% of aluminium and 4% of vanadium in its composition and showcase lightweight, high stiffness, and high resistance properties for usage [1]. In case of Ti-6Al-4V titanium alloy, defects can arise at both the surface or sub-surface level due to several reasons which include improper heat treatment, welding, machining, casting, or finishing of surface of the material [2]. Common defects generated during the Ti-6Al-4V titanium alloy production include porosity, inclusions, cracks, surface and subsurface defects, which define the irregularities or imperfections of the material surface which hampers the appearance, roughness, and performance of the product. Hence, detecting and evaluating any defect in real-time within the manufactured titanium-based alloy material is crucial to ensure the quality and reliability of the final product formed before its usage in various application domains [1-6].

For the purpose of defect detection via a non-destructive, non-contact, and real-time testing methodology without damaging or affecting the material properties, several common non-destructive testing (NDT) techniques are being employed widely for characterizing Ti-6Al-4V titanium alloy [1, 2]. These techniques include: X-ray radiography [1, 2], ultrasonic testing [3], eddy current testing [4], and magnetic particle testing [5]. In the last few decades, infrared thermographic testing [7-19] has emerged as a potent and reliable defect detection modality in various industrial and medical sectors. Infrared thermography is a rapidly emerging technique which evaluates a rapid and real-time defect detection by observing the thermal inhomogeneities within the testing material. The presence of thermal inhomogeneities causes in the disturbances in the surface bounded thermal propagation and impedes the diffusion of heat across the material to identify defects such as cracks, voids, inclusions, or delamination. This ultimately results in the temperature variation over the defective surface in comparison to that observed for the non-defective region of the material. This type of temperature contrast is observed directly by the infrared camera at precise locations of the material being monitored. Various conventional thermographic techniques are used for defect detection in titanium alloys, which include pulsed thermography (PT) [7-13], lock-in thermography (LT) [14-16], and Pulse phase thermography (PPT) [17-19]. Each technique has its advantages and limitations.

Pulse thermography provides better resolution and is a fast technique because short-duration high peak power is utilized in this technique to experiment. So, to acquire higher resolution and probe a high band of frequencies in the test specimen, high peak power heat sources are required, which is the main limitation of pulse-based thermographic techniques (PT and PPT). On the contrary, in lock-in thermography, there is no such requirement for high peak power sources, but due to the fixed frequency used in the sinusoidal excitation limits the depth resolution. This can be improved by repeating experimentation, which is time-consuming [7-19]. So, to overcome all the limitations associated with these conventional thermographic techniques (PT, LT, and PPT), the current work highlights the defect detection capability of barker-coded thermal wave imaging (BCTWI) modality [20-22]. This has been followed up by modeling a numerical model of Titanium alloy Ti-6Al-4V with 25 flat bottom holes under adiabatic boundary conditions with constant initial conditions. The 7-bit Barker coded thermal excitation is used to illuminate the sample surface, and a corresponding thermal pattern has been recorded. This recorded data is then processed with the frequency and time domain-based data processing approaches to analyse the proposed technique's subsurface defect detection capability. Further, the defect depth scanning capability of the proposed scheme is illustrated by considering the time domain correlation coefficient as a figure of merit.

2 Theory

2.1 Barker coded excitation

Compared to other modulation methodologies, the Barker-coded method is the most straightforward binary phase code, with the least compression side lobes. Moreover, this code's autocorrelation feature provides a proportionate compression ratio to the code's length. However, choosing the correct code length requires balancing the time needed for experimentation and the requirement for side lobe minimization. In thermography, lengthy testing reduces the technique's advantages, but shorter experiments may require high peak power heat sources. The best solution, thus, is achieved by using an appropriate code length and experimental period. This current study emphasizes the suggested technique's detection capabilities using a 7-bit code length that provides the lowest compression ratio of any other code length, as shown in figure.1 [20-22].

2.2 Coded excitation thermal waves solution for a finite system:

To study the thermal waves generated by the incident-coded excitation are analysed by a one-dimensional Fourier heat equation given as follows [23-27]:

$$\frac{\partial^2 U(x,t)}{\partial x^2} - \frac{1}{\alpha}\frac{\partial U(x,t)}{\partial t} = 0 \qquad (1)$$

where, $z_1, z, z_2;\ \ \tau > 0$

where $U(x,\tau)$ temporal thermal distribution over the test specimen surface at location x at time t; Specimen thermal diffusivity has been represented by $\alpha = (k/\rho c)$; k -Thermal conductivity; ρ - Specimen Density; c - Specific heat of the specimen.

The temporal thermal distribution over the test specimen surface (at $x=0$) is obtained by solving Eq. (1) under the 7-bit Barker coded excitation with a peak power Q_o (figure.1) with adiabatic boundary conditions and constant initial conditions. The current excitation used for this thermographic study is the measure of the combination of delayed step responses which can be defined as follow [20-22]:

$$Q = Q_o \sum_{i=1}^{4} (-1)^{n_i}\, u(t - a_i T) \qquad (2)$$

where $n_i = 0,\ 1,\ 2,\ 3;\ a_i = 0,\ 3,\ 5,\ 6.$

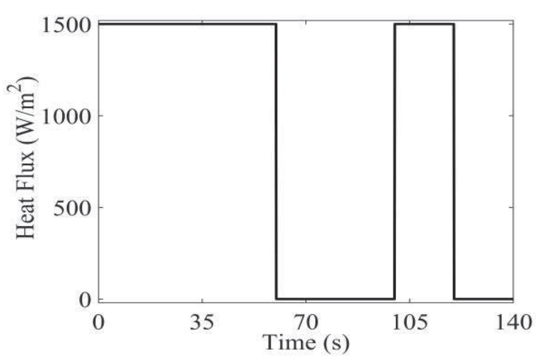

Fig.1 7-bit Barker coded thermal wave excitation used the numerical studies for defect detection in Ti-6Al-4V

Q -Thermal heat flux (W/m2); Q_o -Peak power of the heat flux (W/m^2); t -time (s); T - Total duration of the heat flux (s).

Boundary conditions at $x = L$ [23-27]:

$$Q(L,t) = -k\frac{\partial U(x,t)}{\partial x} = 0 \qquad (3)$$

Initial condition: *when*; $0 \le x \le L;\ t = 0$ [23-27]:

$$U(x,0) = U(x) = U_o = 293.15\ \mathrm{K} \qquad (4)$$

The above Eq. (1) can be solved using Green's function approach for adiabatic boundary condition (presented by Eq. (2) and Eq. (3)) and constant initial condition (Eq. (4)). The overall obtained solutions can be written as [23-27]:

$$U(x,t) = U_o + \left(\frac{Q_o\alpha}{kL}\right)\sum_{i=1}^{4}\left[(-1)^{n_i}(t - a_i T)\,u(t - a_i T)\right] + \left(\frac{2Q_o}{kL}\right)\sum_{m=1}^{\infty}\left[\sum_{i=1}^{4}\left[\frac{(-1)^{n_i}}{\lambda_m^2}\mathrm{Cos}(\lambda_m x)\left(1 - e^{-\alpha\lambda_m^2(t - a_i T)}\right)u(t - a_i T)\right]\right] \qquad (5)$$

where Eigenvalues - $\lambda_m = (m\pi/L)$; L- Specimen thickness; U_o -Initial temperature of the specimen

temporal thermal variation so depicted as a function of the hidden anomaly and the applied thermal excitation. The findings show that even with low peak power excitation sources, this thermographic technique with time-domain pulse compression approaches improves resolution compared to frequency domain approaches and results from high peak power, short duration pulsed excitation.

3 Pulse Compression Approaches for BCTWI Technique

By boosting the SNR of the response signals, time domain pulse compression of coded modulated signals via matched filtering, as employed in radar systems, improves the range resolution and sensitivity to offer improved subsurface fault identification even in randomly noisy situations. Depending on the temporal delay between the signals utilized, it focuses the energy that results from the application into a pseudo pulse whose peak concentrates at a delayed instant. As a result, new insight for coded modulation approaches was gained by probing via low peak powers and focusing energy in the main lobe similar to pulsed-based excitation schemes [28].

3.1 Frequency Domain Analysis

Fast Fourier Transform has been executed on the captured temporal thermal signature over the sample surface pixel by pixel for each pixel $g(x)$ in the field of view, as shown below [18, 19, 28].

$$Z(\omega) = \frac{1}{n}\sum_{i=0}^{n-1} g(x)\ e^{\left[\frac{-j2\pi\omega x}{n}\right]} = Re(\omega) + j\,Im(\omega) \qquad (6)$$

where, $R(\omega)$ is the real and $\mathrm{Im}(\omega)$ is imaginary parts of the Fast Fourier Transformed thermal data □ (ω); x represents the image sequence index.

Then, these obtained real and imaginary components of this FFT data of the captured thermal signature as shown in Eq. (6) can be utilized for the reconstruction of the phase images (Figure.2) as follow [19, 28]:

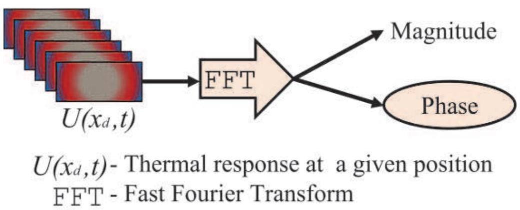

Fig.2 The frequency domain processing approach flow chart adopted for construction of frequency domain phasegrams.

$$\varphi(\omega)=\mathrm{Tan}^{-1}\left(\frac{\mathrm{Im}(\omega)}{\mathrm{Re}(\omega)}\right) \tag{7}$$

3.2 Time Domain Analysis

The Hilbert transform (HT) analysis has been utilized to recover the time domain temporal temperature distribution's correlation coefficient and phase profiles [28-29]:

$$\mathtt{HT}(t)=\frac{1}{\pi}\int_{-\infty}^{\infty}\frac{U(x_r,\tau)}{t-\tau}d\tau \tag{8}$$

where, $U(x_r,\tau)$ is the selected reference thermal signal for the analysis. Then by utilizing the inverse fast Fourier transform (IFFT) properties, the cross-correlation coefficient (Figure.3) has been calculated as follows [29]:

$$\textit{Correlation coefficient}$$
$$(CC)\ =\mathtt{IFFT}\left\{U(x_r,\omega)^{*}U(x_d,\omega)\right\} \tag{9}$$

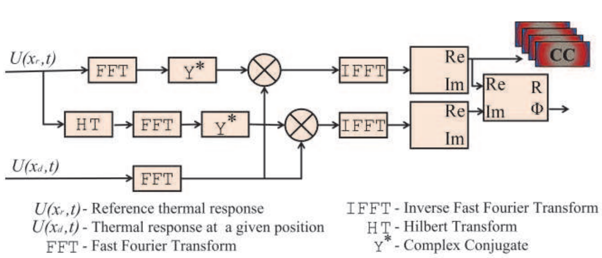

Fig.3 Time domain processing approach flow chart adopted for construction of pulsed compressed correlation profiles and phasegrams

where $U(x_r,\omega)$ and $U(x_d,\omega)$ represent the Fourier transforms of the chosen reference thermal response and the temporal thermal response at a defect location, respectively. The time domain phase (Figure.3) has been reconstructed as follows by using the Fourier analysis [28, 29]:

$$\Phi=\mathrm{Tan}^{-1}\left(\frac{\mathtt{IFFT}\left\{\mathtt{HT}\,(\omega)^{*}U(x_d,\omega)\right\}}{\mathtt{IFFT}\left\{U(x_r,\omega)^{*}U(x_d,\omega)\right\}}\right) \tag{10}$$

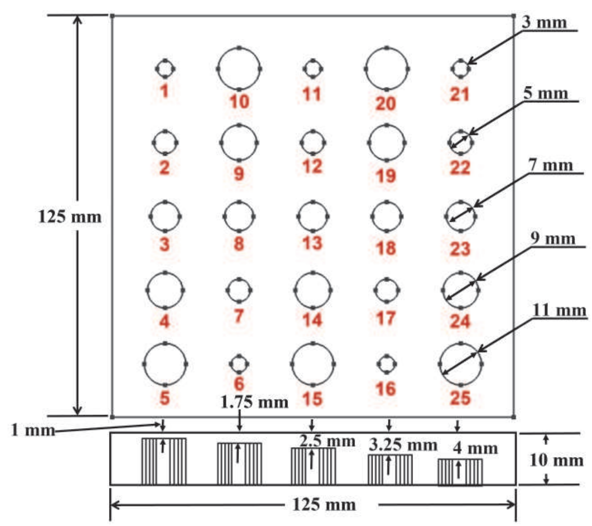

Fig.4 Schematic of modeled Titanium alloy Ti-6Al-4V with 25 flat bottom holes (FBH) used for defect detection analysis of BCTWI technique

Table.1 Thermal properties for Titanium alloy (Ti-6Al-4V) [1-6, 30]

Density (ρ) (kg/m^3)	**Specific heat capacity (C_p) (J/kg-K)**	**Thermal Conductivity (k) (W/m-K)**	**Thermal Diffusivity (α) (m^2/s)**
4512	570	7.3	2.8384 0^{-6}

4 Numerical Modeling and Simulation

A Titanium alloy (Ti-6Al-4V) specimen (Figure.4) with dimensions of 125×125×10 mm containing twenty-five flat bottom hole defects was modeled and simulated for this investigation. The diameters of the modeled flat bottom holes are 3, 5, 7, 9, and 11 mm, respectively, which are at depths of 1, 1.75, 2.5, 3.25, and 4 mm for each diameter from the front surface of the test specimen (descripted in table.1). Figure.4 shows the schematic of this modeled test specimen with its specified dimensions. Table.1 summarizes the thermophysical parameters of the investigated model. Then the numerical simulation studies had performed using finite element modeling and assessment software COMSOL Multiphysics with the heat transfer module in the solids. The modeled specimen consists of a finer mesh size with tetrahedral-shaped elements. The mesh comprises 96,775 domain elements, 16,918 boundary elements, and 1,679 edge elements.

Table.2 Description of flat bottom hole defects in modeled sample

Flat Bottom Hole (FBH) Diameters in millimetre	**Flat Bottom Hole (FBH) Numbers as Mention in the figure.4**				
	Defect depth (H) from specimen surface at: H1 = 1 mm	**H2 = 1.75 mm**	**H3 = 2.5 mm**	**H4 = 3.25 mm**	**H1 = 4 mm**
3 mm	1	6	11	16	21
5 mm	2	7	12	17	22
7 mm	3	8	13	18	23
9 mm	4	9	14	19	24
11 mm	5	10	15	20	25

Further, the specimen surface was exposed to Barker Coded thermal excitation (Figure.1) at 1500 W/m^2 for 140 seconds. Then the corresponding thermal signatures were recorded. These thermal data have been then processed with the time domain pulse compression-based data processing approaches to analyse the defect detection capability of the BCTWI technique in the Titanium alloy (Ti-6Al-4V).

5 Results and Discussions

A numerical simulation has been conducted to validate the defect detection capability of the purposed Barker-coded thermal wave imaging (BCTWI) modality in titanium-based alloys (Ti-6Al-4V). There are 25 flat bottom holes (FBH) modeled in the test specimen with different diameters at different depths, as shown in figure.4. Table 1 presents the thermophysical properties of the modeled titanium alloy specimen, Ti-6Al-4V. Subsequently, the Barker-coded excitation (Figure.1) was used to illuminate the sample's surface for 140 seconds.

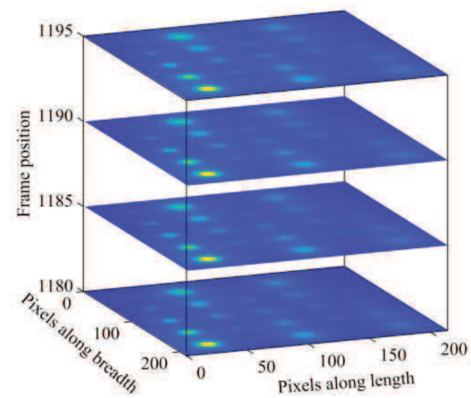

Fig.5 Raw temporal thermal profiles captured over the specimen surface

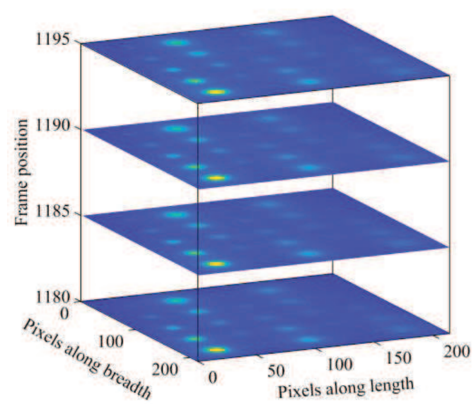

Fig.6 Raw temporal thermal profiles with added Additive White Gaussian Noise (AWGN) with an SNR of 20 dB

The resulting temporal thermal variation across the specimen surface was recorded at a frame rate of 20 Hz. These findings have presented in figure.5. The recorded raw thermal data was intentionally subjected to Additive White Gaussian Noise (AWGN) with an SNR of 20 dB to assess the suggested approach's detection potential under real-time conditions. The resulting noisy temporal thermal data (as shown in figure.6) is then processed using an appropriate polynomial fit of the first order to produce zero mean temporal thermal data. It is clear from the obtained fitted raw thermograms with added noise that the defects detectability at various depths of varying diameters is very difficult due to the insufficient thermal contrast provided over modeled specimen surface. Post-processing approaches such as frequency and time domain are employed to analyse this processed data.

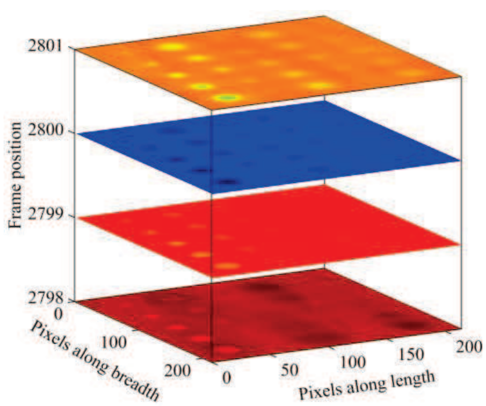

Fig.7 Schematic of phasegrams obtained using frequency domain analysis

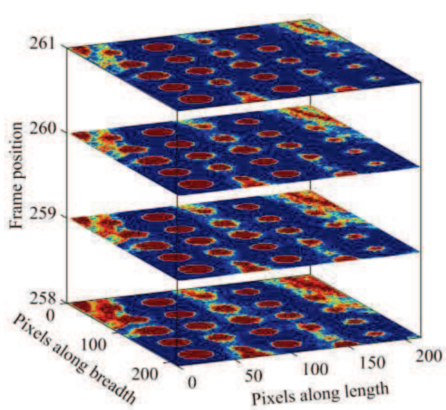

Fig.8 Schematic of phasegrams obtained using time domain analysis

Figure.7 shows the obtained frequency domain phase profiles constructed for different frames. The generated frequency domain phasegrams offer poor contrast over the test specimen surface and are not significant enough to reveal the defects at various depths with varying diameters.

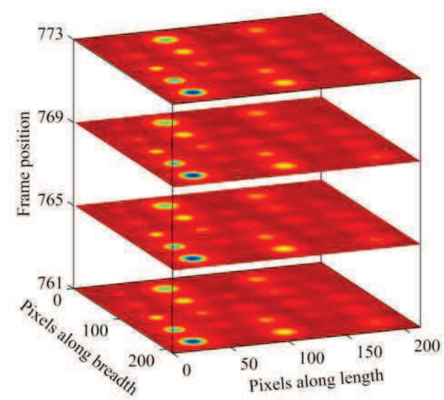

Fig.9 Schematic of correlation profiles obtained using matched filtered data processing approaches in time domain analysis

Further, figure.8 depicts the time-domain phasegrams obtained at different time steps using a cross-correlation-based post-processing approach. In contrast to this, figure.9 illustrates the constructed correlation coefficient profiles at different time instants from the matched filter-based data post-processing approach. The obtained time domain phase and correlation images show a noticeable contrast improvement in defect detection using the Barker-coded thermal wave imaging for the adopted time domain-based data processing methodologies.

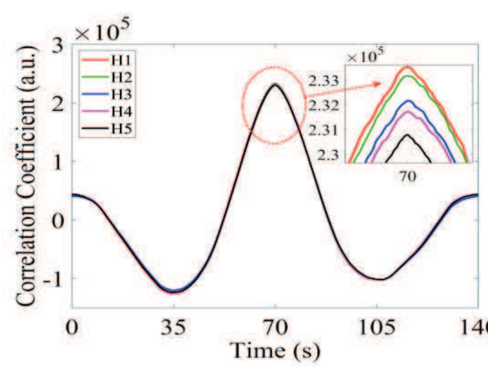

Fig.10a Single-pixel pulse compressed time domain correlation profiles for varying defects depths (H1, H2, H3, H4, and H5) as shown in Table.2 for 3 mm defect diameter

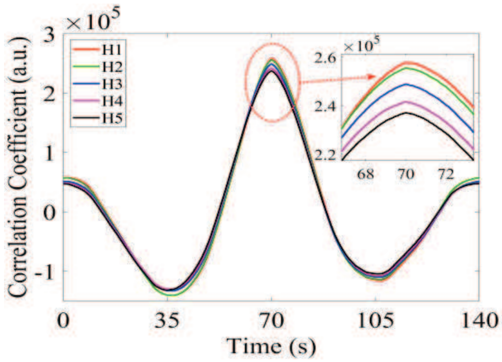

Fig.10b Single-pixel pulse compressed time domain correlation profiles for varying defects depths (H1, H2, H3, H4, and H5) as shown in Table.2 for 5 mm defect diameter

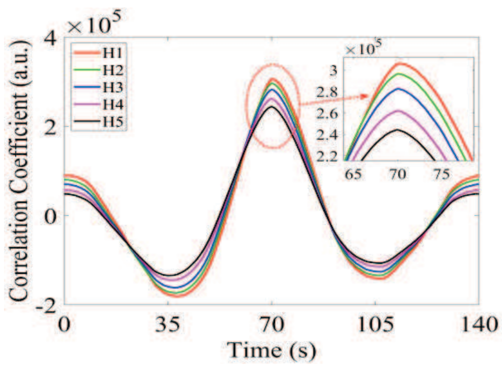

Fig.10c Single-pixel pulse compressed time domain correlation profiles for varying defects depths (H1, H2, H3, H4, and H5) as shown in Table.2 for 7 mm defect diameter

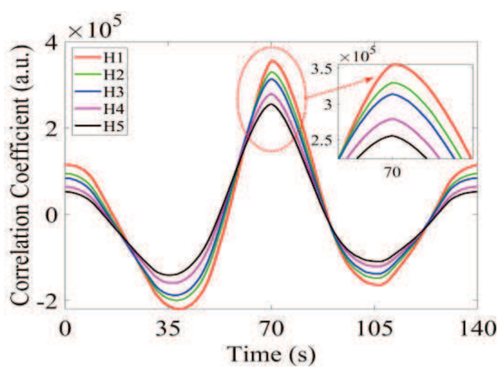

Fig.10d Single-pixel pulse compressed time domain correlation profiles for varying defects depths (H1, H2, H3, H4, and H5) as shown in Table.2 for 9 mm defect diameter

In addition, the single-pixel correlation coefficient profiles at the defect's centre shown in figure.10a, figure.10b, figure.10c, figure.10d, and figure.10e for the defect diameters 3 mm, 5 mm, 7 mm, 9 mm and 11 mm, respectively (pattern of the defects listed in

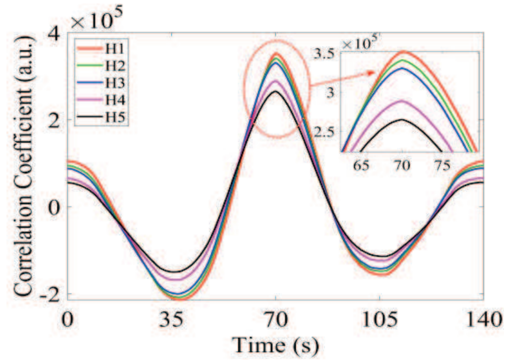

Fig.10e Single-pixel pulse compressed time domain correlation profiles for varying defects depths (H1, H2, H3, H4, and H5) as shown in Table.2 for 11 mm defect diameter

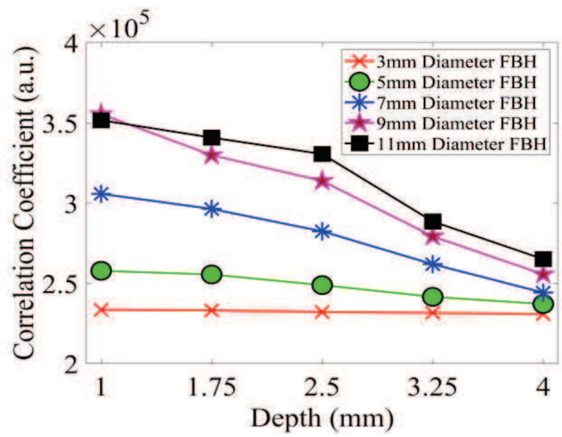

Fig.11 Schematic of time domain correlation coefficient versus defect depths in modeled Titanium alloy Ti-6Al-4V specimen for different defect diameters.

table.2). These computed single-pixel correlation profiles reveal that shallow depths have larger values than deeper depths. To examine the defect scanning capabilities of BCTWI modality employing matched filter-based data post-processing, the obtained single-pixel time-domain correlation coefficient values are plotted with regard to depths of defects of various sizes as shown in figure.11. The defects depth parameter presents over the x-axis, in contrast, the correlation coefficient standards over the y-axis as plotted in figureg.11. The correlation values show a monotonically declining trend as the depth of the defect from the sample surface increases for all faults with varied sizes. Hence, it can be concluded that the pulse compression-based time domain correlation approach is significant in the defect depth estimation in the Titanium alloy Ti-6Al-4V with the BCTWI technique.

6 Conclusions

Subsurface defect detection and estimation capability of the proposed Barker-coded thermal wave excitation has been presented for Titanium alloy Ti-6Al-4V. The results show that the suggested excitation approach with time domain correlation and phase-based data processing surpasses frequency domain-based phase analysis in terms of defect identification by producing the better thermal contrast in time domain. The results demonstrated that most of the energy focused in the main lobe creates a pseudo pulse through correlation, which improves defect detection in the correlation profiles. This approach also delivers improved defect depth resolution even with low peak power heat sources and a shorter code length. Furthermore, significant defects providing better thermal contrast, like phase contrast in time domain phase analysis, have also been observed.

7 References

[1] Dieter, G. E. (1986), "Mechanical Metallurgy", McGraw-Hill Book Company, New York, NY, USA

[2] Davis, J. R. (2003), "Handbook of Materials for Aerospace Engineering", Butterworth-Heinemann, Oxford, UK

[3] Gittos, M. F., & Smith, R. C. (1984), "Ultrasonic detection of defects in titanium alloys", Ultrasonics, 22(1), 11-19

[4] Evans, R. D., & Halbig, M. C. (1998), "Eddy current testing of titanium alloys", Materials Evaluation, 56(9), 1052-1056

[5] Bollinger, R. A., & McQuaid, R. A. (1983), "Magnetic particle inspection of titanium alloys", Materials Evaluation, 41(3), 342-345

[6] Lee, C. H., Lee, K., & Lee, S. H. (2018), "Nondestructive testing of titanium and titanium alloys", Metals, 8(7), 523

[7] Maldague, X. P. V. (2001), "Theory and practice of infrared technology for nondestructive testing", John Wiley & Sons

[8] Bahrami, M., & Bakhtiari-Nejad, F. (2013), "Applications of infrared thermography in nondestructive evaluation of materials: A review article", Journal of Nondestructive Evaluation, 32(2), 89-103

[9] Salazar, A., & Díaz, A. (2015), "Thermography as a non-destructive testing tool", Infrared Physics & Technology, 70, 28-47

[10] Fernández, F. F., López-Higuera, J. M., & Salgado, J. A. (2015), "Application of infrared thermography for defect detection in aerospace structures", Sensors, 15(9), 23549-23578

[11] Sakagami, T., and Kubo, S. (2002), "Applications of pulse heating thermography and lock-in thermography to quantitative non-destructive evaluations", Infrared Physics and Technology, vol. 43, no. 3-5, pp. 211-218

[12] Rosencwaig, A, (1982), "Thermal-wave imaging", Science, vol. 218, no. 4569, pp. 223-228

[13] Busse, G., and Eyerer, P. (1983), "Thermal wave remote and nondestructive inspection of polymers", Applied Physics Letters, vol. 43, no. 4, pp. 355-357, DOI: 10.1063/1.94335

[14] Dillenz, A., Zweschper, T., Riegert, G., and Busse, G. (2003), "Progress in phase angle thermography", Review of Scientific Instruments, vol. 74, no. 1 II, pp. 417-419

[15] Peng, D., and Jones, R. (2013), "Modelling of the lock-in thermography process through finite element method for estimating the rail squat defects", Engineering Failure Analysis, vol. 28, pp. 275-288

[16] Yang, R., and He, Y. (2016), "Optically and non-optically excited thermography for composites: A review", Infrared Physics & Technology, vol. 75, pp. 26-50

[17] Vavilov, V. P., and Marinetti, S.(1999), "Pulsed phase thermography and fourier-analysis thermal tomography", Russian Journal of Nondestructive Testing, vol. 35, no. 2, pp.134-145

[18] Maldague, X., and Marinetti, S. (1996), "Pulse phase infrared thermography", Journal of Applied Physics, 79 (5), pp. 2694- 2698

[19] Maldague, X., Galmiche, F., and Ziadi, A. (2002), "Advances in pulsed phase thermography", Infrared Physics and Technology, vol. 43, no. (3-5), pp. 175-181

[20] Mulaveesala, R., & Venkata Ghali, S. (2011), "Coded excitation for infrared non-destructive testing of carbon fiber reinforced plastics", Review of Scientific Instruments, 82(5), 054902

[21] Ghali, V.S., Panda, S.S.B., Mulaveesala, R. (2011), "Barker coded thermal wave imaging for defect detection in carbon fbre-reinforced plastics, Insight: Non-Destructive Testing & Condition Monitoring, vol. 53, No 11, pp. 621-624

[22] Dua, G., and Mulaveesala, R. (2013), "Applications of Barker coded infrared imaging method for characterisation of glass fibre reinforced plastic materials", Electronics Letters, 49 (17), pp. 1071-1073

[23] Carslaw, H. S., and Jaeger, J. C. (1959), "Conduction of Heat in Solids. Oxford Clarendon Press", London

[24] Özısık, M. N. (1993), "Heat conduction", John Wiley & Sons

[25] Sharma, A., Mulaveesala, R., Dua, G. and Kumar, N. (2020), "Linear frequency modulated thermal wave imaging for estimation of osteoporosis: An analytical approach", Electronics Letters, vol., 56, no. 19, pp. 1007-1010, doi: 10.1049/el.2020.0671

[26] Sharma, A., Mulaveesala, R., Dua, G., Arora, V. and Kumar, N. (2021), "Digitized Frequency Modulated Thermal Wave Imaging for Detection and Estimation of Osteoporosis", IEEE Sensors Journal, Article vol. 21, no. 13, pp. 14003-14010, Art. no. 9286563

[27] Sharma, A., Mulaveesala, R., and Arora, V. (2020), "Novel analytical approach for estimation of thermal diffusivity and effusivity for detection of osteoporosis", IEEE Sensors Journal, 20(11), pp. 6046-6054, doi:10.1109/JSEN.2020.2973233

[28] R Mulaveesala, J S Vaddi and P Singh (2008), "Pulse compression approach to infrared non-destructive characterisation", Review of Scientific Instruments, 79 (9), art no 094901

[29] N Tabatabaei, A Mandelis and B T Amaechi (2011), 'Thermophotonic radar imaging: an emissivity-normalised modality with advantages over phase lock-in thermography", Applied Physics Letters, 98 (16), art no 163706

[30] Sharma, A., Dua, G., Arora, V., Kumar, N., Mulaveesala, R. (2022), "A Novel Analytical Approach for Nondestructive Testing and Evaluation of Bone Implants Using Frequency Modulated Thermal Wave Imaging", Lecture Notes in Mechanical Engineering, pp. 273–285

Numerical Approach for Characterization of Structural Steel Sample using Frequency Modulated Thermal Wave Imaging

Vanita Arora[1], Ravibabu Mulaveesala[2], Anshul Sharma[2], Geetika Dua, Suresh Kumar Bhambhu[2]

[1]Indian Institute of Information Technology Una, Vill. Saloh, Teh. Haroli, Distt. Una Himachal Pradesh, India-177209.
[2]InfraRed Imaging Laboratory (IRIL) Laboratory, Centre for Sensors, Instrumentation and cyber-physical Systems Engineering (SeNSE), Indian Institute of Technology Delhi, Hauz Khas, New Delhi-110016, India
[3]Thapar Institute of Engineering and Technology, Patiala.147004
[a]*Email: mulaveesala@sense.iitd.ac.in*

Abstract

This work demonstrates a finite element analysis based modeling and simulation study for finding out the defect detection capabilities of frequency modulated thermal wave imaging technique. A structural steel specimen with hidden subsurface slags and inclusions such as calcium fluoride, silicon dioxide and air of various sizes and shapes, is considered. Pulse compression based correlation processing scheme is adopted on the generated temporal temperature data and comparisons have been made with the conventional widely used frequency domain phase based approach.

Keywords: *Non-destructive testing; Phase analysis; Frequency modulated thermal wave imaging; Finite element analysis*

1. Introduction

Over the years, Thermal Wave Imaging (TWI) is intensively used for the characterization of various solid materials due to its inherent merits like non-destructive, non-contact, rapid and full-field inspection capabilities[1-5]. In active TWI approach, the test object is thermally stimulated to generate heat flow within it. The presence of defects within the material alters heat flow, causing thermal contrast over it, which can be monitored using infrared camera. Based on the shape of applied heat flux on to the test sample, these thermograhic methods are named either as Pulse (Pulsed Thermography (PT), Pulsed Phase Thermography (PPT), Step Thermography (ST)) or modulated thermographic methods (mono-frequency sinusoidal Lock-in Thermography (LT)) [6-11]. The requirement of high peak power heat sources in case of pulse based techniques and limited depth resolution in a single experimentation cycle in LT are the key issues. Further various research groups all over the world are working on modulated non-stationary transient thermographic techniques such as Frequency Modulated Thermal Wave Imaging (FMTWI), Digitized Frequency Modulated Thermal Wave Imaging (DFMTWI), Barker Coded Thermal Wave Imaging (BCTWI), Golay Coded Thermal Wave Imaging (GCTWI), etc. to overcome these constraints and also on various data processing schemes to improve test resolution and sensitivity [12-18].

This paper describes the application of Finite Element Analysis (FEA) approach for the assessment of a structural steel sample having defects of different shapes such as circular, square and triangular, using FMTWI. This method employs a pre-determined band of frequencies decided by sample thermal properties and its thickness. Hence the whole sample can be inspected in a single run using relatively moderate peak power heat sources in a limited span of time. In simulation, three types of inclusions are incorporated as defects of various shapes at a given depth inside the test sample. Further, in order to test the capabilities of FMTWI, frequency domain based phase and correlation based analysis schemes are carried out on the resultant temporal thermal response.

2. Theory

Heat flux incident onto the test sample generates thermal waves which propagate into the sample by diffusion. The presence of surface and sub-surface defects modify the heat flow, producing thermal gradients over the test sample. The resultant temperature response for a given incident heat flux can be obtained from 1D heat diffusion equation in the absence of any heat source and sink as follows [19]:

$$\frac{\partial^2 T(x,t)}{\partial x^2} = \frac{1}{\alpha}\frac{\partial T(x,t)}{\partial t} \tag{1}$$

where $T(x,t)$ is the temperature at a given depth x at a time instant t and α is the thermal diffusivity of the sample being inspected. The thermal diffusion length for the temperature variations due to a linear frequency modulated heat flux incident onto a semi-infinite solid is expressed as follows:

$$\mu = \sqrt{\frac{\alpha}{\pi\left(f+\frac{Bt}{\tau}\right)}} \tag{2}$$

where f is the initial frequency, B is the bandwidth and τ is the total duration of excitation. The thermal diffusion length determines the decay of thermal wave as it penetrates through the material. The dependence of diffusion length on the slope of time frequency response (B/τ) of applied stimulus assures complete sample depth scanning.

The presence of subsurface defects can be identified either by conventional frequency domain based phase approach or recently proposed correlation coefficient based approach as shown in Fig.1 and 2 respectively.

2.1 Frequency Domain Phase Analysis

In this method, one-dimensional Fast Fourier Transform (FFT) is considered to compute the phase angle of captured temporal thermal profile of each pixel $f(t)$ (where t is the index in image sequence of length N) [20]:

$$F(u) = \frac{1}{N}\sum_{t=0}^{N-1} f(t)\, e^{\left[\frac{-j2\pi ut}{N}\right]} = R(u) + jI(u) \tag{3}$$

where $R(u)$ and $I(u)$ are the real and imaginary components of $F(u)$ respectively. Then the phase angle corresponding to different frequencies is determined using:

$$\emptyset\,(u) = tan^{-1}\left(\frac{I(u)}{R(u)}\right) \tag{4}$$

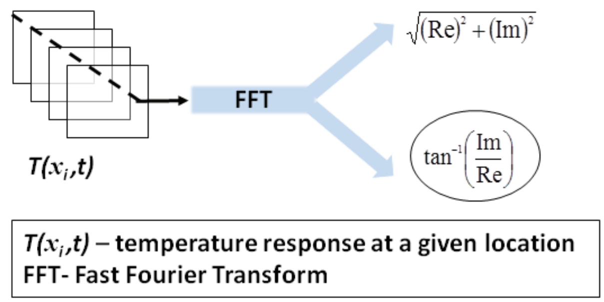

Fig.1 Data processing approach adopted for the construction of frequency domain based phasegrams

2.2 Correlation Coefficient Based Analysis

In this approach, data analysis is carried out to achieve pulse compression in order to reconstruct the correlation coefficient images of the captured temporal thermal sequence as follows [20]:

$$Correlation\ coefficient\ (CC) = IFFT\{T(x_r,\omega)^*\ T(x_i,\omega)\} \tag{5}$$

where $T(x_r,\omega)$ and $T(x_i,\omega)$ are the Fourier transforms of thermal profiles at reference location and at a given location respectively.

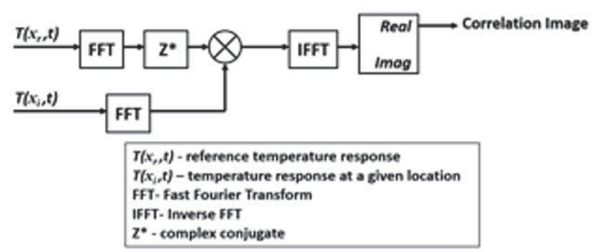

Fig.2 Data processing approach adopted for the construction of correlation coefficient based images

3. FEA Modeling

A FEA model has been developed using the heat transfer module in Comsol Multiphysics version 4.2. The details of the model and simulation parameters are given below.

<u>*Model Geometry*</u>
Numerical analysis is carried out on a structural steel sample of thickness 7 mm, of 100×110 mm lateral dimensions, containing circular, square and triangular shape defects located at a depth of 0.3 mm from the front surface of the sample. The defect thickness is 5.7 mm. The dimensional layout of the simulated sample is as shown in Fig.3. The first row containing all the three different shape defects is filled with air, whereas

second and third rows are filled with silicon dioxide and calcium fluoride respectively, to simulate artificial inclusion and slag.

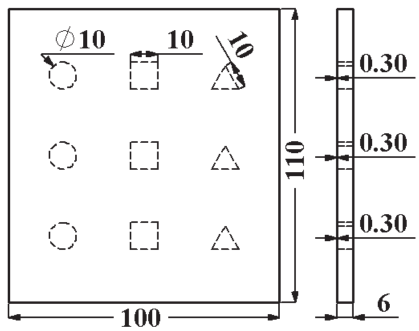

Fig.3 Schematic layout of simulated structural steel sample (all dimensions are in mm)

Sample Parameters and Mesh
The model geometry is discretized with a finer mesh using 38133 tetrahedral elements. Table.1 summarizes the parameters used for the test sample.

Table.1 Parameters used for the test sample

Material	**Thermal Conductivity** k $[W/(m \cdot K)]$	**Heat Capacity** C_p $[J/(Kg \cdot K)]$	**Density** ρ $[Kg/m^3]$
Structural steel	44.5	475	7850
Air	0.0258	1005.4	1.0215
Silicon dioxide	1.5	730	2650
Calcium Fluoride	9.71	854	3180

4. Numerical Results

The simulations are performed by imposing linear frequency modulated heat flux of 200 W/m^2 with frequency sweep of 0.01 to 0.11 Hz in a time span of 100 s. The temperature map over the sample is recorded at a frame rate of 20 Hz. The mean rise in temporal thermal profile of each pixel is removed by proper polynomial fit. The frequency domain phase and correlation information is then calculated from mean removed thermal data. Figure 4(a)-(d) show the depth scanning performance obtained from frequency domain phase images for four different cross–sectional views.

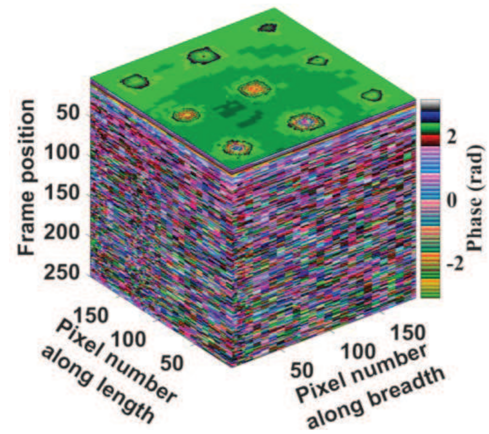

(a)

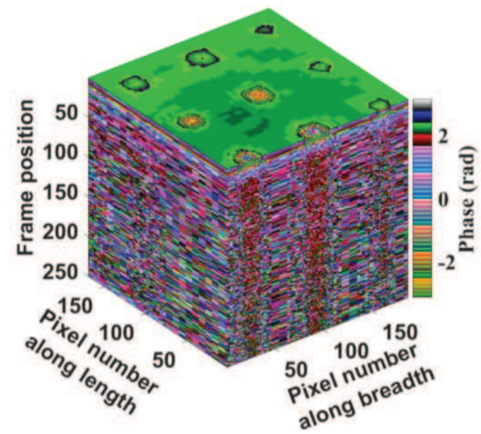

(b)

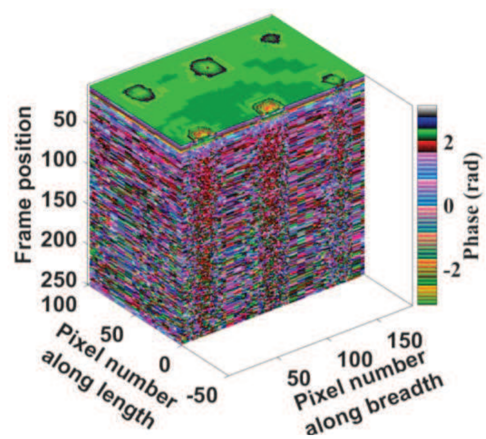

(c)

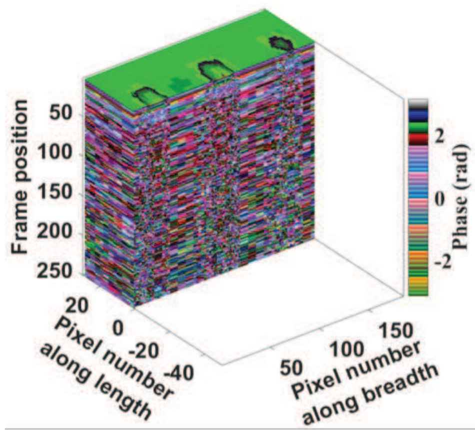

(d)

Fig.4 Depth scanning performance obtained from frequency domain phase analysis

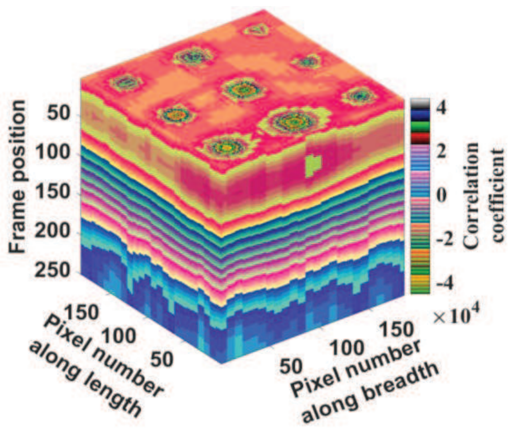

(a)

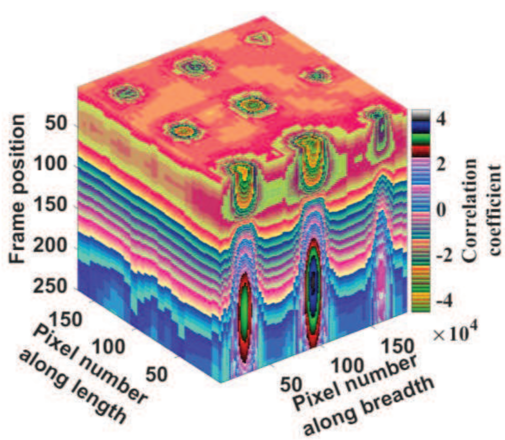

(b)

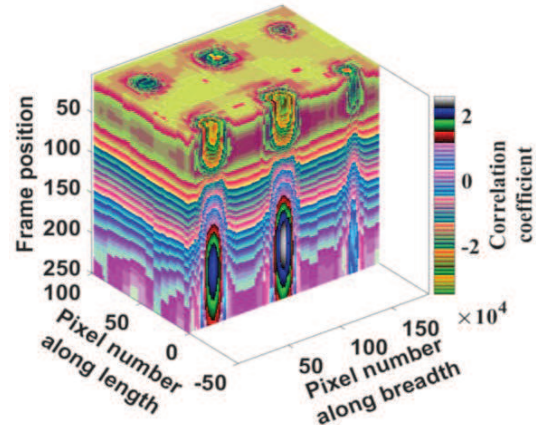

(c)

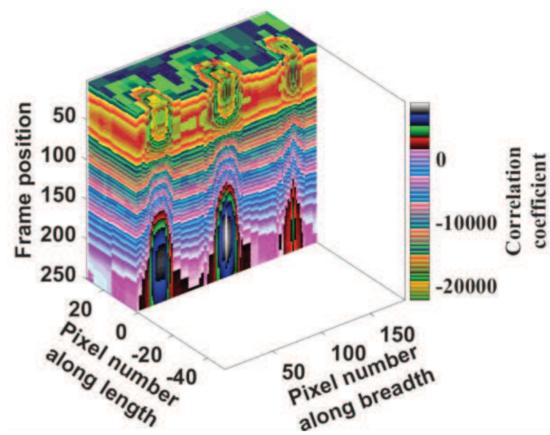

(d)

Fig.5 Depth scanning performance obtained from correlation coefficient images

whereas Figure 5(a)-(d) show the depth scanning performance obtained from correlation coefficient images for four different cross–sectional views.

The results demonstrate that correlation coefficient approach show better detectability for revealing sub-surface anomalies over the frequency domain phase images. The enhanced detection capabilities provided by correlation based processing scheme are due to its inherent potential capabilities like concentration of energy into a very narrow duration pulse and immunity to random noise.

5. Conclusions

This paper highlights the capabilities of correlation based approach for defect detection in structural steel sample. This method provides better detection capabilities than that of frequency domain based phase approach. This technique utilizes the merits of matched filter based pulse compression process which is immune to random noise makes this approach more robust than that of conventional frequency domain phase approach.

6. References

[1] Maldague, X.P.V. Theory and Practice of Infrared Thermography for Nondestructive Testing. New York: Wiley, 2001.

[2] Avdelidis, N. P., C. Ibarra-Castanedo, X. Maldague, Z. P. Marioli-Riga, and D. P. Almond, "A thermographic comparison study or the assessment of composite patches," Infrared Physics & Technology, Vol. 45, No. 4, 291-299, 2004.

[3] Maldague, X. and S. Marinetti, "Pulse phase infrared thermography," Journal of Applied Physics, Vol. 79, No. 5, 2694-2698, 1996.

[4] Avdelidis, N. P., C. Ibarra-Castanedo, X. Maldague, Z. P. Marioli-Riga, and D. P. Almond, "A thermographic comparison study or the assessment of composite patches," Infrared Physics & Technology, Vol. 45, No. 4, 291-299, 2004.

[5] Liu, J. Y., W. Yang, and J. M. Dai, "Research on thermal wave processing of lock-in thermography based on analyzing image sequences for NDT," Infrared Physics & Technology, Vol. 53, No. 5, 348-357, 2010.

[6] Rosencwaig, A., “Thermal-wave imaging,” Science, Vol. 218, No. 4569, 223-228, 1982.

[7] Busse, G, and, P. Eyerer, “Thermal wave remote and nondestructive inspection of polymers,” Applied Physics Letters, Vol. 43, No. 4, 355-357,1983.

[8] Busse, G., D. Wu, and W. Karpen, "Thermal wave imaging with phase sensitive modulated thermography," J. Appl. Phys., Vol. 71, No. 8, 3962-3965, 1992.

[9] Meola, C., Carlomagno, G.M., Squillace, A., Giorleo, G, “Non-destructive control of industrial materials by means of lock-in thermography” Measurement Science and Technology, Vol. 13, No.10, 1583-1590, 2002.

[10] Dillenz, A., Zweschper, T., Riegert, G, and Busse, G, “Progress in phase angle thermography” Review of Scientific Instruments, Vol. 74 No. 1, 417-419, 2003.

[11] Peng, D, and R, Jones, “Modelling of the lock-in thermography process through finite element method for estimating the rail squat defects,” Engineering Failure Analysis, Vol. 28, 275-288, 2013.

[12] Mulaveesala, R. and S. Tuli, "Theory of frequency modulated thermal wave imaging for nondestructive subsurface defect detection," Appl. Phys. Lett., Vol. 89, 191913, 2006.

[13] Ghali, V. S. and N. Jonnalagadda R. Mulaveesala, "Three dimentional pulse compression for infraed non destructive testing," IEEE Sensors, Vol. 9, No. 7, 832-833, 2009.

[14] Tabatabaei, N. and A. Mandelis, "Thermal-wave radar: A novel subsurface imaging modality with extended depth-resolution dynamic range," Rev. Sci. Instru., Vol. 80, No. 3, 034902, 2009.

[15] Mulaveesala, R. and V. S. Ghali, "Coded excitation for infrared non-destructive testing of carbon fiber reinforced plastics," Rev. Sci. Instru., Vol. 82, No. 5, 054902, 2011.

[16] Mulaveesala, R., V. J. Somayajulu, and P. Singh, "Pulse compression approach to infrared non destructive characterization," Rev. Sci. Instru., Vol. 79, No. 9, 094901, 2008.

[17] Mulaveesala, R., V. S. Ghali, and V. Arora, “Applications of non-stationary thermal wave imaging methods for characterisation of fibre-reinforced plastic materials,” Electronics Letters, Vol. 49, No. 2, 118-119, 2013.

[18] Tabatabaei, N., A. Mandelis, and B. T. Amaechi, "Thermo photonic radar imaging: an emissivity-normalized modality with advantages over phase lock-in thermography," Appl. Phys. Lett., Vol. 98, No. 16, 163706, 2011.

[19] Carslaw, H. S. and J. C. Jaeger, "Conduction of Heat in Solids," Oxford Clarendon Press, London, 1959.

[20] Ghali, V. S. and R. Mulaveesala, "Comparative data processing approaches for thermal wave imaging techniques for non-destructive testing," Sensing and Imaging, Vol. 12, No. 1-2, 15-33, 2011.

Neural Network Based Automatic Defect Detection in Infrared Thermography

Geetika Dua[1a], Pranav Yogesh Mahajan[1], Aneesh Bajwa[1,] Vanita Arora[2]

[1]Thapar Institute of Engineering and Technology, Patiala.147004
[2]Indian Institute of Information Technology Una, Vill. Saloh, Teh. Haroli, Distt. Una Himachal Pradesh, India-177209.
[a]*Email: geetikadua09@gmail.com*

Abstract

Early, accurate, and automatic detection of defects is an essential aspect of quality improvement. This paper employs a classification-based automatic defect detection method using Gabor filter features. The thermal patterns of various defects are used to provide the primary information for defect detection. Considering the desirable characteristics of spatial locality and orientation selectivities of the Gabor filter, we design filters for extracting defect features from the thermogram. The feature vector based on Gabor filters is used as the classifier's input, a Feed forward neural network (FFNN) on a reduced feature subspace. A finite element method and experiment were adopted to simulate a Carbon fiber reinforced polymer (CFRP) material with void holes as defects. The thermogram will be convolved with Gabor filters by multiplying the image by Gabor filters in the frequency domain. Features are a cell array containing the result of the convolution of the image with each of the forty Gabor filters. The input vector of the network will have large values, which means a large amount of computation. So we reduce the matrix size to one-third of its original size by deleting some rows and columns. This work aims to implement a classifier based on neural networks (Multi-layer Perceptron) to differentiate defect and non-defect patterns.

Keywords:*Defect detection, Gabor wavelet, Gabor Filter, feed forward neural network classifier.*

1. Introduction

Inefficiencies in industrial processes are costly regarding time, money, and consumer satisfaction. In order to sustain or increase the current level of performance in the highly competitive global market, the industry should improve the quality of the production process. It has been learned that the price of a material is reduced by 45%–65% due to the presence of defects. Early and accurate detection of defects and classification is an essential aspect of quality improvement. The accuracy of manual inspection is not good enough due to fatigue and tediousness. The solution to the problem of manual inspection is the automated, i.e., neural network-based part inspection system. Automated part inspection systems mainly involve two challenging problems: defect detection and classification.

Feature selection plays a vital role in developing automated defect classification capability. For an appropriate feature set, the distinguishing qualities of the features should be high, and the number of features should be small. Moreover, an appropriate set of features considers the difficulties in the feature extraction process [1]. A defect inspection system aims to detect and classify surface defects that impair product quality with regard to the requirements set by the user. The requirements mainly deal with the product's suitability for its intended use. In the worst case, the defects may make the product functionally deficient or unusable.

Infrared thermography (IRT) has emerged widely as a method for Non-destructive testing (NDT) as it offers non-contact, comprehensive area detection of material defects. It is based on the physical phenomenon that any object of a temperature above absolute zero emits electromagnetic radiation. The infrared camera further covers the emitted radiation into temperature and produces thermograms [2-7]. This work uses Frequency modulated thermal wave imaging (FMTWI) [8-12] to get the thermograms actively. FMTWI imposed a suitable band of frequencies over the test sample within single experimentation. This work aims to implement a classifier based on Multi-layer Perceptron for automatic defect detection in a

CFRP sample. This work presents an approach combining FMTWI with FFNN for a fast, accurate way to detect and classify sub-surface defects. The multi-layer feed-forward neural network is just several layers of single-layer perceptron neurons bonded to one another [13]. This explains the term 'multi-layer'. The term 'feed-forward' means that any neuron's output will be recurrent to the previous layers of the network.

2. Modeling and simulation

In this work, a 3D Finite element analysis (FEA) has been carried out on a steel sample using COMSOL Multiphysics. This software simulates designs, devices, and processes in all engineering, manufacturing, and scientific research fields [14-17]. COMSOL Multiphysics is a simulation platform that provides fully coupled multiphysics and single-physics modeling capabilities. The Model Builder includes all of the steps in the modeling workflow, from defining geometries, material properties, and the physics that describe specific phenomena to solving and post-processing models for producing accurate results. A CFRP sample is modeled with six blind holes as defects (shown in Fig.1), and has been modeled with a finer mesh using 3D tetrahedral elements.

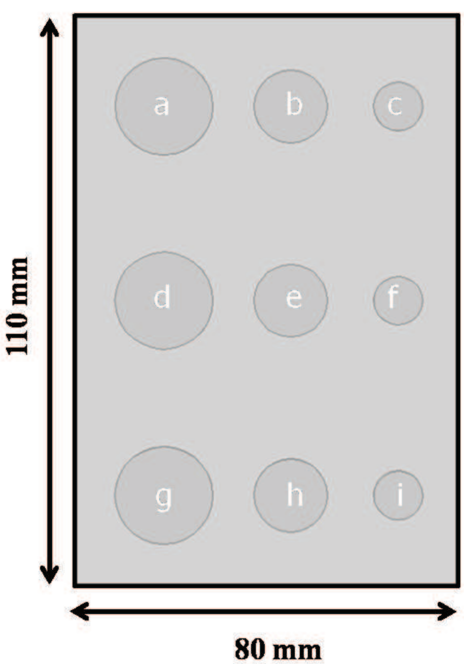

Fig.1 Layout of the modeled CFRP sample with blind holes.

The defects dimensions are shown in Table 1.

Table.1 Defects dimensions

Defect	Diameter (mm)	Depth (mm) from the front surface
a	10	2
b	7.5	2
c	5	2
d	10	1
e	7.5	1
f	5	1
g	10	0.5
h	7.5	0.5
i	5	05

The FEA is carried out by imposing an LFM heat flux (with frequency varying from 0.01 Hz to 0.1 Hz for 100 s) over the surface of the test material, and the infrared camera captures the resultant surface thermal response at a frequency of 25 Hz. The simulations are carried out under adiabatic boundary conditions, with the sample at an ambient temperature of 300 K. The simulated data is further processed using FFNN.

3. Training and testing

3.1 Multi-layer feed-forward neural network

It is just several layers of single-layer perceptron neurons bonded to one another. This explains the term 'multi-layer'. The term 'feed-forward' means that any neuron's output will be recurrent to the previous layers of the network.A multi-layer feed-forward neural network can be created with:

net = newff(P,T,[S1 S2 …])

Where P is an R-by-Q matrix of Q input vectors of R elements each and T is an S-by-Q matrix of Q target vectors of Q elements each.

S1 is the number of neurons in the first layer of the network. In this work as we want to distinguish between defects and non-defects we only need one neuron in the last layer which is called usually the output layer.

So, if we want to have 10 neurons in the first layer and 1 output neuron in the output layer, and we want to create this network, we should write:

net = newff(P,T,[10 1])

Consider that we have 30 images containing defect and 40 images containing non-defect. Each of the images is of size 27x18. with a height of 27 pixels and a width of 18 pixels. So each is actually a matrix and the size of all the matrixes is equal.

Training

The Multy-layer perceptron with the training algorithm of feed propagation is a universal mapper, which can, in theory, approximate any continuous decision region arbitrarily well. However, the convergence of feed-forward algorithms is still an open problem. It is well known that the time cost of feed-forward training often exhibits remarkable variability. It has been demonstrated that, in most cases, the rapid restart method can prominently suppress the heavy-tailed nature of training instances and improve the computation efficiency.

Multi-layer perceptron (MLP) with feed-forward learning algorithms is chosen for the proposed system because of its simplicity and capability in supervised pattern matching [13]. Our problem has been considered suitable with the supervised rule since the input-output pairs are available. For training the network, we used the classical feed-forward algorithm. An example is picked from the training set, and the output is computed.

The training phases are like changing the weights and bias of the neural network and testing it on our training set. Then it adds small corrections to the initialized weights and again tests it. To train the neural network we should write:

net = train(net,P,T);

This line simply trains the network, ‘net’ based on the P and T inputs and their desired outputs, and then it puts back the trained network inside ‘net’.

Testing

For distinguishing between defect and non-defect, we only need one output neuron. This is true as long as we do not want to use orthogonal codes for the desired output of our network. As an example, assume that we have one output neuron, and the value of this neuron for defect patterns is 0, and for the non-defect pattern is 1 for Log sigmoid neurons (or -1 and 1 for tangent sigmoid). If we want to use orthogonal codes, we should have two output neurons with tangent sigmoid as their activation functions. For defect patterns, the value of one output neuron is -1, and the second is 1. For non-defect patterns, the values are reversed. Here we have an advantage in that if the value of two output neurons is both the same, we can conclude that the network is not sure about the type of the input pattern. Even it can be added to the training set for clarification.

In the defect detection system, we have chosen the high value (near 1) as the representative of defects and the low value (near -1) as the non-defects. So we have used one output neuron, and in each call to the network, we only ask for the simulation of one feature vector, one feature vector at a time. So that means our answer always will be a scalar value.

3.2 Generating train sets

We created two folders. One is called ‘defect’, and the other is 'non-defect'. There are several images in PNG format in each of them. These images are the training sets that we have generated. As we can see, all of the images are 27x18. We searched the internet, found some defect images, and put them in the folder. We added some more defect images to the folder. Finding non-defect images was usually strange because a defect is defined, but a non-defect can be anything. To do this, we started with 5 or 6 random non-defect images. First, we trained the neural network for the first time and tested it over an image without any defects.

Testing employed cutting every possible 27x18 patch from the image and converting them into a vector format. Then we gave each vector to input the trained neural network. During testing holes, we got a high response for some of them, say over 0.9. In those cases, we got them and put them in the non-defect folder. Then we trained the network again and did the same procedure again.

One thing is very important due. Our training set should always have a balance between the number of defects and the number of non-defects. Every non-defect image we add to the training set will lower the effect of detecting defect images.

3.3 Gabor feature extraction

Gabor features are simply the coefficients of the response of Gabor filters. Gabor filters are related to Gabor wavelets. Each Gabor wavelet is formed from two components; a complex sinusoidal carrier placed under a Gaussian envelope [18-21].

When the input data is too large or is suspected to be redundant (it does not have much useful information), it will be transformed into a reduced representation set named features. The process to obtain this vector of features is feature extraction. Consider that we have a different defect image from different defects. In defect detection, we are interested in highlighting those parts of the defects common for all defects. All the defects have holes. We need features that can highlight them. Of course, in defect recognition, we need features that can successfully distinguish different defects. Gabor features can do both. Gabor features have been used for both purposes. These help in removing useless and redundant information, and what is left can be used for defect detection or recognition. Now the aim of the later stage, the classifier, which in our case is a neural network, can be to recognize or detect them.

Gabor filtering is done by convolving images with Gabor kernels. Each window that contains a Gabor wavelet is a Gabor kernel, and as described before, the size of the kernel are always odd pixels. After creating all the required kernels, which are about 40, each kernel should be convolved with the window. The convolution of f and g is written by f*g. In 2D, we can consider that we put both images on top of each other and we multiply each of their pixels. Then we sum them all into one scalar value, which belongs to the location of the pixel at the center of the window. After that, one should move the kernel and compute the results for another location until we have the result for all the values of the pixels.

3.4 Pre-selection

To cross-corelate a defect-like sub-image of size 27x18 with theinput image to produce the defect-like image, a template defect.Cross-correlation is a measure of similarity that we can read more about here9. It is simply aconvolution but theoretically speaking, we do not rotate the kernel. Our only intention is to roughlyguess the location of the defects to avoid inspecting every location.

3.5 Search Algorithm

In the pre-selection stage, we recorded the location of all the pixels that should be checked in aimage-like matrix caled cell.state. Actually the word ‘state’is coming from the fact that each pixelcontains a 1 or a 0 as its value. The ON pixels which have 1 as their values, are the location of thecenter of the 27x18 windows that should be checked.

Now we should make sure that when the algorithm finishes, the values of all the pixels are -1. Duringthis phase the value of some pixels may change. According to defined rules, some pixels may changetheir velues form -1 to 1. Other pixels may change their values to -1.Now, according to the result for this pixel, we should make a decision about other pixels in the neighbourhood.Now, according to the result for this pixel, we should make a decision about other pixels in the neighbourhood.

4. Results and discussions

The present works highlight the capability of the proposed approach in detecting the defects present in a CFRP sample. In this approach, the test material can undergo a known controlled frequency modulated thermal stimulation sweeping its entire frequency range from 0.01Hz to 0.1 Hz in 100 s, and the infrared camera captures the corresponding thermal response over the surface. Additive white Gaussian noise with a signal-to-noise ratio being 40 dB is added to the obtained thermal response for the imposed incident heat flux. Noise is artificially added to test the capability of the proposed approach to detect the subsurface density variations.

The neural network responds to most of the candidate locations. There is only a matter of deciding which locations to choose as defects.Fig.2 illustrates the candidate locations.Fig.3 shows the marked detected defects.

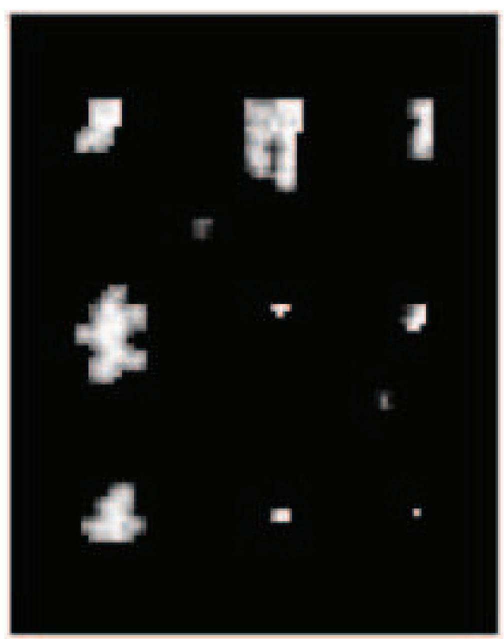

Fig.2 Chosen candidate locations for defects.

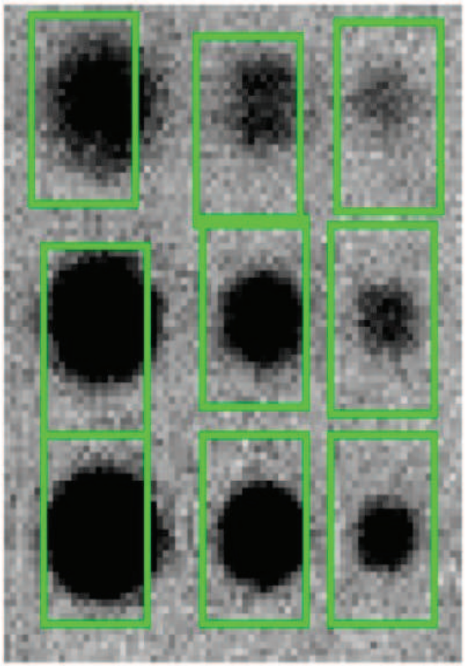

Fig.3 Marked defects

5. Conclusions

It is well known that the aerospace composite materials need to be light in weight, but still highly functional and dependable. The defect could cause catastrophic component failure, incur unnecessary costs. Non-destructive testing prior to installation of aerospace components, and periodically throughout their functional lifetime, can effectively prevent these failures. This study does try to evaluate NDT with neural networks on the simulated CFRP specimen. The results imply that the proposed method can effectively discriminate between the defect and non-defect patterns.

6. References

[1] J. Tou, R. Gonzalez, Pattern Recognition Principles. Massachusetts, USA: Addison-WesleyPublishing Company, 1981.

[2] X. P. V. Maldague (2001), “Theory and Practice of Infrared Thermography for Non- Destructive Testing,” John Wiley & Sons Inc.

[3] D. P. Almond and S. K. Lau (1994), “Defect sizing by transient thermography I: An analytical treatment,” Journal of Physics D: Applied Physics, 27 (5), pp. 1063-1069.

[4] D. L. Balageas, J.C. Krapez, P. Cielo (1986), “Pulsed photothermal modeling of layered materials,” Journal of Applied Physics, 59 (2), pp. 348-357.

[5] X. Maldague and S. Marinetti (2003), “Pulse Phase Infrared Thermography,” Review of Scientific Instruments, 74 (1 II), pp. 417-419.

[6] X. Maldague and S. Marinetti (1996), “Pulse phase infrared thermography,” Journal of applied physics, vol. 79, no. 5, pp. 2694-2698.

[7] G. Busse (1979), “Optoacoustic phase angle measurement for probing a metal,” Applied Physics Letters, 35 (10), pp. 759-760.

[8] G. Busse, D. Wu, W. Karpen (1992), “Thermal wave imaging with phase-sensitive modulated thermography,” Journal of Applied Physics, 71 (8), pp. 3962-3965.

[9] R. Mulaveesala and S. Tuli (2006), “Theory of frequency modulated thermal wave imaging for nondestructive subsurface defect detection,” Applied Physics Letters, 89 (19), art.no. 91913.

[10] S. Tuli and R. Mulaveesala (2005), "Defect detection by pulse compression in frequency modulated thermal wave imaging," Quantitative InfraRed Thermography Journal, vol. 2(1), pp. 41-54.

[11] Ghali V S and Mulaveesala R (2010). “Frequency modulated thermal wave imaging techniques for non-destructive testing,” Insight: Non-Destructive Testing and Condition Monitoring52, 475-480.

[12] Arora V, Mulaveesala R and Bison P (2016), “Effect of Spectral Reshaping on Frequency Modulated Thermal Wave Imaging for Non-destructive Testing and Evaluation of Steel Material,” Journal of Nondestructive Evaluation35, 1-7.

[13] Yang F and Paindavoine M (2003). “Prefiltering for pattern RecognitionUsing Wavelet Transform and Neural Networks,” Adavances in imaging and Electron physics, Vol. 127.

[14] Fang Q, Nguyen B D, Castanedo C I, Duan Y and Maldague II X (2020), “Automatic defect detection in infrared thermography by deep learning algorithm”, Thermosense: thermal infrared applications XLII SPIE) pp 180-195.

[15] Mulaveesala R and Dua G (2016), “Non-invasive and non-ionizing depth resolved infra-red imaging for detection and evaluation of breast cancer: A numerical study”, Biomedical Physics and Engineering Express, 2, 055004.

[16] Dua G, Arora V and Mulaveesala R (2021), “Defect Detection Capabilities of Pulse Compression Based Infrared Non-Destructive Testing and Evaluation”, IEEE Sensors Journal21, 7940-7947.

[17] Arora V, Mulaveesala R, Rani A, Kumar S, Kher V, Mishra P, Kaur J, Dua G and Jha R (2021),"Infrared Image Correlation for Non-destructive Testing and Evaluation of Materials", Journal of Nondestructive Evaluation, 40, 1-7.

[18] Lyons M J, Budynek J and Akamatsu S (1999), "Automatic Classification of Single Facial Images",IEEE Trans. on PAMI, Vol. 21(12).

[19] Kanade T (1973), "Picture processing by computer complex and recognition of human faces",Technical report, Kyoto University, Dept. of Information Science.

[20] Turk M and Pentland A (1991), "Eigenfaces for recognition", Journal of Cognitive Science, pp.71-86.

Reliability of Thermal Images and Numerical Modelling on Passive Infrared Thermography for Concrete Structures

Kavya R. Nair [1a], Vimal Mohan [2], P. Srinivasan [2]

[1] Project Associate, CSIR- Structural Engineering Research Centre, Taramani, Chennai
[1] Scientist, CSIR-Structural Engineering Research Centre, Taramani, Chennai
[a]*Email: krn.kavyanair@gmail.com*

Abstract

Premature deterioration of reinforced concrete (RC) structures resulting from exposure to aggressive environments is a serious challenge faced by civil engineers. Highway bridges, marine structures, and industrial power plants are typical examples of structures facing premature deterioration. Evaluation of concrete quality and deterioration in concrete structural elements using non-destructive testing methods such as Infrared Thermography (IRT) plays a vital role. Defects such as honeycombs, delamination etc can be identified based on the temperature variation on the thermograms. But, the depth of delamination cannot be determined. In this paper, experimental studies were carried with different depths of delamination & numerical studies based on heat transfer were performed. The depth of delamination obtained from the numerical model was found to be matching with the experimental studies and the numerical model was validated.

Keywords: *Concrete deterioration, Non-destructive testing, Infrared thermography, Numerical modelling, Defect quantification*

1. Introduction

Concrete is one of the most versatile man-made building materials available. But due to various factors like extreme weather condition, improper construction methods, corrosion etc. premature deterioration occurs in concrete structures [1]. These deteriorations in the form of cracks, delaminations and air voids, which will start slowly will progress to failure and can be expensive in terms of money and life. The ability to detect these deteriorations at early stage itself act as a useful tool for maintenance and restoration of structure. The methods include Non-destructive tests (NDT) which cause no damage to the structure and also methods like core test, pull out test etc. which affects the integrity of the structure and require repair after the test. With the advances in image processing, signal processing and increased access to powerful computers NDT has become a powerful tool for the analysis of old as well as new concrete structures (Hiasa, 2014). Currently various methods like impact echo, coin tapping, ultrasonic pulse echo, ultrasonic surface wave, ground penetrating radar and infrared thermography are applied for defect detection in concrete [2].

Infrared thermography (IRT) is a global inspection method which allows to detect subsurface delaminations and voids with accuracy. It is having the advantage of inspecting large surface area without direct contact in a short span of time which make it useful for application in wide range of civil engineering structures [3]. Infrared thermography is the science of detecting infrared energy emitted from an object, converting it into apparent temperature and displaying the result as an infrared image. Using an infrared camera, the thermal image can be obtained from an object without making direct contact with the object and this makes IRT an ideal method for investigating inaccessible structures [4].

All objects above zero Kelvin emit infrared energy. IR camera detects this IR energy and convert that to temperature and gives thermogram as output. Heat flows from warmer to cooler area and sound concrete have least resistance to heat conduction. Presence of defects/deteriorations reduces the conductivity as it is having thermal conductivity less than concrete. Thus, the portion of concrete above the defect will be having higher temperature than surrounding during day time (Fig.1 a) and during night that portion will be cold (Fig.1 b). This variation in temperature can be identified from thermogram indicating defects [5].

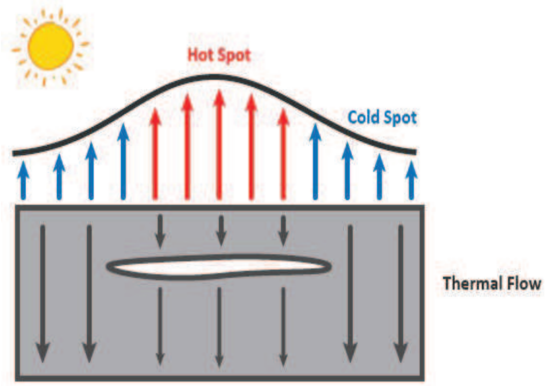

(a)

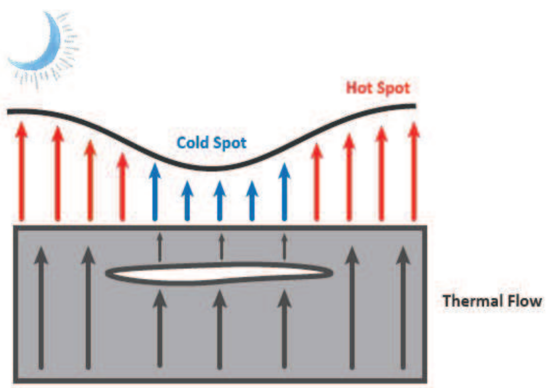

(b)

Fig.1: (a) Temperature variation during day time (b) during night

Concrete testing can involve large areas, the heat source should be low cost and capable of heating the surface uniformly. Sun fulfils all these requirements and this method is called passive infrared thermography. For areas not accessible to sunlight an external source of heat is to be provided and this method is called active thermography. Since concrete is having low thermal diffusivity it requires long heating time which is practically not possible with active IRT. Also, concrete is highly non-homogenous which means that the use of active IRT is less widely reported in civil engineering than in other fields [6]. Estimating the depth of delamination is a major limitation of IRT. Quang Huy Tran et.al [7] conducted study using square pulse thermography which is a method of active IRT for defect quantification. A relation between observation time and square of real depth was derived to find the depth of defect. Also, a method for evaluation of depth and thickness of defect based maximum thermal contrast, defect size, sample thickness and heating time under active IRT was suggested. But for passive thermography these methods cannot be used.

This study aims at conducting an experimental investigation on concrete specimens with defects of thickness 3 mm and 10 mm kept at various depths from surface. Passive infrared thermography is utilized for defect detection. The variation in temperature of delaminated area with depth of defect, thickness and time of investigation is studied in detail. Also, this study investigates the possibility to estimate the depth of defect using FE modelling.

2. Experimental Program

2.1 Specimen details

In this study four specimens with defects simulated with different thickness and depth were used. Details about the dimension of specimen and depth and type of defects in each is given in Table I. Fig.2 shows the details about the specimen and arrangement of defects. Artificial delamination was simulated using Expanded Polyethylene (EPE) foam and cardboard and one with air gap. EPE foam was chosen because it is having a thermal conductivity of 0.024 W/m K which is similar to that of air and cardboard is having lot of air voids in it which simulate the condition similar to an air void/delamination. For SA-1 an air gap was created at one edge of the specimen to study the effect of boundary condition on defect detection. A steel plate was placed at a depth of 20 mm during casting and was removed after four hours leaving an air gap inside. Concrete of M30 grade was used for the preparation of specimens.

Table.I: Statistical Parameters of UPV Values

Specimen	Size of specimen (mm)	Defect type	Size of defect(mm)	Defect depth (mm)
SA-1	500 x 500 x 125	Air void	165 x 165 x 3	20
S-1	500 x 500 x 150	Card board EPE foam	100 x 100 x 3 100 x 100 x 10	12
S-2	500 x 500 x 150	Card board EPE foam	100 x 100 x 3 100 x 100 x 10	25
S-3	500 x 500 x 100	Card board EPE foam	100 x 100 x 3 100 x 100 x 10	30 & 40

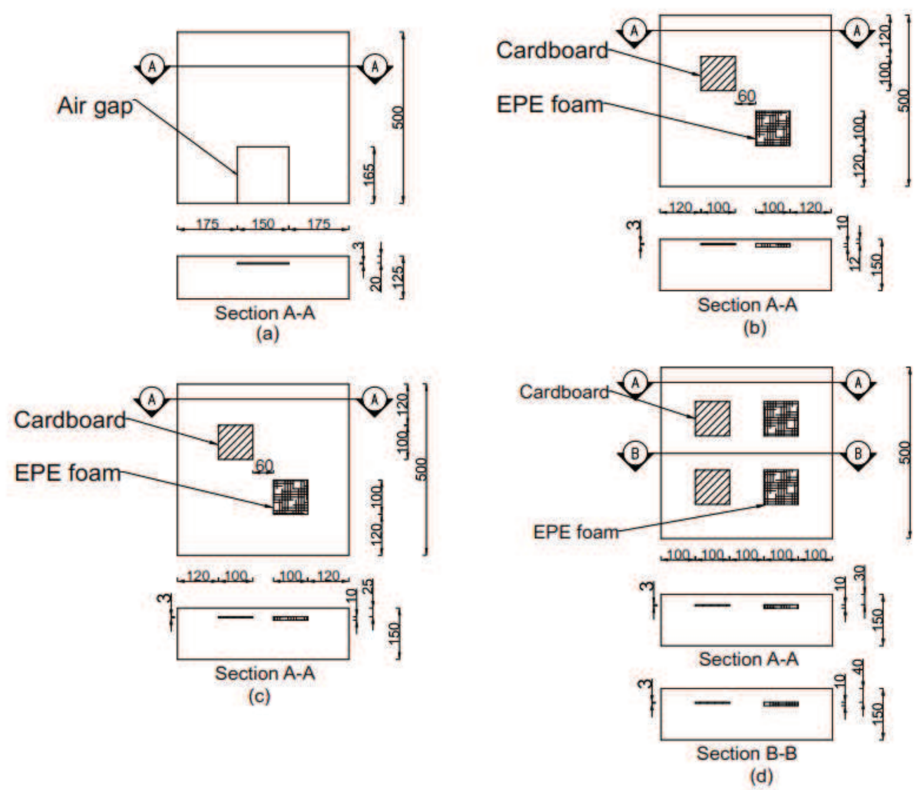

Fig.2: (a) Specimen 1(SA-1) (b) Specimen 2(S-1) (c) Specimen 3(S-2) (d) Specimen 4 (S-3)

2.2 Test procedure

Specimens were arranged on an open ground over concrete cubes of 100 mm size to ensure wind flow for proper heat transfer. Infrared images were taken using IR camera from 9 AM to 6 PM at one-hour interval. The emissivity value was set as 0.95 which is the value for concrete and the reflected apparent temperature was set as 6°C. Slabs were arranged in north- south direction and images were taken from a height of 1.5 m from concrete surface. Specifications of camera is given is Table II.

Table II: IR Camera specifications

Detector type	Uncooled microbolometer
IR resolution	320 x 240 pixels
Spectral range	7.5 - 13 µm
Field of view	45^{O} x 34^{O}

3. Experimental Output

3.1 IR output for SA-1

In the image from 9 AM, the defect was partially detected and then as time passes it became more visible upto 12 PM. After 12PM the edge with air gap was having less temperature as the sun shifts to opposite side and the air gap was not detected. At 2 PM the defect was only partially detected and after that is was not visible. Table III summarizes the IRT results for SA-1. Also, in terms of difference in temperature between sound and delaminated portion (ΔT) it was found that during 10 AM to 1 PM even with ΔT of 1.4^{o}C the defect was detected were as at 9 AM and 6 PM even with ΔT of 2 ^{o}C and 2.6 ^{o}C defects was not detected. Thus, it can be inferred that the delamination being near to the boundary is having an effect on defect detectability. But this will not be a problem for actual structures which have larger surface area. Fig. 3 shows the IR images for SA-1 at 9 AM, 1 PM and 4 PM.

Table III: Summary of IRT results

Time	9 AM	10 AM	11 AM	12 PM	1 PM	2 PM	3 PM	4 PM	5 PM	6 PM
Sun loading	C	C	C	C	C	C	C	C	O	O
Defect indication	P	C	C	C	C	P	O	O	O	O
Heating/ cooling	Hg	Hg	Hg	Hg	Hg	Cg	Cg	Cg	Cg	Cg

Indications: C- defect completely detected, P- defect partially detected, O- defect not detected, Hg- Heating
Cg- Cooling

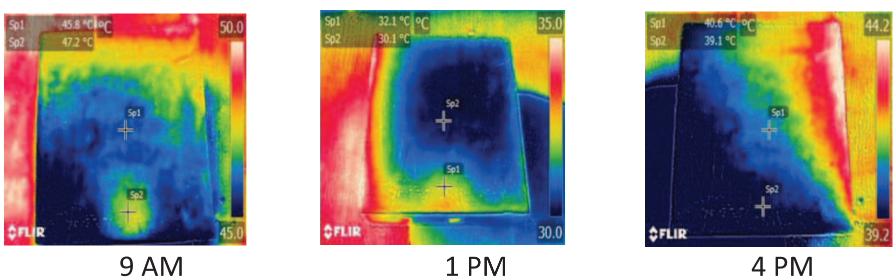

Fig. 3: IR images for SA-1

3.2 IR output for S-1 to S-3

From IR images it was observed that the defect detectability is affected by the thickness of the defect and depth of defect. For specimen 1 in which defect is at 12 mm depth both the defects were completely detected from 10 AM to 2 PM and during 6 PM. During 9 AM, 2 PM and 5 PM defects were only partially detected. This is because of the interchange of heating and cooling cycle. And it was observed that during 4 PM defects were not detected, and this is because of the intersection of heating and cooling cycle. This was found to be true for all the specimens. For specimen 2 in which defect was at 25 mm depth from surface 3mm thick defects were not detected at any instant of time. For 10 mm defect also, it was only partially detected from 10 AM to 3PM. Table IV summarizes the IRT results for S-1 and S2 respectively. A defect like portion is seen on the left top corner for specimen-2 in all the images. But this was identified as a stain mark on the top of the specimen from digital image.

From the IR images for specimen 3 it was observed that the defects; both 3 mm and 10 mm was not detected at any time. Some portions similar to defects was identified. But the temperature for that portion is less than sound region which is not true for day time heating condition. It was found from digital image that such observations are due to the smooth finish of the surface. Fig.4-6 shows the IR images obtained for three specimens.

Table IV: Summary of IRT results for S1 and S2

Time	9AM	10AM	11AM	12PM	1PM	2PM	3PM	4 PM	5 PM	6 PM
Sun loading	C	C	C	C	C	C	C	C	O	O
Defect indication S-1 (10mm)	C	C	C	C	C	C	P	O	P	C
Defect indication S-1 (3mm)	P	C	C	C	C	C	P	O	P	C
Defect indication S-2 (10 mm)	O	P	P	P	C	P	P	O	O	O
Defect indication S-2 (3mm)	O	O	O	O	O	O	O	O	O	O

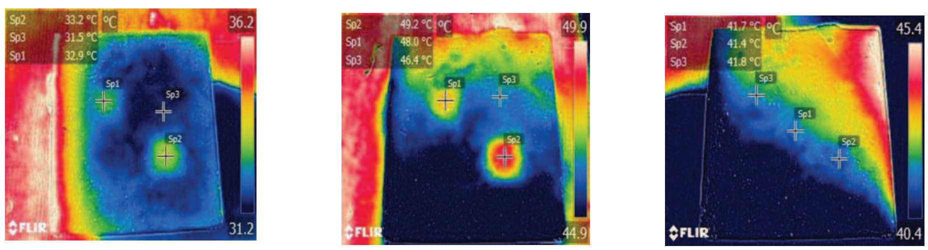

9 AM 1 PM 4 PM

Fig. 4: IR images for S-1

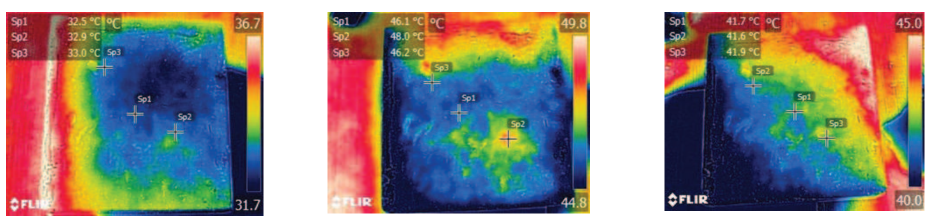

9 AM 1 PM 4 PM

Fig. 5: IR images for S-2

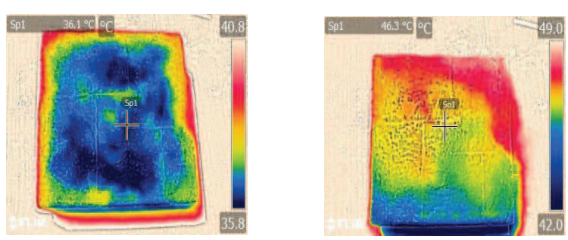

11 AM 12 PM

Fig. 6: IR images for S-3

3.3 Discussion of experimental outputs

From experimental investigation it was found that defects up to 25 mm depth could be detected. Also, at 25 mm depth only delamination with 10 mm thickness could be detected. At 4 PM, defects were not detected in any of the specimens. This is due to the intersection of heating and cooling cycle. Also, for specimen SA-1 defect were not detected after 3PM. This is due to the boundary condition and interchanging period. It was observed that the surface temperature of delamination (T_{del}) was higher than temperature of sound area (T_{sound}) during heating cycle. And during cooling cycle T_{del} is less than T_{sound}. Also, it was observed that the T_{del} value decreases with increase in depth of defect. Fig. 7 shows the variation of T_{sound} and T_{del} with time. It was observed that T_{del} value varies with the thickness of defect. T_{del} value was more for 10 mm thick defects during heating cycle and T_{del} for 3mm thick defect more than that for 10 mm defects during cooling cycle. Fig.8 shows the variation of T_{del} with thickness of defect. Thus, a correlation between the depth of defect and thickness of defect with T_{del} is obtained such that T_{del} decreases with increase in depth and increases with increase in thickness.

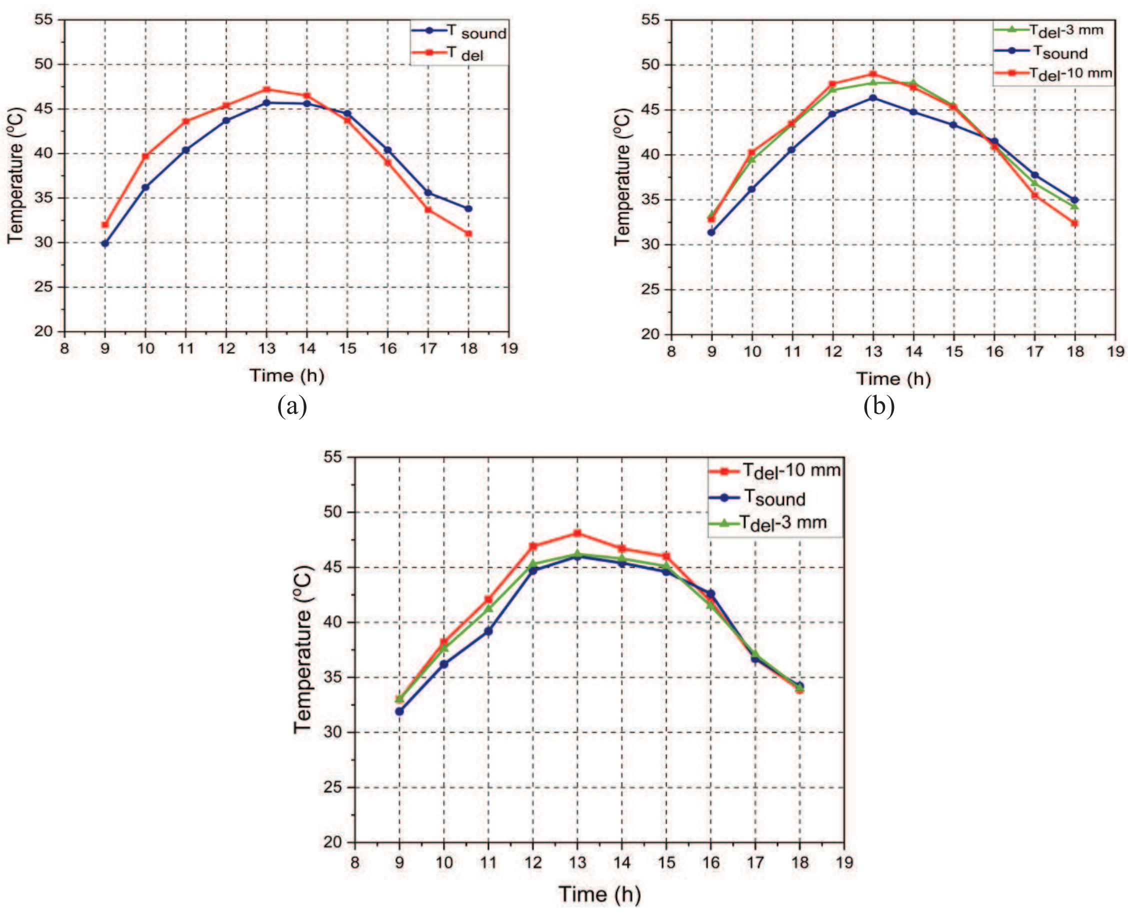

(a) (b)

(c)

Fig.7: Variation of T_{sound} and T_{del} with time. (a)SA-1 (b)S-1 (c)S-2

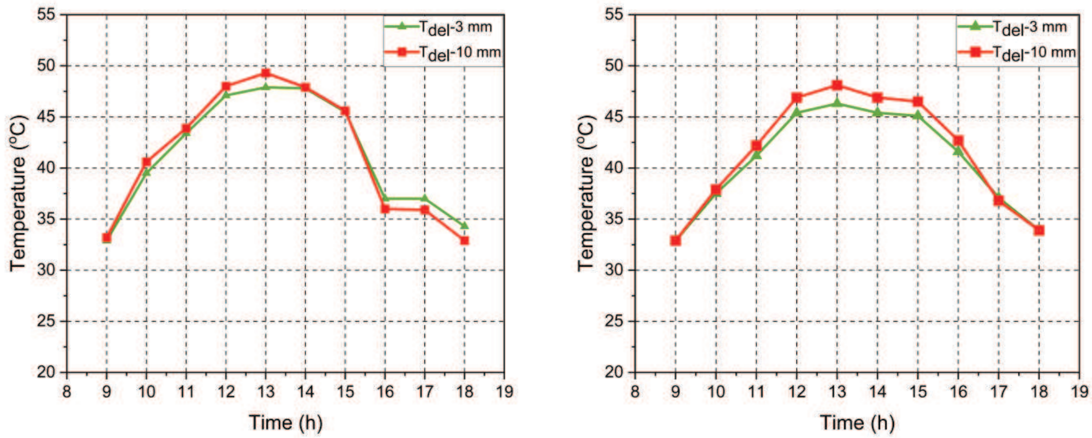

(a) (b)

Fig. 8: Variation of T_{del} with thickness of defect(a) S-1 (b)S-2

4. Numerical Model

4.1 Model development

Finite element modelling of the specimens was done and results were compared with IRT results to validate the model. Modelling was done using the Heat transfer module of COMSOL Multiphysics software.

The concrete blocks of size 500 mm x 500 mm x 150 mm were established over a large ground of size 6 x 6 x 1 m. Defects in form of EPE foam was arranged similar to specimen at depth of 12mm, 20mm, 25 mm. The blocks were arranged over concrete stand of width 100 mm and height 150 mm.

Fig.9(a)shows the FE model of the specimen along with ground. Meshing of the model was done using "Finer" element size physics-controlled mesh available in the software. The material properties fed are given in Table V. The parameters like solar irradiance, ambient temperature, convective heat transfer coefficient, location information and date of experimental investigation are required for forming the FE model. The solar irradiance I_s=605 W/m^2 was set in software for all the models. The ambient temperature input was given based on the weather condition reported by the nearest weather station. The ambient temperature value given as input is given in Fig.9(b).

In this model the primary heat source is the solar radiation. The value of solar radiation and direction of sunlight with time was automatically calculated by the software using latitude, longitude, time zone, date and time. The information was fed as follows: latitude=13.083, longitude=80.2707, time zone= +5:30 h. Convective heat transfer co-efficient h_w was calculated using wind speed. The average value of wind speed for the day was found to be 5.04 m/s. And h_w was obtained as 23 W/ m^{2}K.

Table V: Material properties

Material properties	Units	Concrete	EPE foam	Ground
Thermal conductivity	W/ (m K)	1.6	0.024	0.6
Heat capacity at constant pressure	J/ (kg K)	880	1130	800
Density	Kg/m^3	2300	25	1500
Surface emissivity	-	0.95	-	0.76

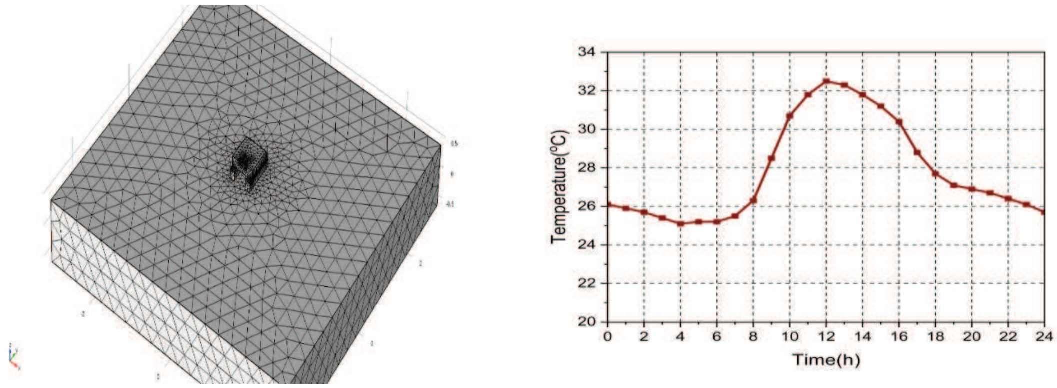

Fig.9: (a)FE model of specimen along with ground (b)Ambient temperature for 4th March 2022

5. Comparison of Simulation and IR Results

Simulation results were obtained from 9 AM to 6 PM. Fig.10-12 shows the simulation results for 9 AM, 1 PM and 4 PM. The defects are clearly visible in simulation results similar to IR results. At 4 PM the simulation result also shows the interchange period during which the defects were not visible in the image. Fig. 7 shows the comparison between IR results and simulation results. The simulation results also follow a similar pattern with experimental values. Surface temperature values from 12 PM to 3 PM is almost same for both simulation and experimental results for S-1 and S-2 (Fig.13). And it is same at 2PM for SA-1. This exceptional behaviour of SA-1 is due to the boundary condition. During other times of the day the temperature readings are bit higher for simulation results. This might be because of the assumption that the sky was clear entire day which was made while doing FE modelling.

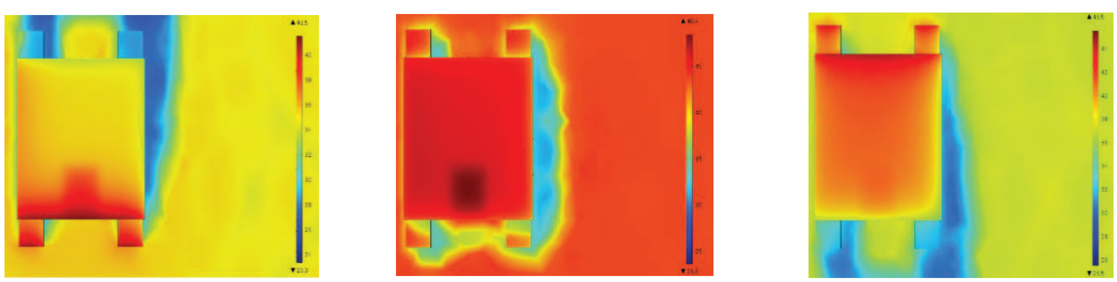

9 AM 1 PM 4 PM

Fig.10: Simulation result for SA-1

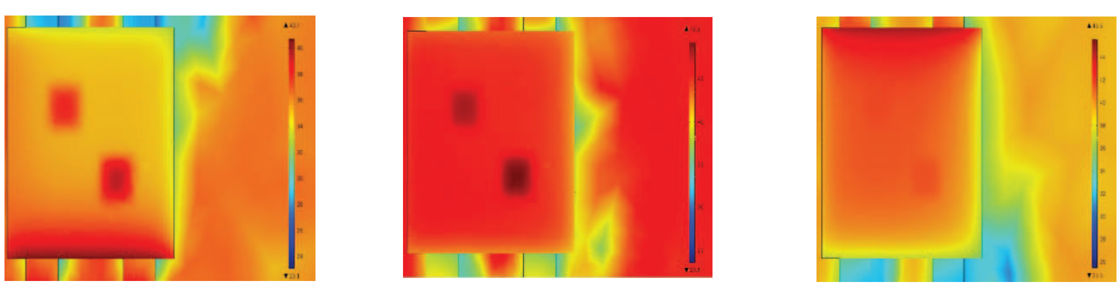

9 AM 1 PM 4 PM

Fig.11: Simulation results for S-1

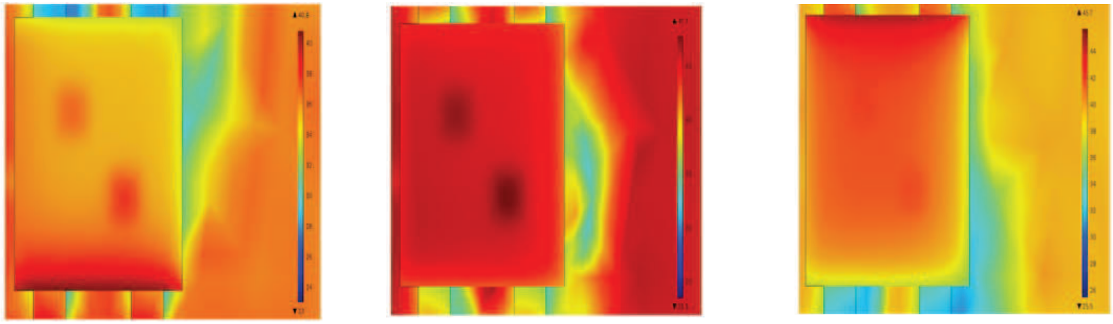

9 AM 1 PM 4 PM

Fig.12: Simulation results for S-2

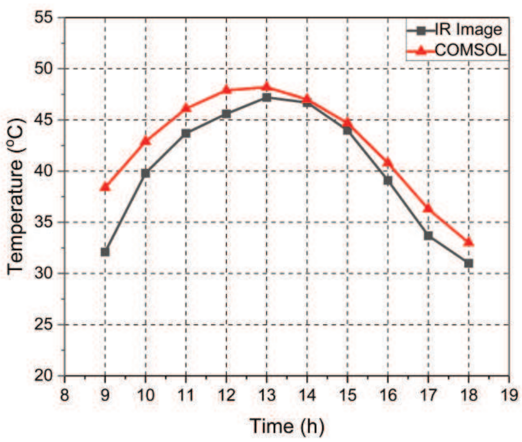

(a)

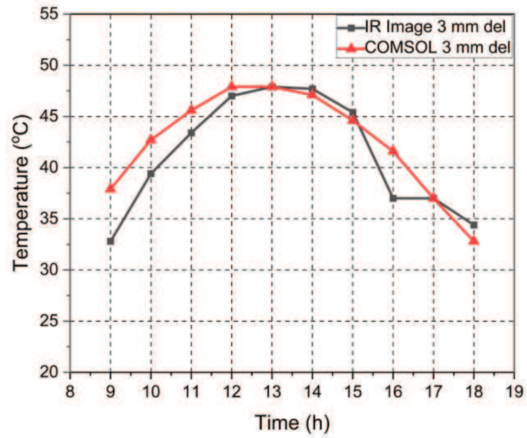

(b)

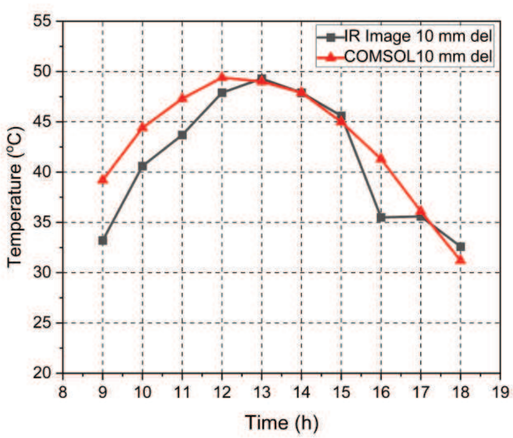

(c)

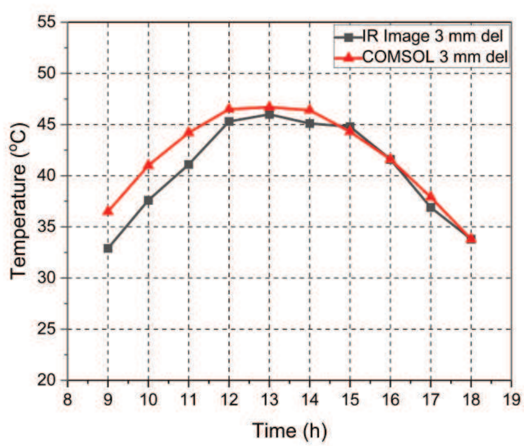

(d)

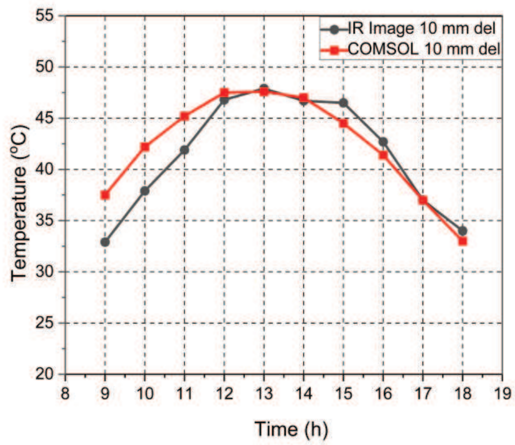

(e)

Fig.13: Comparison of simulation result and IR result (a)SA- 1 (b)S-1, defect 3mm thick (c)S-1, defect 10 mm thick (d) S-2, defect 3mm thick (e)S-2, defect 10 mm thick

From the comparison of simulation and IRT results it can be concluded that the FE model was established properly. A similar pattern of T_{del} values was obtained from simulation results. The values of temperature were almost same during 12 PM to 3 PM. But it can be found that during other time the values of temperature was higher than the IR results. This can be due to the assumption of clear sky condition made while creating FE model. The other reasons include some external agents like wind, photographic angle, thermal sensitivity of camera etc. Thus, it can be concluded that an inverse study can be conducted using FE modelling by simulating several depths and thicknesses of delamination models from which the depth of delamination can be obtained.

6. Conclusion

Experimental investigation was done on specimens with simulated defects to study the effectiveness of IR thermography for detecting delaminations in concrete structures. It was found that IRT can be used effectively for evaluating quality of cover concrete. Defects upto a depth of 25mm can be detected from IR images. An interchange period between heating and cooling cycle was observed and during which the defects are not detected in IR images. From SA-1 it was found that the boundary condition is having much effect on the defect detectability and temperature values. But this will not be a problem for actual structures which have larger surface area. Sometimes the portion identified as defect from the image can be some stains or marking on the surface of the defect. Comparing IR image with digital image helps to overcome this problem. A correlation between the depth of defect and thickness of defect with T_{del} was obtained such as T_{del} increases with increase in thickness of defect and decreases with increase in depth from surface. Numerical model was established successfully using COMSOL Multiphysics software and the temperature values between 12 PM and 3 PM shows a similar trend with IR results. Thus, it could be concluded that an inverse study can be conducted using FE modelling by simulating several depths and thickness of delamination models from which the depth of delamination can be obtained.

7. References

[1] Jungwon Huh, Quang Huy Tran, Jong-Han Lee, DongYeob Han, Jin-Hee Ahn, and Solomon Yim (2016). "Experimental study on detection of deterioration in concrete using infrared thermography technique". Advances in Materials Science and Engineering, https://doi.org/10.1155/2016/1053856.

[2] Shuhei Hiasa, Recep Birgul, Azusa Watase, Masato Matsumoto, Koji Mitani and F. Necati Catbas (2014). "A Review of Field Implementation of Infrared Thermography as a Non-destructive Evaluation Technology". Computing in Civil and Building Engineering ASCE 1715-1722, 10.1061/9780784413616.213.

[3] Shuhei Hiasa, Recep Birgul, F. Necati Catbas (2017). “Effect of Defect Size on Subsurface Defect Detectability and Defect Depth Estimation for Concrete Structures by Infrared Thermography”. J Nondestruct Eval 36:57, https://doi.org/10.1007/s10921-017-0435-3

[4] M. Hain, J. Bartl, V. Jacko (2009). “Active Infrared Thermography in Non-destructive Testing”. Institute of Measurement Science Slovak Academy of Sciences, Bratislava, Slovak Republic, 5, 339–343, 10.1117/12.881599.

[5] Azusa Watase, Recep Birgul, Shuhei Hiasa, Masato Matsumoto, Koji Mitani, F. Necati Catbas (2015). “Practical identification of favorable time windows for infrared thermography for concrete bridge evaluation”. Construction and Building Materials 101 1016–1030, 10.1016/j.conbuildmat.2015.10.156.

[6] Patricia Cotič, DejanKolarič, Violeta Bokan Bosiljkov, Vlatko Bosiljkov, Zvonko Jagličić (2015). “Determination of the applicability and limits of void and delamination detection in concrete structures using infrared thermography”. NDT&E International74, 87–93, https://doi.org/10.1016/j.ndteint.2015.05.003.

[7] Tran Q. H, Huh J, Mac V. H, Kang C, & Han D (2018). “Effects of rebars on the detectability of subsurface defects in concrete bridges using square pulse thermography”. NDT and E International, 100, 92–100, https://doi.org/10.1016/j.ndteint.2018.09.001.

[8] Shuhei Hiasa, Recep Birgul, F. Necati Catbas (2017). “A data processing methodology for infrared thermography images of concrete bridges”. Computers and Structures 190 ,205–218, https://doi.org/10.1016/j.compstruc.2017.05.011.

[9] Jungwon Huh, Quang Huy Tran, Jong-Han Lee, DongYeob Han, Jin-Hee Ahn, and Solomon Yim (2016). “Experimental study on detection of deterioration in concrete using infrared thermography technique”. Advances in Materials Science and Engineering, 10.1155/2016/1053856

[10] A. Karunarathne (2016). “Modelling of Thermal Effects due to Solar Radiation on Concrete Pavements”. Int. Conf. Int. Inst. Infrastruct. Resil. Reconstr., no. 8, p. 277.

[11] Basic Guide to Thermography (2004), Land Instruments International.

[12] B. Milovanovic (2012). “The Role of Infrared Thermography in Nondestructive Testing of Concrete Structures”. vol. 385, no. 1, pp. 7–12.

[13] Glenn Washer, Richard Fenwick, and Naveen Bolleni (2010). “Effects of Solar Loading on Infrared Imaging of Subsurface Features in Concrete”. J. Bridge Eng.15:384-390, https://doi.org/10.1061/(ASCE)BE.1943-5592.0000117.

[14] Hiasa S, Birgul R, MatsumotoM & Necati Catbas F (2018). “Experimental and numerical studies for suitable infrared thermography implementation on concrete bridge decks. Measurement”. Journal of the International Measurement Confederation, 121(February), 144–159, https://doi.org/10.1016/j.measurement.2018.02.019

[15] Malhotra V.M, Carino N.J. Handbook on Nondestructive Testing of Concrete, 2nd ed.; CRC Press: Boca Raton, FL, USA, 2004.

[16] Shuhei Hiasa, Recep Birgul, Masato Matsumoto and F. Necati Catbas(2018). “Experimental and Numerical Studies for Suitable Infrared Thermography Implementation”. https://doi.org/10.1016/j.measurement.2018.02.019.

[17] M. Mirsadeghi, D. Cóstola, B. Blocken, and J. L. M. Hensen (2013) “Review of external convective heat transfer coefficient models in building energy simulation programs: Implementation and uncertainty,” Appl. Therm. Eng., vol. 56, no. 1–2, pp. 134–151, https://doi.org/10.1016/j.applthermaleng.2013.03.003

NDE PATENTS

Dr.Shyamsunder Mandayam

Through this feature every quarter, we intend to provide you a snapshot of some latest and important patents in the world of NDE. We also intend to use this feature to encourage the Indian NDE community to file more patents based on your innovations. We will be happy to provide guidance and assistance in different ways – Answering queries, Conducting Tutorials and webinars, One-on-one discussions, Networking with Intellectual property experts, etc.

Need help understanding, What are Patents? Why to Patent? When to Patent? What is the Patenting Process? …… Please feel free to reach out to me by email at mandayam.shyamsunder@gmail.com

Here we list below a few interesting patents related to a mix of different modalities in ***NDE and Inspection.***

United States Patent 11,590,676

Guided wave-based system for cure monitoring of composites using piezoelectric discs and fiber Bragg gratings/phase-shifted Bragg gratings

Inventors: Tyler B. Hudson, Fuh-Gwo Yuan, Nicolas Auwaijan, Frank L. Palmieri

Assignee: UNITED STATES OF AMERICA AS REPRESENTED BY THE ADMINISTRATOR OF NASA,Washington, DC (US)

System and method for in-process cure monitoring of a material utilizes one or more sensors such as fiber Bragg gratings (FBGs) or phase-shifted FBGs (PS-FBGs) and at least one optical line fiber connected to the sensor(s). The sensor(s) and the optical line may be embedded in the material prior to curing the material may comprise a fiber reinforced polymer. Waves are excited into the material during curing thereof to form guided waves that propagate through the material. At least one wave metric of the guidedwaves is measured utilizing the sensor(s).

United States Patent 20230052887

Robotic Platforms and Robots for Nondestructive Testing Applications, Including Their Production and Use

Inventors: Erin Along, Christoph Schaal

Robotic platforms and methods of use are disclosed that include: at least one robot or robotic device, at least one computer-based control system, wherein the system is at least in part located on the at least one robot, at least one communications system, wherein the communications system is designed to communicate between the computer- based control system and the at least one robot, and at least one evaluation system that is designed to implement and process at least one nondestructive testing method.

United States Patent11,526,168

ROBOTIC INSPECTION OF IN-SERVICE TANKS THROUGH LOWER WALL

Inventors: Zeeshan Farooq Lodhi, Mir Asif Khan

Assignee: Saudi Arabian Oil Company, Dhahran CN (SA)

To implement robotic inspection of anin-service tank through the lower wall, a launch system is operatively coupled to the in-service tank carrying a multiphase fluid separated into a first fluid phase settled at the bottom of the in-service tank and a second fluid phase floating above the first fluid phase. The launch system includes multiple valves and is coupled to the bottom of the in-service tank. By operating the launch system, a robotic tank inspection device is introduced into the first fluid phase in the in-service tank while bypassing the second fluid phase. By operating the robotic tank inspection device, the bottom of the in- service tank is inspected for corrosion.

United States Patent 20230012228

Detection of Corrosion Under Paint and Other Coatings Using Microwave Reflectometry

Inventors: Brad D. Moore, JayL. Fisher, Christopher A. Bang,

Assignee: Southwest Research Institute, San Antonio, TX (US)

A test system for detecting corrosion under a coating on a structure, the coating being transmissive to microwaves and the surface being reflective to microwaves. A microwave generator generates microwaves of a desired power and frequency, which are delivered to a test head that both transmits the microwaves to the surface and receives the microwaves as reflected from the structure. A corrosion detection processor measures the phase and amplitude of the reflected signal, and compares measurement data to reference data to determine if corrosion under the coating is indicated.

United States Patent 11,220,356

NON-DESTRUCTIVE INSPECTION USINGUNMANNED AERIAL VEHICLE

Inventors: James J. Troy, Gary E. Georgeson, Joseph L. Flafenrichter, Scott W. Lea

Assignee: The Boeing Company, Chicago, IL (US)

Provided is a nondestructive inspection ("NDI") system that includes an unmanned aerial vehicle ("UAV") comprising a body structure and at least one support arm. The support arm includes a first arm portion having a first end coupled to the body structure and a second end coupled to a second armportion. The second arm portion includes a first end coupledto the second end of the first arm portion and a second end coupled to an NDI scanning device. The support arm also includes a compliant member disposed between the first arm portion and the second arm portion. The NDI scanning device includes one or more NDI sensors., accurate, efficient on-machine wall thickness measurement of the large panel.

Indian Society for Non-destructive Testing (ISNT)

Enriching Lives through NDE

CIRCULAR

No: ISNT/2023/01 **Date: 2nd January 2023**

Schedule of ISNT meetings

YEAR: 2023

Month	Meeting	Day/Date of mtg.	Timing	Mode / Venue
JANUARY 2023	Past President's Meeting	Sunday, 8th January	03:30 pm–05:30 pm	ONLINE
	Finance / Treasurers Meeting	Saturday, 21st January	03:30 pm–05:30 pm	ONLINE
FEBRUARY 2023	Byelaw Enforcement & Advisory and RA Committee	Saturday, 4th February	03:30 pm–05:30 pm	ONLINE
MARCH 2023	Chapter Chairmen Meeting	Saturday, 4th March	03:30 pm–05:30 pm	ONLINE
	PFMB	Saturday, 11th March	10.00 am– 11.30 am	HYBRID Online / ISNT HO, Chennai
	TMB		11.45 am – 1.30 pm	
	NCB		2.30 pm – 4.30 pm	
	NGC	Sunday, 12th March	10.00 am – 3.30 pm	
MAY 2023	Finance / Treasurers Meeting	Saturday, 20th May	03:30 pm–05:30 pm	ONLINE
JUNE 2023	PFMB	Saturday, 10th June	10.00 am– 11.30 am	HYBRID Online / ISNT HO, Chennai
	TMB		11.45 am – 1.30 pm	
	NCB		2.30 pm – 4.30 pm	
	NGC	Sunday, 11th June	10.00 am – 3.30 pm	
JULY 2023	Past President's Meeting	Sunday, 9th July	03:30 pm–05:30 pm	ONLINE
AUGUST 2023	Byelaw Enforcement & Advisory and RA Committee	Saturday, 5th August	03:30 pm–05:30 pm	ONLINE
SEPTEMBER 2023	Chapter Chairmen Meeting	Saturday, 2nd September	03:30 pm–05:30 pm	ONLINE
	PFMB	Saturday, 9th September	10.00 am– 11.30 am	HYBRID Venue to be decided by March NGC
	TMB		11.45 am – 1.30 pm	
	NCB		2.30 pm – 4.30 pm	
	NGC	Sunday, 10th September	10.00 am – 3.30 pm	
	Finance / Treasurers Meeting	Saturday, 16th September	03:30 pm–05:30 pm	ONLINE
OCTOBER 2023	Award Committee	Saturday, 14th October	03:30 pm–05:30 pm	ONLINE
DECEMBER 2023	PFMB	Wednesday, 6th December NDE 2023	02.00 pm– 03.00 pm	PHYSICAL NDE 2023 Venue, Pune
	TMB		03.00 pm - 04.00 pm	
	NCB		04.30 pm– 0530 pm	
	NGC		05.30 m - 07.30 pm	

Notes: 1. Separate notifications will be sent to the members of the committee / Board for each meeting

2. Each meeting should be attended only by the members and invitees

Bikash Ghose

Hon Gen Secretary, ISNT

The First International Conference on NDE 4.0 - April 2021 in Virtual Mode

The Second International Conference on NDE 4.0 – October 2022 at Berlin, Germany

And Now Proudly Announcing

The Third International Conference on NDE 4.0

to be held during

February 2025 in INDIA !

Watch this space for more details

ORGANISED BY

INDIAN SOCIETY FOR
NON-DESTRUCTIVE TESTING

NDE 2023

DEC 7-9, 2023 • PUNE

33rd Annual Conference & Exhibition on NON DESTRUCTIVE EVALUATION

theme

Transformative NDE:
Unleashing the Power of Advanced Technologies

venue

The Orchid Hotel, Pune
Maharashtra, INDIA

www.isntnde.in


IPLEX GX/GT
Videoscope
IPLEX


Vanta Element™
Handheld XRF Analyzer


OmniScan X3 Phased
Array Flaw Detector
FlexoForm Scanner
INDEX
FlexoFORM
CLOSE
OLYMPUS

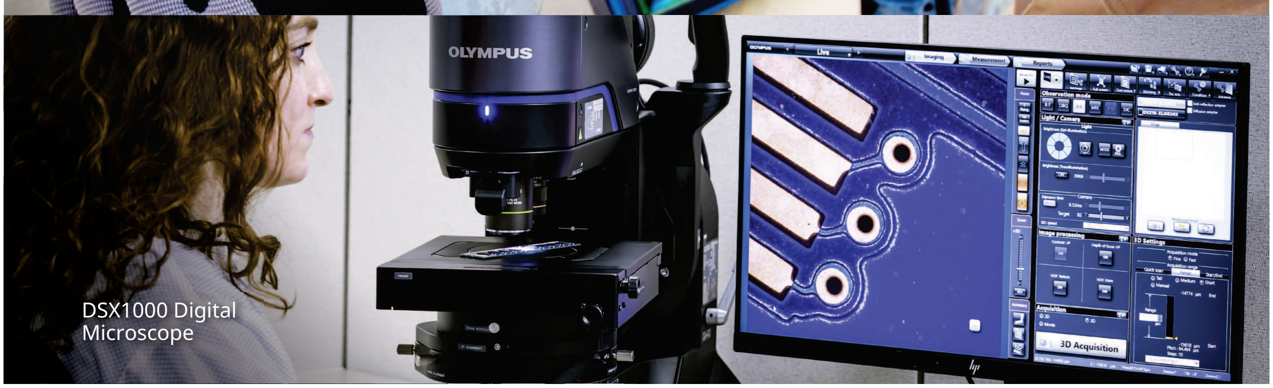
DSX1000 Digital
Microscope
OLYMPUS
3D Acquisition